1-1-2016

Calponin And Cytoskeleton Dynamics In Macrophage Functions And The Pathogenesis Of Atherosclerosis

Rong Liu
Wayne State University,

CALPONIN AND CYTOSKELETON DYNAMICS IN MACROPHAGE FUNCTIONS AND THE PATHOGENESIS OF ATHEROSCLEROSIS

by

RONG LIU

DISSERTATION

Submitted to the Graduate School

of Wayne State University,

Detroit, Michigan

in partial fulfilment of the requirements

for the degree of

DOCTOR OF PHILOSOPHY

2016

MAJOR: PHYSIOLOGY

Approved By:

_____

Advisor Date

_____

_____

_____

_____

DEDICATION

To my departed loving father for your guidance and encouragement during my youth and career development; to my dear mother for your love and support.

ACKNOWLEDGEMENTS

I am grateful to my dissertation advisor, Dr. J.-P. Jin. Your training and insights have been invaluable to me. Thank you for your tireless teaching and guidance.

I sincerely thank the members of my dissertation committee, Dr. Steven Cala, Dr. Robert Lasley, Dr. Takeshi Sakamoto, Dr. Assia Shisheva and Dr. Jianjun Wang, for their support and advice. I want to thank all the Jin lab members for their help and friendship, particularly Dr. Hanzhong Feng who is my first instructor of research skills. The following Jin lab members and collaborators have also helped my dissertation research in significant ways: Dr. M. Moazzem Hossain, Dr. Xuequn Chen, and Dr. Alan Daugherty at the University of Kentucky. I want to further thank the Physiology Ph.D. Program and the Department of Physiology and our graduate officers, Dr. Douglas Yingst and Dr. Steven Cala. The Physiology Department at Wayne State University is my first home in the United States.

Lastly, my many thanks go to Ms. Christine Cupps. I am grateful to your patience and all the help in the past four years which has been the best time of my life.

TABLE OF CONTENTS

LIST OF TABLES

LIST OF FIGURES

LIST OF ABBREVIATIONS

AMVRT	Avian Myeloblastosis virus reverse transcriptase
APC	Antigen presenting cells
ApoB-LP	Apolipoprotein B-containing lipoprotein
ApoE	Apolipoprotein E
BSA	Bovine serum albumin
CH domain	Calponin homology domain
CHD	Coronary heart disease
CVD	Cardiovascular disease
DMEM	Dulbecco's modified eagle's medium
ELISA	Enzyme-linked immunosorbent assay
ERK	Extra-cellular regulated kinase
FBS	fetal bovine serum
GAPDH	glyceraldehyde-3-phosphate
HAT	hypoxanthine, aminopterin, thymidine
HT	hypoxanthine thymidine
IL-1β	Interleukin-1β
IPTG	Isopropyl 1-thio-β-galactopyranoside
LDL	Low density lipoprotein
M-CSF	Macrophage colony stimulating factor
MLC	Myosin light chain
ORO	Oil red O
PBS	Phosphate buffered saline

PKC	Protein kinase C
SDS-PAGE	SDS-polyacrylamide gel electrophoresis
TNF-α	Tumor necrosis factor-α
TnI	Troponin I
TnT	Troponin T
VCAM-1	Vascular cell adhesion molecule-1

CHAPTER 1 - INTRODUCTION

The cardiovascular system and coronary heart disease

The cardiovascular system consists of the heart, which is an anatomical pump, with its intricate conduits (arteries, veins and capillaries) that traverse the whole human body carrying blood. While the heart is the power source responsible for maintaining adequate circulation of oxygenated blood, arteries are the elastic and contractile vessels to carry blood away from the heart under high pressure and regulate the flow volumes [3]. The wall of an artery consists of three distinct layers: The inner most tunica interna is made of a layer of simple squamous epithelium known as endothelium. It rests on a connective tissue membrane with many elastic and collagenous fibers, named basal membrane. The middle tunica media makes up most of an arterial wall, including smooth muscle fibers and a thick elastic connective tissue layer. The outer tunica externa (tunica adventitia) is thinner, mostly made up of connective tissue with irregular fibers. The heart is a highly energy-consuming muscular organ and is supplied with oxygen-rich blood by the coronary arteries.

Arterial atherosclerosis is characterized as the formation of atherosclerotic lesions at the inner layer of arteries, including coronary arteries. Atherosclerosis causes arterial walls thicken and lose elasticity. Progressively, the growth and erupt of atherosclerotic plaques cause blockages of coronary arteries and severe damage of the cardiac muscle, a syndrome described as the coronary heart diseases (CHD). Currently, arterial atherosclerosis is the leading cause of morbidity and mortality in the U.S. and in most developed countries. Arterial atherosclerosis-caused CHD is also rapidly increasing in prevalence in developing countries. Therefore, the prevention and

treatment of atherosclerosis is of paramount importance in the prevention and treatment of cardiovascular diseases (CVDs).

Atherosclerosis was formerly considered a cholesterol storage disease, based on strong evidence of experimental and clinical relationships between hypercholesterolemia and atheroma [4]. In the past two decades, extensive research on the pathophysiology of the disease has established that atherosclerosis is an inflammatory disease [5] [6] [7].

Atherosclerosis is an inflammatory disease

Atherosclerosis is initiated by the subendothelial accumulation of cholesterol-rich, apolipoprotein B-containing lipoproteins (ApoB-LPs) in the susceptible areas of arterial vasculature [8]. The sequestered ApoB-LPs within the intima are isolated from plasma antioxidants, thus become vulnerable to various modifications, such as oxidation, enzymatic and non-enzymatic cleavage, and aggregation. These modifications cause the damage of ApoB-LPs and render these particles pro-inflammatory. Both innate and adaptive immune responses are activated with the progression of the disease [9] [10]. The key early inflammatory response to oxidative ApoB-LPs is the activation of overlying endothelial cells and recruitment of monocytes/macrophages [11] (Figure 1). It is rapidly followed by an adaptive immune response to an array of potential antigens presented to effector T lymphocytes. Both the innate and adaptive immune responses play important roles in the initiation and development of atherosclerosis. In fact, Atherosclerotic lesions contain large number of immune cells, particularly macrophages and T cells [12]. The reduction of macrophages in mice deficient for macrophage colony-stimulating factor (M-CSF) protects against atherosclerosis [13]. Defective

generation of T and B lymphocytes also significantly inhibits lesion development [14] [15].

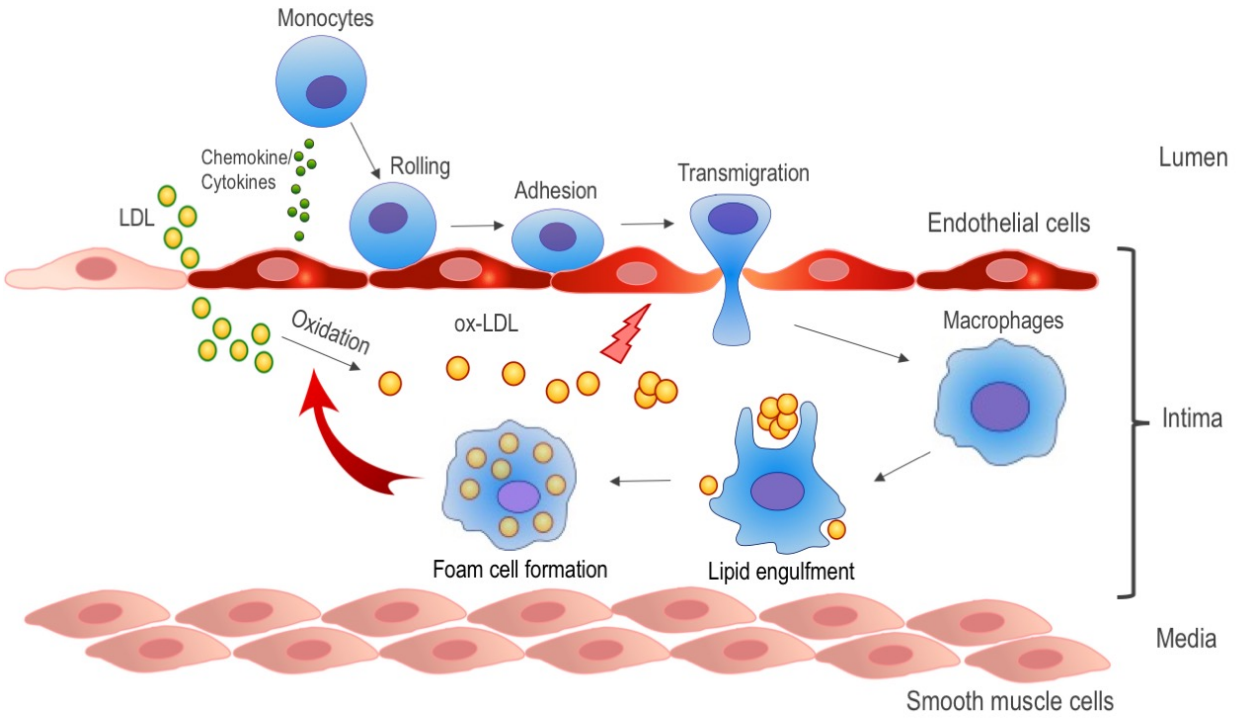

Figure 1. The initial inflammatory response in atherosclerosis. ApoB-LPs (take the LDL as an example in the figure) enter the intima and undergo various modifications, such as oxidation. These modifications incite an inflammatory response characterized by chemokine/cytokine secretion and altered expression of adhesion molecules by the overlying endothelial cells. The inflammatory signals lead to monocyte recruitment into the intima, where they differentiate into macrophages and internalize modified lipoproteins, resulting in the formation of foam cells, a landmark of atherosclerosis lesion. (Modified from [8])

Role of macrophage in the development of atherosclerosis

While subendothelial retention of oxidative lipoproteins is the initiating step of atherogenesis, the ensuing immune response is mediated by the recruited monocytes that differentiate into macrophages and ingest the accumulated oxidative lipoproteins, which transforms them into the cholesterol-laden foam cells. Activated endothelial cells secrete chemoattractants to guide monocytes directional migration. While endothelial cells normally resist leukocyte adhesion, activated endothelial cells express adhesion molecules such as vascular cell adhesion molecule-1 (VCAM-1) and P-selectin that

mediate monocyte rolling, adhesion and migration into the intima [16]. Within the intima, monocytes mature into macrophages with the up-regulation of scavenger receptors, under the influence of M-CSF [17]. Macrophages engulf oxidative lipoproteins through scavenger receptors. The accumulation of cholesteryl esters in the cytoplasm produces the characteristic change of macrophages into foam cells (Figure 1). Macrophages and foam cells derived from them amplify the inflammatory response through the secretion of numerous growth factors and cytokines, including tumor necrosis factor-α (TNF-α) and interleukin-1β (IL-1β). The two key cytokines are central mediators of inflammatory pathways relevant to atherosclerosis [16].

Notably, macrophages that accumulate in atherosclerotic plaques seem to have a diminished capacity to migrate, which contributes to their failure to resolve inflammation and to the progression of the lesion to more advanced, complex plaques in which other immune cells subsets and vascular smooth muscle cells participate in the inflammatory process [18]. In these advanced plaques, macrophages continue to be major contributors to the inflammatory response through their secretion of pro-inflammatory mediators (including chemokines, cytokines and reactive oxygen and nitrogen species) and their eventual death by necrosis or apoptosis. Dying macrophages release their lipid contents and tissue factors, which leads to the formation of a pro-thrombotic necrotic core, a key component of unstable plaques, and contributes to their rupture and the ensuing intravascular blood clot that underlies myocardial infarction and stroke.

Therefore, the regulation of macrophage activation and function has become a focus of the exploration of new therapeutic approaches for arterial atherosclerosis. To

date, the regulation of macrophage function in atherosclerosis and other inflammatory diseases has been investigated mainly in the context of ligand-receptor recognitions and the effects on cell signaling. While the motility and substrate adhesion of macrophages play essential roles in the development and resolution of inflammation [19] [20], very little is known about how the regulation and mechanisms by which these cytoskeleton mechanical tension-based functions determine the development and prognosis of atherosclerosis.

Calponin and isoforms

Calponin is a family of actin filament associated regulatory proteins. It was first identified in chicken gizzard smooth muscle, with a proposed function as a striated muscle troponin T-like protein that binds actin thin filaments to regulate smooth muscle contraction [21]. Extensive research subsequently found that calponin is an actin filament-associated regulatory protein of 34-37 kDa (292-330 amino acids) expressed in both smooth muscle and many non-muscle cell types and functions as an inhibitor of actin-activated myosin ATPase.

Three isoforms of calponin encoded by three homologous genes have been found in vertebrate species: A basic calponin (calponin 1, isoelectric point (pI) = 9.4) encoded by *CNN1* [22], a neutral calponin (calponin 2, pI = 7.5) encoded by *CNN2* [23] [24] and an acidic calponin (calponin 3, pI = 5.2) encoded by *CNN3* [25] (Table 1).

Comparisons of cDNA sequences and the deduced protein primary structures demonstrated that calponin 1, 2 and 3 have largely conserved structures. The phylogenetic tree produced by alignment of amino acid sequences of the three calponin isoforms in vertebrate species investigated to date showed that each of the calponin

isoforms is conserved in the vertebrate phylum whereas the three isoforms have significantly diverged early during evolution (Figure 2). This relationship likely reflects adaptations of the calponin isoforms to their potentially differentiated cellular functions.

Table 1. Calponin isoform genes and their tissue-specific expression.

Isoform Genes	*CNN1*	*CNN2*	*CNN3*
Protein product	Calponin 1	Calponin 2	Calponin 3
Location in human chromosome genome	19p13.2-p13.1	19p13.3	1p22-p21
Number of Exons	7	7	7
Number of amino acids	297	309	329
Molecular Weight	33.2-kDa	33.7-kDa	36.4-kDa
Isoelectric Point	9.10	7.23	5.84
Tissue expression	Smooth muscle	Smooth muscle Neuronal tissue Fibroblast Myoblasts Epithelial cells Endothelial cells Monocytes/Macrophages B lymphocytes	Smooth muscle Neuronal tissue Fibroblast Myoblasts Trophoblasts B lymphocytes

The data presented are based on human calponin isoforms and genes, except for the tissue- and cell-specific expressions that are from studies of multiple vertebrate species.

Tissue distribution of calponin isoforms

The three calponin isoforms exhibit different patterns of tissue and cell type-specific expressions. The expression of calponin 1 is highly specific to smooth muscle cells (Table 1). The contents of calponin 1 vary among different types of smooth muscle. For example, a high level of expression is seen in phasic smooth muscle of the digestive tract and a very low level of expression is found in avian trachea [26]. The

expression of calponin 1 in smooth muscle is up-regulated during development [27]. The mature smooth muscle cell-specific high level expression of calponin 1 suggests a role in smooth muscle differentiation and contractile functions.

Calponin 2 is found in a broader range of tissue and cell types, including developing and remodeling smooth muscles and adult mature smooth muscles [27], epidermal keratinocytes [28], fibroblasts [29], lung alveolar cells [30], endothelial cells [31], myeloid white blood cells [1], myoblasts [32], prostate cancer cells [2] and platelets [33] (Table 1). These cell types can be placed in three groups: a) cells that are physiologically under high mechanical tension, e.g., smooth muscle cells in the wall of hollow organs, epithelial and endothelial cells; b) cells that have high rates of proliferation, e.g., myoblasts; and c) cells that are actively migrating, e.g., fibroblasts and macrophages. The tissue distributions of calponin 2 may imply a role in regulating cytoskeleton tension and related functions, such as adhesion, proliferation and migration [34].

Calponin 3 is found in the brain with expressions in neurons [35], astrocytes [36], and glial cells [37] (Table 1), where it may function in regulating the actin cytoskeleton with a proposed role in the plasticity of neural tissues [38, 39]. Calponin 3 is also found in embryonic trophoblasts and myoblasts with a function in cell fusion during embryonic development and myogenesis [40, 41]. Gene targeting studies showed that mice with the knockout of either *Cnn1* or *Cnn2* gene are viable and fertile [42] [1]. In contrast, *Cnn3* knockout resulted in embryonic and postnatal lethality due to defective development of the central nervous system [43], suggesting the critical of calponin 3 in embryonic and neural system development.

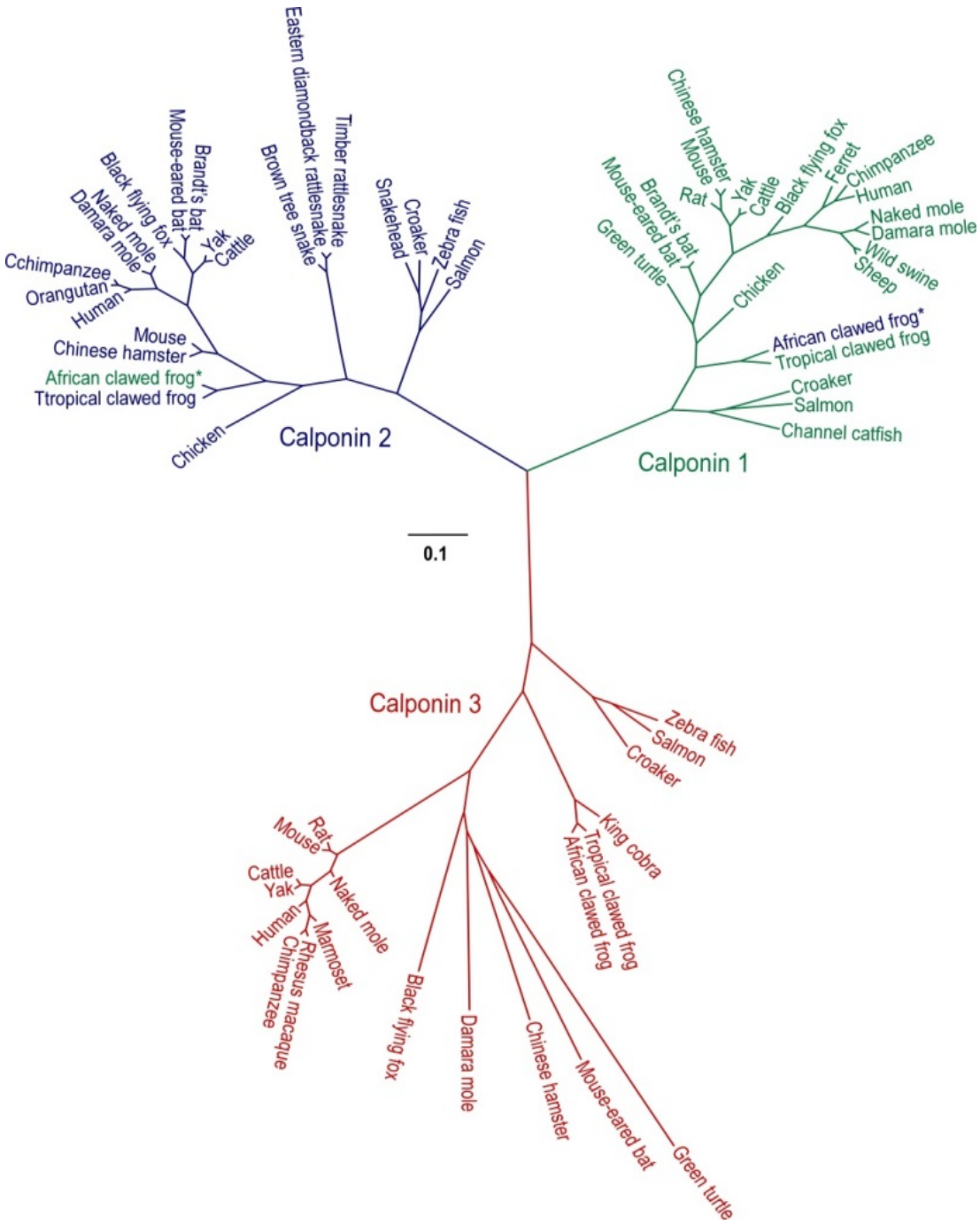

Figure 2. Evolutionary lineage of vertebrate calponin isoforms. The phylogenetic tree of vertebrate calponin isoform genes is derived from protein sequence alignment performed with the Clustal V method using the MegAlign computer program (Lasergene; DNASTAR, Inc, Madison, WI). The degrees of evolutionary divergence are indicated by the lengths of lineage lines. Calponin isoforms 1, 2 and 3 are marked in green, blue and red, respectively. *The aliases of Africa clawed frog *Cnn1 and Cnn2* genes deposited in NCBI database are annotated as *Cnn2* and *Cnn1*, respectively, which is inconsistent with the sequence homology analysis and requires further validation. (See Appendix B)

Structure-function relationship of calponin

Current knowledge of the structure-function relationship of calponin was largely learned from biochemical studies of calponin 1 in smooth muscles. Summarized in Figure 3, primary structure of the three calponin isoforms consists of a conserved N-terminal calponin homology (CH) domain, a conserved middle region containing two actin-binding sites, and a C-terminal variable region that constitutes the main differences among the isoforms.

Outlined in Figure 3, a sequence motif of ~100 amino acids in the N-terminal region of calponin (residues 29-129) is identified as the "calponin homology (CH) domain". CH domains have been found as tandem repeats in many actin-binding proteins with functions including actin cross-linking to cell signaling and are proposed to be either autonomous actin binding motifs or to serve as regulatory structure [44] [45]. However, in contrast to its observed functions in various other proteins, the single CH domain in calponin is not the binding site between calponin and F-actin nor regulates the modes of calponin F-actin binding [46]. CH domain of calponin was found to bind to extra-cellular regulated kinase (ERK) 1 and 2, suggesting a function in ERK signaling of smooth muscle and non-muscle cells [47].

A large collection of evidence demonstrated the role of calponin as an actin-binding protein that inhibits the MgATPase activity of smooth muscle myosin [48, 49] [50] [51] and hinders the movement of actin filaments over immobilized myosin heads [52] [53]. Calponin binds to F-actin through two binding sites (residues 144-162 and 171-188 in chicken calponin 1) (Figure 3) that are conserved among the three calponin isoforms. *In vitro* data show calponin induces actin polymerization and inhibits

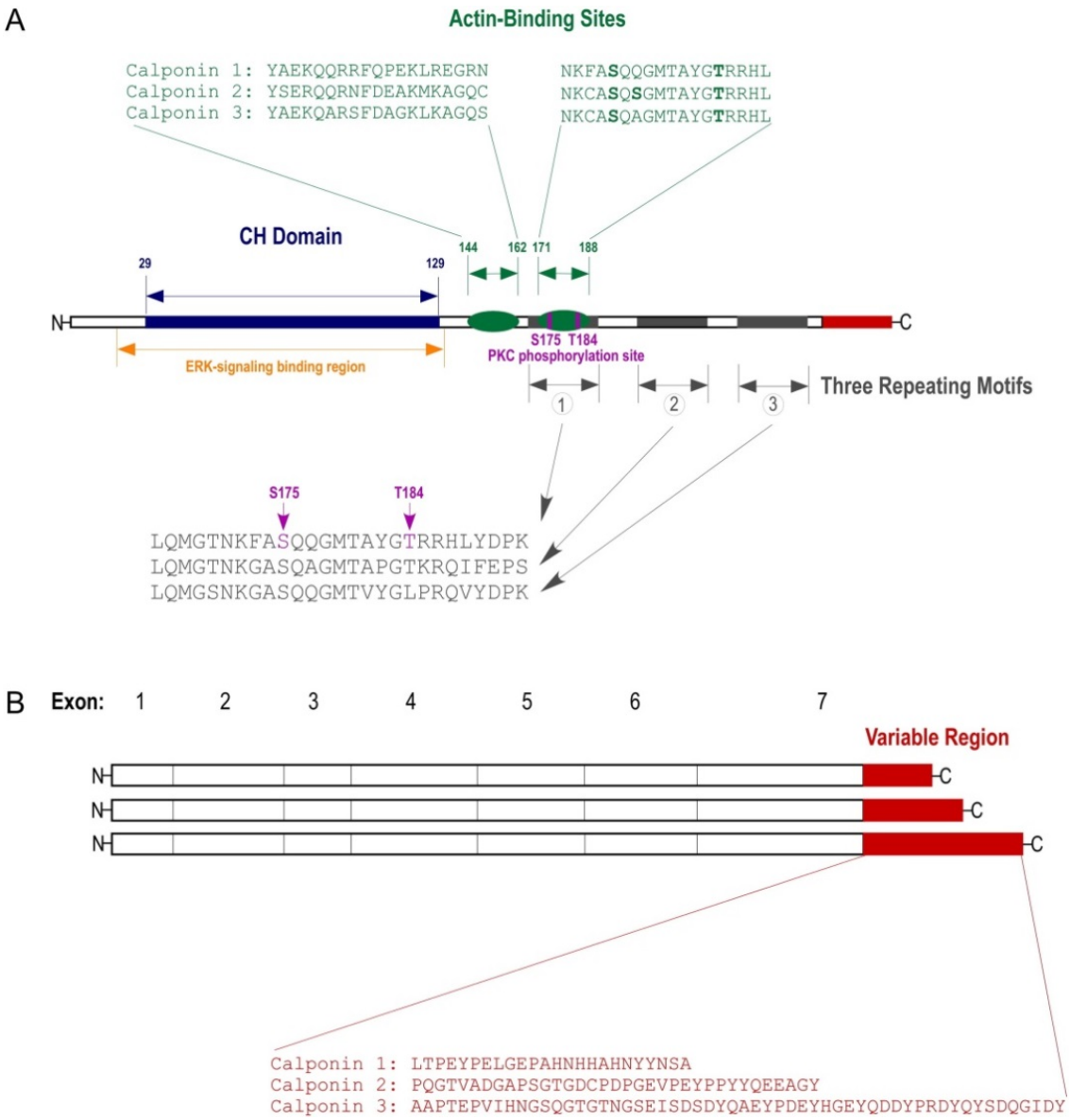

Figure 3. Linear structure and comparison of calponin isoforms. The illustrations summarize the primary structures and comparison of the three calponin isoforms. (A) The linear structural map primarily summarized from studies of chicken calponin 1 outlines the structural and functional domains of calponin. The N-terminal CH domain, the two actin-binding sites, the three repeating sequence motifs, and the C-terminal variable region are shown. The CH domain overlaps with the ERK binding region. Amino acid sequences of the two actin-binding sites in the three isoforms and the three repeating motifs of calponin 1 are shown in the insets. The regulatory phosphorylation sites Ser_{175} and Thr_{184} are located in the second actin-binding site that overlaps with the first repeating motif. Potentially phosphorylatable serine residues corresponding to Ser_{175} are conserved in both repeats 2 and 3, whereas a Thr_{184} equivalent is conserved in repeat 2. Different from calponin 1 and calponin 3, calponin 2 has an additional, potentially phosphorylatable, serine at position 177. (B) Each of the three calponin isoform genes contains seven exons. While the three isoforms are largely conserved in the N-terminal and middle regions, they have a C-terminal variable region encoded by exon 7 that is significantly diverged in length and amino acid sequences.

depolymerization of actin filaments. Addition of calponin greatly retarded the actin depolymerization process [54]. These findings are consistent with the results in living cells that transfective expression of calponin 2 increases resistance of actin filaments to cytochalasin B, indicating the role of calponin 2 in stabilizing actin skeleton [29].

There are three repeating sequence motifs in calponin next to the C-terminal region. This repeating structure is also conserved in all three isoforms and across species. Illustrated in Figure 3, the first repeating motif overlaps with the second actin-binding site (residues 171-188) and contains the protein kinase C (PKC) phosphorylation residues Ser_{175} and Thr_{184} that have no counterparts in the first actin-binding site (residues 144-162). This structural feature is consistent with the hypothesis that the second actin-binding site plays a regulatory role in the binding of calponin to the actin filament. Similar sequences as well as potential phosphorylation sites are present in repeats 2 and 3 although their functions and regulation have not been determined. Therefore, the biological significance of these repeating motifs in calponin remains to be established.

The C-terminal segment of calponin is a variable region that has diverged significantly among the three isoforms. The variable lengths and amino acid compositions of the C-terminal segment produce the size and charge differences among the three calponin isoforms (Table 1). The corresponding charge features rendered calponin 1, 2 and 3 the name of “basic”, “neutral” and “acidic” calponins, respectively ([55] [56]. The C-terminal segments of calponin have been shown to have differentiated effects on weakening the binding of calponin to F-actin. Deletion of the C-

terminal tail segment of calponin strongly enhanced the actin-binding and bundling activities of all three isoforms, indicating a regulatory inhibition effect of the C-terminal variable region [57] [58]. The C-terminal tail regulates the interaction with F-actin by altering the function of the second actin-binding site of calponin [59]. These findings suggest that C-terminal variable region may determine the cell type-specific functions and/or subcellular distributions of the calponin isoforms.

Role of calponin 2 in the regulation of actin cytoskeleton in non-muscle cells

Various cellular functions that are regulated by calponin 2 have been identified in different cell types. Calponin 2 was first found to regulate the rate of cell proliferation. Significant amounts of calponin 2 are found in growing smooth muscle tissues such as embryonic stomach and urinary bladder as well as the uterus during early pregnancy [27]. The expression of calponin 2 decreases to lower levels in quiescent adult smooth muscle cells while the expression of calponin 1 is up-regulated [27]. Over expression of calponin 2 in a rabbit smooth muscle cell line hindered cell proliferation with increased number of binuclear cells indicating a blocking of cytokinesis [27]. These data suggest that although calponin 2 is an inhibitory regulator, it is required in rapidly proliferating cells, possibly as an equilibrium factor for the regulated dynamic changes of the actin cytoskeleton during cell proliferation and cytokinesis.

The dynamics of actin cytoskeleton plays a critical role in cell motility function. As an actin-associated protein, calponin 2 regulates cell motility, presumably through inhibiting the actin activated myosin motor functions. Primary fibroblasts isolated from calponin 2 knockout mice were found to migrate faster than that of wild type control cells [60].

Calponin 2 also facilitates adhesion in multiple types of cells. Significant amounts of calponin 2 are found in human and mouse platelets [33]. In a microfluidic flow-based thrombosis assay, blood samples from *Cnn2* knockout mice exhibits prolonged time of platelet accumulation and thrombosis compared to wild-type control mice, suggested the weakened adhesion of calponin 2-null platelet [33]. Primary fibroblasts isolated from calponin 2 knockout mice were also found weakened adhesion that wild-type control cells [60]. The effect of calponin 2 on facilitating the velocity of cell adhesion was also shown when prostate cancer cells expression high or low calponin 2 were compared on substrates of high or low stiffness [2].

The mechanism by which calponin 2 regulates the functions of actin cytoskeleton remains to be investigated. In addition to stabilization of actin filaments [29], our recent study demonstrated that calponin 2-null fibroblasts isolated from *Cnn2* knockout mice have increased cell traction force that is generated by myosin II motor activity [61]. This finding is consistent with the established role of calponin 1 as an inhibitory regulator of smooth muscle actomyosin ATPase and contractility [62].

Calponin 2 in the regulation of macrophage function

Macrophages are mobile cells and their actin cytoskeleton plays a fundamental role in the adhesion, locomotion and phagocytosis. These activities are essential for the function of macrophages in defensive and autoimmune responses [63]. Significant amounts of calponin 2 are found in blood cells of myeloid lineage, indicating a regulatory role. Calponin 2 is known to increase actin cytoskeleton stability and inhibit myosin motor activity. The removal of calponin 2 from macrophages may make the actin cytoskeleton more dynamic. Previous *in vitro* experimental data demonstrated

that calponin 2-null macrophages possessed faster migration ability (Figure 4) and enhanced phagocytotic activity (Figure 5) [1]. Macrophages play critical roles in the pathogenesis of inflammatory diseases. Function changes of macrophage may change the resolution of inflammatory diseases. For instance, in global as well as in myeloid cell-specific *Cnn2* knockout mice, the development of inflammatory arthritis induced by anti-glucose-6-phosphate isomerase serum was significantly attenuated as compared with that in control mice [64]. These data demonstrate that calponin 2 regulates macrophage activities and controlling calponin 2 expression and function in macrophages may be explored for applications in the treatment and prevention of inflammatory diseases.

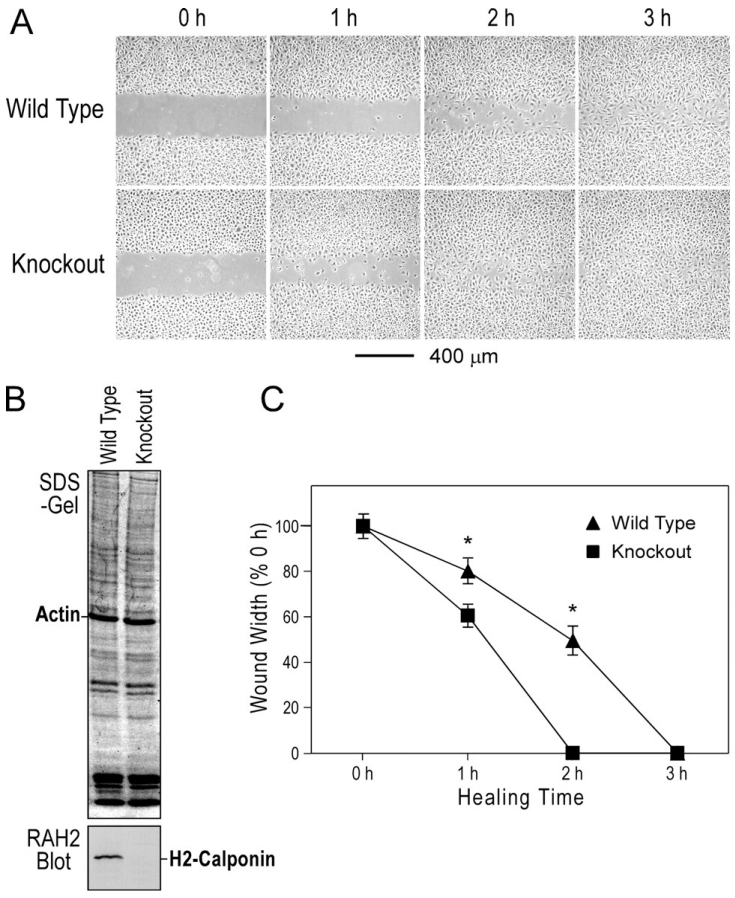

Figure 4. Faster migration of calponin 2-free macrophages during *in vitro* wound healing. *A*, scratch wounds were made in monolayer cultures of peritoneal residential macrophage 24 h after plating. Healing of the wound by cell migration was monitored for 6 h. The micrographs showed an earlier closure of the wound in the h2-calponin-free macrophage culture than the wild type control. *B*, SDS-PAGE and Western blot using RAH2 antibody on total protein extracts from cells collected at the end of the wound healing experiments confirmed the presence and absence of h2-calponin in the wild type and *Cnn2* knock-out cells, respectively. *C*, quantification of the wound healing data demonstrates the faster migration rate of the h2-calponin knockout macrophages than the wild type control. *, $p < 0.05$.

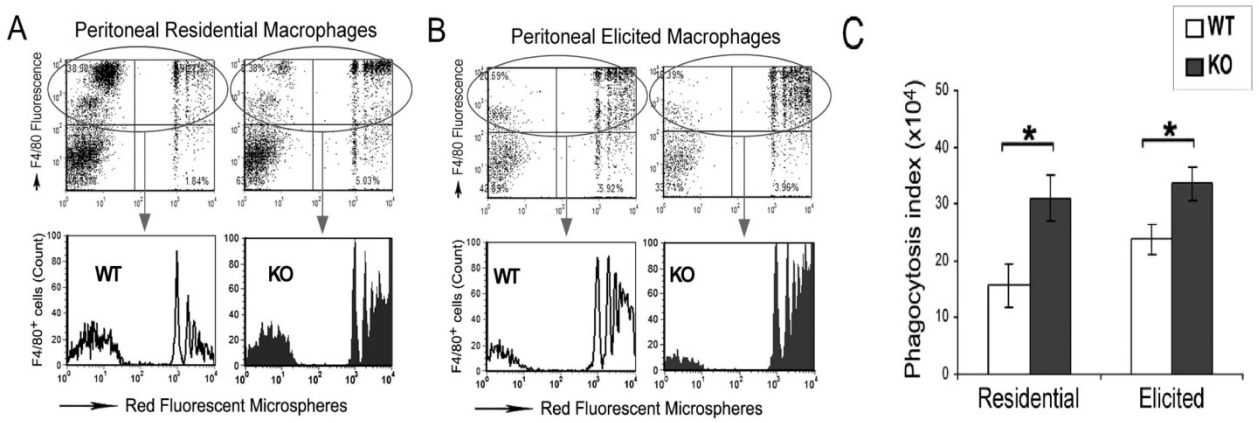

Figure 5. Calponin 2-free macrophages had enhanced phagocytosis. Residential (*A*) and elicited (*B*) peritoneal cells isolated from calponin 2 knock-out (*KO*) and wild type (*WT*) mice were incubated with red fluorescent carboxyl microspheres to test phagocytosis activity. In the representative flow cytometric histograms of the F4/80-positive WT and KO macrophages, the *x* axis represents the fluorescent intensity indicating phagocytosis of the beads and the *y* axis indicates the gating for macrophages (*upper panels*) and the relative cell counts (*lower panels*). The *peaks* from *left to right* represent cell populations with no bead-ingested, 1 bead ingested, and 2 to more than 5 bead ingested. *C*, the phagocytosis activities measured on peritoneal residential (n = 7 for both WT and KO) and 72-h elicited (n = 7 for WT, n = 5 for KO) macrophages are summarized as phagocytosis index (percent of beads-ingested cells × mean florescence intensity of cells containing beads). The data demonstrated an enhanced phagocytosis activity of both residential and elicited macrophages when h2-calponin was absent (*, $p < 0.05$).

Aims of dissertation research

Based on these novel findings, the central hypothesis to be investigated in my dissertation research is that removal of calponin 2 from macrophages would attenuate the development and/or severity of atherosclerosis. Two integrative Specific Aims are pursued:

Aim 1 is to investigate the overall phenotype of *ApoE-/-* and systemic *Cnn2-/-* double KO (*ApoE-/-,Cnn2-/-)* mice and *ApoE-/-*, myeloid cell-specific *Cnn2* KO (*ApoE-/-,Cnn2f/f,lysM*$^{cre+)}$ mice in the development of atherosclerosis. The development of aortic atherosclerotic plaques in these mouse models is compared to that in age and sex-matched *ApoE-/-* control mice. The hypothesis is that the deletion of calponin 2 from macrophages will attenuate the development of atherosclerosis (Figure 6).

Aim 2 is to investigate the cellular and molecular mechanisms of alleviating atherosclerosis development in calponin 2-null mice. *Cnn2-/-* mouse macrophages and derived foam cells are examined for functions such as adhesion, migration and phagocytosis. The cytokine production profiles in *Cnn2-/-* and control macrophages and foam cells are also investigated. The hypothesis is that deletion of calponin 2 will promote macrophage migration and weaken macrophage adhesion, which leads to attenuated inflammatory response and atherosclerotic lesion (Figure 6).

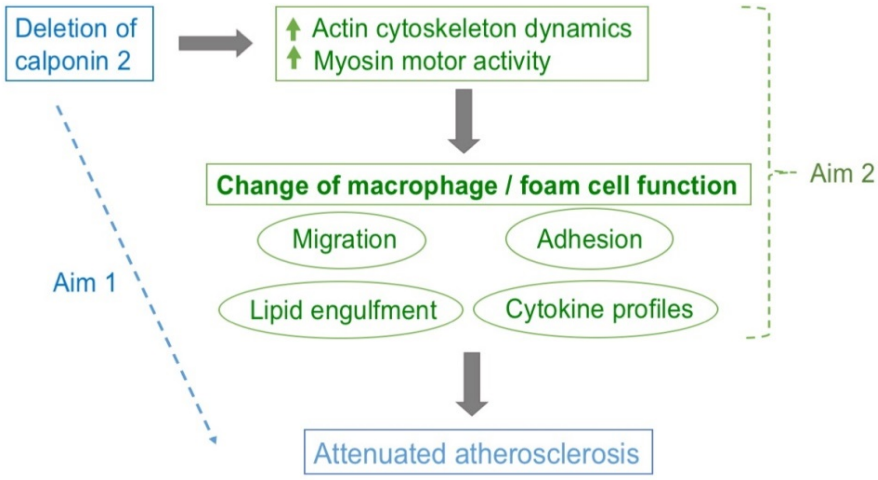

Figure 6. Road map of my Specific Aims. Aim 1 is labeled in blue and Aim 2 is labeled in green. Aim 1 is to investigate the overall phenotypes in the development of atherosclerosis of *ApoE-/-, ApoE-/-,Cnn2-/-* and *ApoE-/-,Cnn2f/f,lysM^{cre+} mice.* Aim 2 is to study the underlying mechanisms focusing on the function changes of macrophages and derived foam cells.

To understand the pathogenesis of atherosclerosis has a major impact on healthcare and the prevention of coronary heart diseases. Based on the notion that atherosclerosis is an inflammatory disease and our recent findings of calponin 2's role in regulating the cytoskeleton-based functions of macrophages, my dissertation research will contribute to a better understanding in the regulation of macrophage's cytoskeleton function in the pathogenesis of atherosclerosis and lay fundamental background information for future development of effective treatment and prevention of the disease.

To reflect my training in a broad range of research approaches and other contributions that I have made to the field of vascular physiology and pathophysiology

research during my Ph.D. study, this dissertation also summarizes the cloning of a cDNA encoding mouse Apolipoprotein E (ApoE) protein, expression of recombinant ApoE in *E. coli* culture, and the approach to develop hybridoma monoclonal antibodies against ApoE (Chapter 2). With the critical role of mechanical regulation in calponin's functions in the development of atherosclerosis, the mechanoregulation of a calponin-related protein, SM22, is investigated in Chapter 4. Related to the mechanical environment of vascular tissue, my studies on the physiological contractility of cardiomyocytes that are present in the wall of mouse and rat thoracic veins are presented in Chapter 5. The results add valuable contributions to our understanding of cardiovascular biology and diseases.

CHAPTER 2 - CLONING OF cDNA ENCODING MOUSE APOE, EXPRESSION OF RECOMBINANT PROTEIN IN BACTERIAL CULTURE, AND APPROACHES TO DEVELOPING HYBRIDOMA MONOCLONAL ANTIBODIES

Abstract

SDS-PAGE and immunoblotting are essential techniques to detect ApoE protein to verify genetically modified mice bearing multiple alleles used in this study. Taking advantages that our laboratory has the capacity to routinely develop and produce hybridoma monoclonal antibodies as well as a part of hands on training in molecular engineering, the development of anti-ApoE monoclonal antibodies was included in my thesis project. cDNA encoding mouse ApoE was reversely transcribed from RNA extracted from adult mouse liver tissue. The *Apo*E cDNA insert was cloned to a Tx_3-included pAED4 vector to facilitate ApoE expression and purification. Tx_3-ApoE fusion protein was expressed by *E. coli* BL21-(DE3)pLysS and purified by a Zn (II) affinity column. Balb/c mice were immunized with Tx_3-ApoE fusion protein and spleen cells were harvested for hybridoma production. The positive hybridoma clones were screened by indirect ELISA against Tx_3-ApoE antigen. The screening results show that all the positive clones demonstrated high specificity and affinity against the Tx_3 peptides in the antigen but none of them was against ApoE. The data indicate that different from many other mouse proteins which were effective immunogens for mouse in generating specific monoclonal antibodies, ApoE has very weak immunogenicity but served as an effective carrier in delivering Tx3 peptides. The fact that mouse ApoE can be recognized by the immune system of mouse as an effective carrier intrigued us to test a novel approach to generating useful antibodies by immunizing *ApoE*-KO mice to avoid the intrinsic issue of immune tolerance in developing antibody tools against plasma proteins like ApoE, especially from the species same as the host to be immunized.

Introduction

Cholesterol is insoluble in plasma and thus packed in lipoproteins when travels in blood stream. Cells uptake cholesterol via low density lipoprotein (LDL) receptor [65] because cholesterol esters are too hydrophobic to pass through membranes. ApoE mediates high-affinity binding of ApoE-containing lipoprotein particles to LDL receptor and is responsible for cellular uptake of these particles. Therefore, homozygous *ApoE* KO mice exhibit high cholesterol in the plasma (five times of normal) and early spontaneous atherosclerotic lesions [66]. Mice with ApoE deficiency are broadly used as an established model in the study of atherosclerosis [67].

SDS-PAGE and immunoblotting are essential techniques to detect ApoE protein to verify the genetically modified mice bearing multiple alleles used in this study, thus the development of anti-ApoE monoclonal antibodies was included in my thesis project. Mouse ApoE cDNA was cloned and subcloned into a Tx_3-included pAED4 vector for facilitating expression. Tx_3-ApoE fusion protein was expressed, purified and used for Balb/c mice immunization. The positive hybridoma clones were screened by indirect ELISA against Tx_3-ApoE antigen. The screening results show that all the positive clones demonstrated high specificity and affinity against the Tx_3 peptides in the antigen but none of them was against ApoE. The results indicate that ApoE had very weak immunogenicity but served as a good carrier in delivering Tx3 peptides. However, when ApoE protein fused with a C-terminal segment of calponin 2, the immunogenicity of ApoE was enhanced and specific monoclonal antibodies against ApoE were produced, suggesting that carriers and antigenic epitopes exhibit preferences for their conjugation

partners, and a specific design of fusion proteins may represent a new approach to increasing immunogenicity of antigens and generating targeted monoclonal antibodies.

Material and Methods

Cloning of cDNA encoding mouse ApoE

Total cellular RNA was extracted from adult mouse liver tissue using the TRIzol reagent (Invitrogen) according to the manufacturer's protocol. Integrity of the isolated RNA was verified using agarose gel electrophoresis. cDNA encoding ApoE was obtained by reverse transcription-coupled polymerase chain reaction (RT-PCR). Reverse transcription was carried out using ApoE exon 4 reverse primer and Avian Myeloblastosis Virus Reverse Transcriptase (AMVRT). PCR amplification of the coding region of ApoE cDNA without the N-terminal secretion peptide was carried out using the following primers: Forward: 5'-CAATTGCG***CATATG***AAGGCTCTGTG-3'; Reverse: 5'-TG***GAATTC***CTCACAGAGACTCAGA-3'). The PCR primers were designed to add unique restriction enzyme sites: *Nde*I and *Eco*RI (Indicated in bold italic font in the primer sequence) at the 5' and 3' ends of the ApoE cDNA insert, respectively, for subsequent cloning into the expression plasmids.

The *ApoE* cDNA insert was double digested with *Nde*I and *Eco*RI at sites engineered in the PCR cloning primers and ligated into a pAED4-based expression vector employing an N-terminal fusion tag of 15 amino acids ($[HEEAH]_3$) derived from the N-terminal variable region of chicken breast muscle Troponin T (TnT) [68] to facilitate the purification via metal affinity chromatography [69] [68]. After transformation of JM109 *E. coli* and plating on ampicillin selection LB plates, antibiotic resistant bacterial colonies were selected and screened by PCR to identify the presence and

appropriate orientation of the *ApoE* cDNA insert. A positive recombinant plasmid was sequenced to confirm the correct insertion of the specific cDNA insert and the absence of PCR-generated mutations.

Large-scale expression of the Tx_3-tagged ApoE protein

Competent BL21-(DE3) pLysS *E. coli* cells were transformed with the expression plasmid encoding mouse ApoE cDNA as described above. Freshly transformed BL21-(DE3) pLysS colonies were used to inoculate 2X tryptone-yeast broth containing 100 μg/mL ampicillin and 12.5 μg/mL chloramphenicol [70]. The culture was incubated at 37 °C with vigorous shaking and induced at $OD_{600\ nm}$ ~0.4-0.5 by adding isopropyl 1-thio-β-D-galactopyranoside (IPTG) to a final concentration of 0.4 mM. The culture was continued for another 3 hrs, harvested by centrifugation and resuspended in a lysis buffer containing 6 M urea, 1 M KCl and 20 mM phosphate buffer pH 7.4. The pellets were lysed by three passes through a French press at 1000 psi. Lysis supernatant was clarified by centrifugation and loaded to a Zn(II) affinity chromatography column [69] [68]. The fractions containing purified ApoE protein were dialyzed against 0.1% formic acid and lyophilized for use in mouse immunization.

Hybridoma production

Seven-week old female Balb/c mouse was immunized intraperitoneally (*i.p.*), intramuscularly and subcutaneously with 100 μg purified Tx_3-ApoE (50 mM imidazole elution fractions) mixed with an equal volume of Freund's complete adjuvant. At the 10th day, the mouse was given *i.p.* boost twice at one-day interval using the same amount of antigen diluted with phosphate buffered saline (PBS).

Cell fusion was carried out at the 13th day after the initial immunization using a

method previously described [71]. Briefly, the mouse was sacrificed to collect spleen after bleeding for obtaining the immune serum. This extensive bleeding also allows us to omit the lysis step for removing red blood cells before fusion. Spleen cells were isolated, washed with DMEM and spun down together with washed Sp2/0-MLK myeloma cells in a ratio of 8:1 and exposed to 0.6 mL of 50% PEG_{1500} (American Type Culture Collection) containing 7.5% dimethyl sulfoxide (DMSO) in Dulbecco's modified Eagle's medium (DMEM) at 37 °C for 2.5 min before being slowly diluted with 10 mL warm DMEM. After incubation for 10 min at 37 °C, the cells were spun down and gently resuspended in 80 mL HAT (0.1 mM hypoxanthine; 0.4 μM aminopterin; 16 μM thymidine) selection medium containing 20% fetal bovine serum (FBS) and plated in four 96-well cell culture plates. After incubation at 37 °C for 5 days, ~50μL of fresh HAT medium was added to each well. After 7 days, half of the medium in each well was replaced by HT media (0.1 mM hypoxanthine; 16 μM thymidine) containing 20% FBS.

Enzyme-linked immunosorbent assay (ELISA) and immunoblotting screening of positive hybridomas and limiting dilution subcloning

The hybridoma screening was carried out using indirect ELISA. 100 μL of the immunogen (Tx_3-ApoE fusion protein, 2 μg/ml) in carbonate buffer was coated on 96-well microtiter plate and incubated at 4 °C overnight. After washing to remove free protein, 100 μL of hybridoma culture supernatant was added at 37 °C and incubated for 2 h. Then the plate was washed and processed to incubate with horseradish peroxidase-conjugated anti-mouse immunoglobulin second antibody (Santa Cruz Biotechnology), and H_2O_2/2,2'-azinobis (3-ethylbenzothiazolinesulfonic acid) substrate reaction. Absorbance at 415 nm of each well was recorded at a series of time points during the substrate development using an automated microplate reader (Bio-Rad

Benchmark).

The positive colonies were confirmed with Western blotting. Briefly, Tx_3-ApoE fusion protein was resolved on 14% Laemmli gel with an acrylamide:bisacrylamide ratio of 180:1. The gel was electrically blotted to nitrocellulose membranes using a semidry transfer apparatus (Bio-Rad, Hercules, CA). The membranes were incubated with culture supernatant from ELISA positive hybridomas at 4 °C overnight. After washes, the membranes were incubated with alkaline phosphatase-conjugated anti-mouse IgG as second antibody (Santa Cruz Biotechnology, Inc., Santa Cruz, CA) at room temperature for 1 h, washed again and developed in 5-bromo-4-chloro-3-indolylphosphate/nitro blue tetrazolium substrate solution to visualize the protein bands.

The positive hybridomas were subcloned multiple times using limiting dilution method to obtain stable cell lines (9 times for 3C10 and 7 times for 3C11). The stable hybridoma cell lines were stored in liquid nitrogen in multiple vials and introduced into Pristane-primed peritoneal cavity of Balb/c mice to produce hybridoma ascites fluids that are enriched with the specific monoclonal antibodies. After centrifugation clarification to remove cell debrides, the monoclonal antibody ascites fluids were lyophilized for long term storage or made into 50% glycerol stock and stored at -20 °C for daily use.

Immunoglobulin isotyping of monoclonal antibodies

The subclass of immunoglobulins was determined using a Mouse Immunoglobulin Isotyping ELISA Kit (BD Pharmingen™). The wells of microtiter plate were coated 4 °C overnight with rat anti-mouseIgG_1, IgG_{2a}, IgG_{2b}, IgG_3, IgM, IgA, Igκ or Igγ purified monoclonal antibodies. Each hybridoma culture supernatant was then

added to one set of the isotype-specific anti-body coated wells for standard sandwich ELISA test. The results showed that 3C10 and 3C11 are both IgG1κ.

ELISA titration of monoclonal antibodies

For optimization of working dilution of monoclonal antibodies, affinity titration was performed. Purified chicken Tx-TnT protein was dissolved at 5 μg/mL and coated as the antigen on 96-well microtiter plate at 4 °C overnight. After washing to remove free protein, serial dilutions (1:10) of hybridoma culture supernatant or mouse ascites fluid were added and incubated at 37 °C for 2 h. The fresh culture medium or normal mouse serum at the same dilutions was used as negative control. Then the plate was processed with standard ELISA procedure as described above. The experiments were performed in triplicate wells.

Results

Mouse ApoE cDNA cloning and ApoE protein preparation

The agarose gel in Figure 7 shows Total RNA extracted from mouse brain and liver and *ApoE* cDNA amplified with RT-PCR. The *ApoE* RNA extracted from liver was used as template for subsequent reverse transcription. A band of ~1-kb in size was observed by PCR amplification of the RT product (the predicted size is 935-bp). Figure 8 shows a circular map of recombined pADED4-Tx_3 plasmid containing *ApoE* cDNA. Compared to the low expression level of ApoE alone in BL21-(DE3)pLysS *E. coli*, the expression efficiency of ApoE protein is dramatically increased with the N-terminal fusion of Tx_3 tag (Figure 9). Tx_3 tagged ApoE protein was purified using Zn (II) affinity chromatography (Figure 10). The Tx_3-ApoE fusion protein exhibits an elution peak at

50-60 mM imidazole.

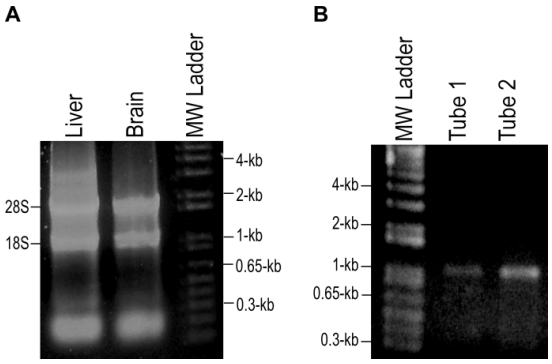

Figure 7. *ApoE* RNA extraction and cDNA amplification. A: Total RNA was extracted from mouse liver and brain tissue. Agarose gel depicted the two subunits of eukaryotic ribosomal RNA: 28S and 18S. B: PCR amplification of *ApoE* cDNA from mouse liver RNA. The agarose gel shows the specific ~1-kb product of *ApoE* cDNA.

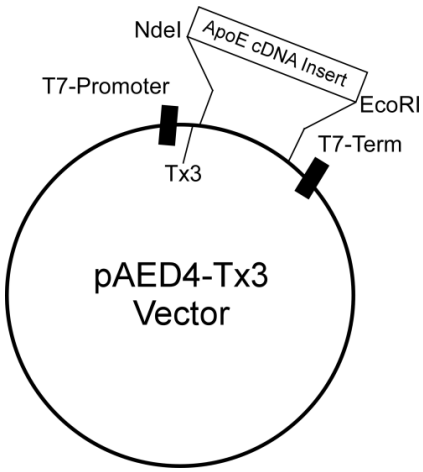

Figure 8. Map of recombined pADED4-Tx_3 vector and ApoE cDNA. *ApoE* cDNA was ligated into pAED4-Tx_3 vector with *Nde*I and *Eco*RI digested 5' and 3' sticky ends, respectively. The Tx_3 segment is incorporated at the NH_2-terminal of ApoE polypeptide. Protein expression is driven by the inducible T7 RNA polymerase.

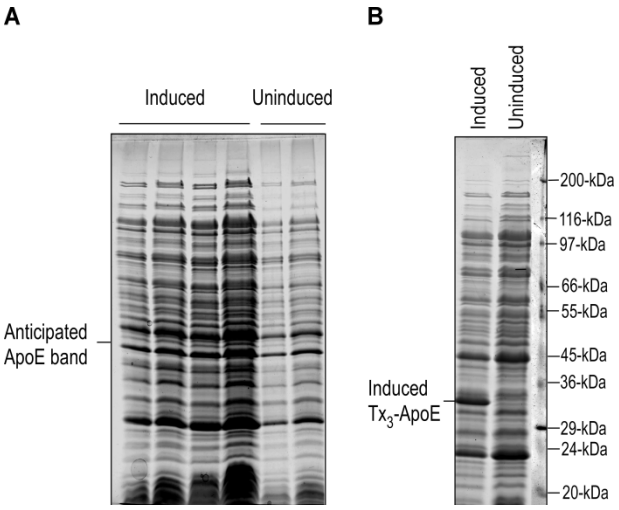

Figure 9. IPTG-induced expression of ApoE and Tx_3-tagged ApoE in BL21-(DE3) pLysS *E. coli*. A: SDS-PAGE examined protein expression after 3 h IPTG induction in ApoE pAED4 transformed BL21-(DE3) pLysS Ecoli. No free ApoE band was found in induced E.coli. B: SDS-PAGE with bacteria lysis from Tx_3-ApoE PAED4 plasmid transformed BL21-(DE3) pLysS Ecoli showed after incorporation of NH_2-terminal Tx_3 tag, the expression of Tx_3-ApoE was dramatically increased.

Titer of monoclonal antibodies 3C10 and 3C11

Serial dilutions (10^{-1}, 10^{-2}, 10^{-3}, 10^{-4} and 10^{-5}) of 3C10 and 3C11 hybridoma

culture supernatant were tested with indirect ELISA against chicken breast muscle Tx-TnT. For 3C11, 10^{-2} dilution maintained 90% of the maximal O.D., and 10^{-3} dropped to 35%. For 3C10, 10^{-2} dilution resulted in 70% of the maximal O.D. and 10^{-3} fell to 20% (Figure 11). Therefore, 3C11 demonstrated higher apparent affinity to chicken breast muscle Tx-TnT than does 3C10.

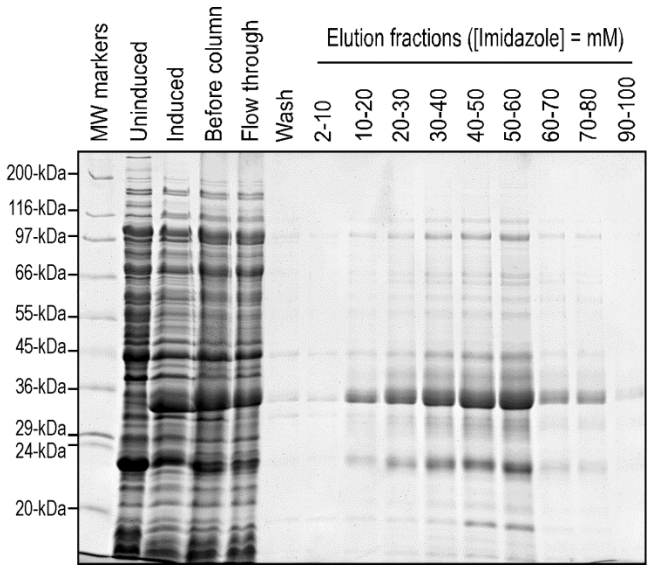

Figure 10. Zn(II) affinity column purification of Tx_3-ApoE. SDS-PAGE was performed to analyze the elution profile. Un-induced and IPTG-induced bacterial lysis were loaded as controls. Most un-bound proteins were washed out in the flow-through from the Zn(II) column. The affinity-bound protein was eluted with increasing concentrations of imidazole. The peak elution of Tx_3-ApoE is between imidazole concentrations of 50 mM and 60 mM.

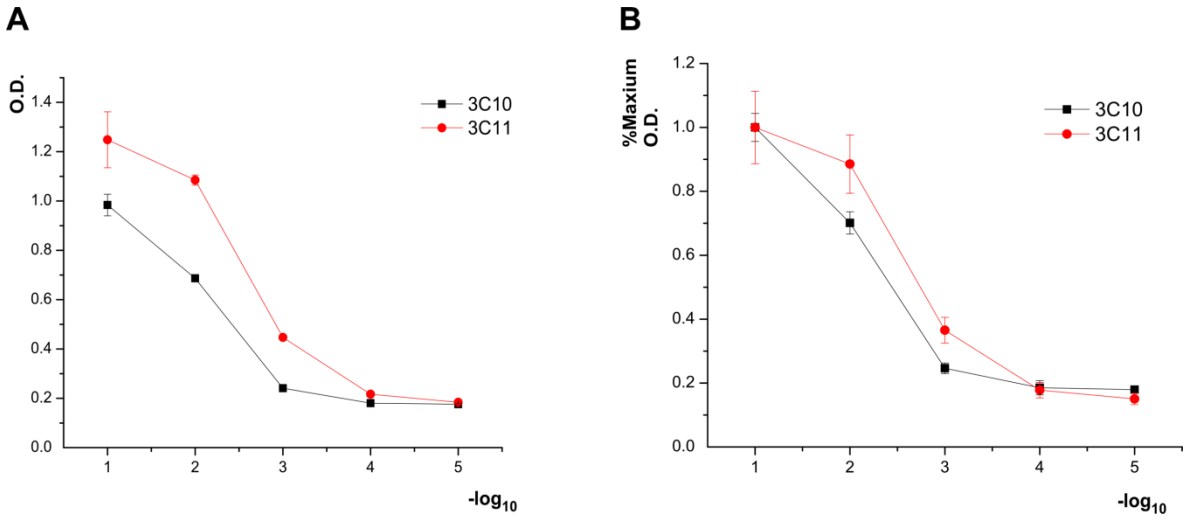

Figure 11. Comparison of ELISA titration curves of 3C10 and 3C11 hybridoma culture supernatants against chicken breast muscle Tx-TnT. The X-axis in both A and B is the series dilutions (10^{-1}, 10^{-2}, 10^{-3}, 10^{-4} and 10^{-5}) of 3C10 and 3C11 hybridoma supernatants in $-\log_{10}$ unit. The Y-axis in A is the absolute O.D. value at 20 min development and the Y-axis in B is the titration curves normalized to the maximal O.D. value of each antibody.

Specific monoclonal antibodies against the Tx epitope

3C10 and 3C11 hybridoma cells were introduced into Pristane-primed peritoneal cavity of Balb/c mice to produce hybridoma ascites fluids that are enriched with specific monoclonal antibodies. Figure 12 is a Western blotting characterization to demonstrate the specificity of monoclonal antibody 3C11 in recognizing the Tx tag on different fusion proteins and in chicken breast muscle fast Troponin T (Tx-TnT) that naturally contains the Tx segment. The results show that regardless the hosting environment of the Tx epitope, monoclonal antibody 3C11 effectively identified the Tx epitope specifically and with high affinity. Interestingly, at the same amounts of protein input as shown in the accompanying SDS gel Tx_9-GRP94 which contains 9 Tx repeats was recognized by 3C11 monoclonal antibody in much higher intensity than that of Tx_2-GRP94 containing only 2 Tx repeats in the Western blot under same conditions. The results indicate that the Tx9 tag contains multiple epitopes which can be simultaneously bound by multiple monoclonal antibody 3C11.

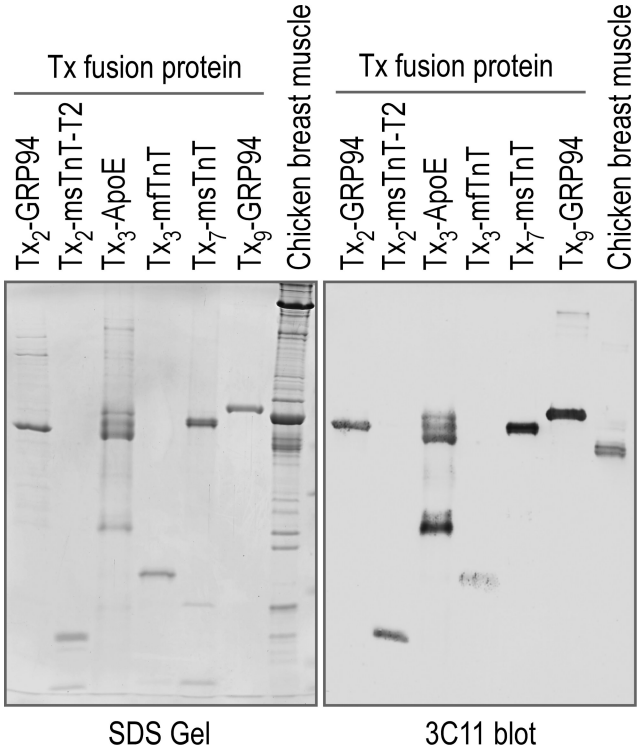

Figure 12. Western blotting using 3C11 ascites fluid against different Tx-fusion proteins and chicken breast muscle. Tx-fusion proteins Tx_2-GRP94, Tx_2-msTnT (mouse slow troponin T), Tx_3-ApoE, Tx_3-mfTnT, Tx7-msTnT (mouse fast troponin T), and Tx_9-GRP94 previously produced in our lab were used to examine the specificity of 3C11 monoclonal antibody. The SDS gel displays the loading of purified Tx-fusion proteins and total protein extracted from chicken breast muscle. The 3C11 Western blot demonstrates that regardless the fusion environment of Tx epitope, 3C11 monoclonal antibody can identify the Tx repeats specifically and with high affinity. The fast troponin T in chicken breast muscle contains 7 Tx repeats, which can also be recognized by 3C11.

Discussion

Monoclonal antibodies (mAbs) are important tools in basic science research as well as clinical diagnosis and therapy. From the time the first hybridoma monoclonal antibody was reported in 1975, the field of hybridoma technology has been rapidly advanced in producing mAbs with high specificity and affinity.

Antigen presenting and monoclonal antibody generation

Monoclonal antibodies are homogenous antibodies which bind to the same epitope and are produced from a single B-lymphocyte clone [72]. In the course of normal immune response, pathogens are recognized by the immune system as foreign (antigen), and eliminated or effectively neutralized to reduce their potential damage. After recognizing an antigen, antigen presenting cells (APCs) such as dendritic cells engulf and digest it in the lysosomes. Within the lysosome, the antigen is degraded into small peptides. The individual peptides are complexed with histocompatibility complex class II (MHC class II) and presented on the membrane surface of APCs. APCs present the processed antigen to a T helper cell ($CD4^+$), which later active B cell and induce B cell maturation and antibody production. Therefore, the structure of protein epitopes plays a critical role in antigen presenting and B cell activation and antibody production.

Immunogenicity of Tx segment and ApoE

Tx segment is defined as the 4-9 repeats of a sequence motif His-(Glu/Ala)-Glu-Ala-His specifically existed in the NH_2-terminal hypervariable region of troponin T (TnT) from avian pectoral muscle [73]. TnT is the tropomyosin (Tm) – binding subunit of the troponin complex and plays an essential role in the Ca^{2+} regulation of vertebrate striated

muscle contraction [74]. Three homologous genes encode cardiac and slow and fast skeletal muscle isoforms of TnT and alternative RNA splicing further produce multiple species and tissue-specific TnT splice forms with functional significance [75] [76] [77] [78]. An intriguing example is the presence of Tx-TnT (the repeating His pairs ([H-X-X-X-H]$_x$; designated Tx) at the NH_2-terminal hypervariable region of TnT in avian pectoral muscle [79] [80] [78]. It has been shown that the Tx segment is a cluster of transition metal ion (Zn^{2+}, Cu^{2+}, Ni^{2+} and Co^{2+}) binding site [81] and the inclusion of the Tx segment results in a more negative NH_2-terminal charge compared to other fast skeletal muscle TnTs [82] [83]. Acidic TnT isoforms is less sensitive to acidosis [84] and exhibits higher sensitivity to Ca^{2+} in the development of force [85], therefore the evolution of avian pectoral TnT and Tx element may reflect functional adaption of flight muscle [73].

Besides the physiological functions in avian breast muscle, Tx segment was found able to facilitate protein expression and purification due to its high metal-binding affinity. After incorporated with Tx segment at the N-terminal, ApoE protein also achieved higher level expression in *E. coli* and was effectively purified through Zn (II) affinity chromatography [69], (Figs. 8, 9 and 10). Therefore, Tx_3 peptides have been often used as a tag for protein expression and purification. In this study, it was found that Tx segment exhibits strong immunogenicity when fused with ApoE protein. Tx segment structure seems particularly recognizable by the immune system possibly due to its unique structure. However, the Tx segment is not strongly immunogenic by itself because of the small size. On the other hand, ApoE is a plasma lipoprotein and should be immunologically tolerated after *de novo* and chronic exposure to the immune cells. Therefore, our result is interesting by showing that ApoE possesses very weak

immunogenicity but served as an effective carrier to deliver the Tx epitope to elucidate immune responses.

Effective enhancement of immunogenicity of ApoE by a C-terminal segment of calponin 2

ApoE plays key roles in lipid transport and mediating cell lipid uptake through low-density lipoprotein receptor (LDLR). To carry out these two essential physiological functions, ApoE protein has a N terminal region able to interact with the LDLR [86] and a C-terminal domain of micromolar binding affinity to phospholipid [87] [88]. In the lipid-free state, ApoE is partially folded which gives ApoE flexibility and adaptability for the substantial conformational changes that accompany lipid or ligand binding [89] [90]. For example, upon binding of lipid, ApoE conformation undergoes a considerable change: Lipid-free ApoE does not bind with high affinity to LDLR. For high-affinity binding, ApoE must be associated with lipid [91]. The features of partially folding and structure flexibility provide the possibilities to expose different epitopes when ApoE was folded differently.

In an attempt to generate a fusion immunogen with enhanced immunogenicity, we fused the C-terminal tail 85 amino acid segment (C85) of calponin 2 that contains mainly acidic amino acids and also has very weak immunogenicity with ApoE. A hybridoma fusion trial showed that the combination of two very weak immunogens did not readily increase the immunogenicity of either of the two proteins. Therefore, the altering of folded structure alone may not be an effective approach in this development.

In summary, ApoE is the key protein involved in cholesterol transportation and metabolism. ApoE has a unique structure which allows lipids binding as well as the binding ability to LDLR. ApoE alone is not well expressed in *E. coli*, but adding the Tx

segment at the N-terminal of ApoE significantly increased the expression of Tx_3-ApoE fusion protein. When fused with Tx_3 peptides, ApoE serves as an exceptional carrier to present the Tx epitope to the immune system. This observation indicates that mouse immune system is able to recognize ApoE although is tolerated when one attempts to produce high affinity antibody as research tools. We are now in the process of testing immune response to mouse ApoE in *ApoE-/-* mice [105] in which the *de novo* deletion of ApoE expression should have prevented the development of immune tolerance. The effectiveness of this potentially novel approach to increasing immunogenicity of antigens and generating useful monoclonal antibodies remains to be evaluated.

CHAPTER 3 - DELETION OF CALPONIN 2 IN MACROPHAGES ALTERS CYTOSKELETON-BASED FUNCTIONS AND ATTENUATES THE DEVELOPMENT OF ATHEROSCLEROSIS

(Chapter contains previously published material. See Appendix C)

Abstract

Arterial atherosclerosis is an inflammatory disease. Macrophages play a major role in the pathogenesis and progression of atherosclerotic lesions. Modulation of macrophage function is a therapeutic target for the treatment of atherosclerosis. Calponin is an actin-filament-associated regulatory protein that inhibits the activity of myosin-ATPase and dynamics of the actin cytoskeleton. Encoded by the *Cnn2* gene, calponin isoform 2 is expressed at significant levels in macrophages. Deletion of calponin 2 increases macrophage migration and phagocytosis. In the present study, we investigated the effect of deletion of calponin 2 in macrophages on the pathogenesis and development of atherosclerosis. The results showed that macrophages isolated from *Cnn2* knockout mice ingested the same level of acetylated low-density lipoprotein (LDL) as that of wild type (WT) macrophages but the resulting foam cells had significantly less impaired velocity of migration. Systemic or myeloid cell-specific *Cnn2* knockouts effectively attenuated the development of arterial atherosclerosis lesions with less macrophage infiltration in apolipoprotein E knockout mice. Consistently, calponin 2-null macrophages produced less pro-inflammatory cytokines than that of WT macrophages, and the up-regulation of pro-inflammatory cytokines in foam cells was also attenuated by the deletion of calponin 2. Calponin 2-null macrophages and foam cells have significantly weakened cell adhesion, indicating a role of cytoskeleton regulation in macrophage functions and inflammatory responses, and a novel therapeutic target for the treatment of arterial atherosclerosis.

Introduction

Atherosclerosis is the primary cause of ischemic heart disease and stroke. In the past two decades, studies have established that atherosclerosis is an inflammatory disease [5] [6] [7]. Increasing levels of circulating low-density lipoprotein (LDL)-cholesterol and the subsequent intramural accumulation of oxidized LDL trigger the recruitment and retention of monocytes to generate subendothelial lesions in arterial wall [92]. In the intima of vessel wall, monocytes differentiate into macrophages to scavenge lipoprotein particles and become foam cells, which is a landmark of atherosclerosis [92]. Macrophages and the lipid ingestion-generated foam cells play active roles in mediating the ensuing inflammatory response and prognosis of atherosclerosis plaques [93]. Therefore, the regulation of macrophage activation and function has become a focus of the exploration of new therapeutic approaches for arterial atherosclerosis.

To date, the regulation of macrophage function in atherosclerosis and other inflammatory diseases has been investigated mainly in the context of ligand-receptor recognitions and the effects on cell signaling. While the motility and substrate adhesion of macrophages play essential roles in the development and resolution of inflammation [19] [20], very little is known about how the regulation and mechanisms by which these cytoskeleton mechanical tension-based functions determine the development and prognosis of atherosclerosis.

Calponin is a family of actin filament-associated regulatory proteins of 34–37 kDa (292–330 amino acids) in size found in smooth muscle [94] and many non-muscle cell types [29] [30]. Through high affinity binding to F-actin, calponin inhibits the actin-

activated myosin MgATPase [49] [50] [51] and motor activity [52] [53]. Three isoforms of calponin have been found in vertebrate species: A basic calponin (calponin 1, isoelectric point (pI) = 9.4) expresses specifically in mature smooth muscle cells and functions in regulating smooth muscle contractility [27, 55, 95, 62, 56]. An acidic calponin (calponin 3, pI = 5.2) is found in brain [35], embryonic trophoblasts [41] and myoblasts [40] to participate in cell fusion during embryonic development and myogenesis. Calponin 2 is an isoform with neutral overall charge (pI=7.5) and presents in a broad range of tissue and cell types, including smooth muscle cells [27], endothelial cells [31], epithelial cells, fibroblasts [29, 30], and myeloid leukocytes [1]. Via decreasing the dynamics and stabilizing the actin cytoskeleton, calponin 2 regulates many actin-cytoskeleton-based cellular functions such as increasing substrate adhesion and inhibiting migration and cytokinesis.

Calponin 2 is expressed at significant levels in macrophages. A previous study in our laboratory has demonstrated that calponin 2 regulates migration and phagocytosis of macrophages. Peritoneal macrophages isolated from *Cnn2* gene knockout (KO) mice exhibited a faster rate of migration and enhanced phagocytosis than that of wild type (WT) control cells, indicating a regulatory role of calponin 2 in the fundamental function of macrophages [1]. Following this novel discovery, the present study investigated the effect of deleting calponin 2 in macrophages on the pathogenesis and development of arterial atherosclerosis. Using cellular and *in vivo* mouse models, the experiments demonstrated that macrophages isolated from *Cnn2* KO mice ingest the same level of LDL as that of WT macrophages but the resulting foam cells had less impaired migration. Consistently, *Cnn2* KO in myeloid cells effectively attenuated the

development of arterial atherosclerosis lesions in apolipoprotein E knockout mice. Supporting the identification of calponin 2 as a novel therapeutic target, calponin 2-null macrophages produce less pro-inflammatory cytokines than that of WT macrophages, and the up-regulation of pro-inflammatory cytokines in foam cells was also attenuated by the deletion of calponin 2. Calponin 2 null macrophages exhibit a weakened adhesion to substrate, linking a cytoskeleton regulation to macrophage activity and inflammatory response.

Materials and Methods

Genetically modified mice

All animal studies were carried out under protocols approved by the Institutional Animal Care and Use Committee of Wayne State University.

The generation and initial characterization of *Cnn2*-floxed ($Cnn2^{f/f}$) mice and induction of systemic *Cnn2* KO have been described previously [1]. The colony of $Cnn2^{-/-}$ mice have been back breeding with wild type C57BL/6 mice for 9 or more generations, ensuring >99% C57BL/6 genetic background. Myeloid cell-specific *Cnn2* KO mice ($Cnn2^{f/f}$,$lysM^{cre+}$) were generated by cross-breeding $Cnn2^{f/f}$ mice with $lysM^{cre+}$ mice, a transgenic line bearing a Cre recombinase gene driven by *lys*M promoter [96] [64]. The effectiveness of lysM-Cre induced floxed-calponion 2 deletion in myeloid cells was assessed in the recent publication in our lab. In $Cnn2^{f/f}$,$lysM^{cre+}$ mice, calponin 2 is undetectable by immunoblotting in macrophages but unaffected in the skin tissue (a representative control tissue) [64]. Apolipoprotein E (*ApoE*) gene KO mice [97] (C57BL/6 strain) were purchased from TACONIC. $ApoE^{-/-}$,$Cnn2^{-/-}$ double homozygotes and $ApoE^{-/-}$,$Cnn2^{f/f}$,$lysM^{cre+}$ triple transgenic mice were produced by crossing $ApoE^{-/-}$

with *Cnn2*$^{-/-}$ and *Cnn2*$^{f/f}$,*lysM*^{cre} lines, respectively. Genotypes of these experimental mice were confirmed using PCR and verified post mortem using Western blot analysis.

Preparation and culture of mouse macrophages

Residential peritoneal macrophages were lavaged with pre-warmed RPMI 1640 medium from WT and *Cnn2*$^{-/-}$ mice. Elicited mouse peritoneal macrophages were obtained by injection of 2 mL of sterile 3% thioglycollate broth for 72 h prior to lavage. A fixed volume (8 mL) of medium was used for each animal so the total number of cells lavaged could be compared. The cells collected were cultured in RPMI-1640 medium containing 10% fetal bovine serum (FBS), 2 mM L-glutamine, 100 i.u./mL penicillin and 50 i.u./mL streptomycin at 37°C in 5% CO_2 unless specified.

Macrophage lipid engulfment

Residential peritoneal macrophages were isolated from WT and *Cnn2*$^{-/-}$ mice as above and seeded onto pre-cleaned coverslips in a 48-well culture plate in RPMI 1640 medium containing 10% FBS. Cells were allowed to adhere to the coverslips at 37°C overnight. Non-adherent cells were removed by gentle washing with pre-warmed RPMI 1640 medium. The adherent macrophages were processed for experiments as described [98]. To load the macrophages with lipid, the culture medium was switched to RPMI 1640 containing 10% FBS and 25 μg/mL acetylated LDL (BT-906, Alfa Aesar). The cells on coverslips were fixed at 4 hrs, 8 hrs and 24 hrs of lipid loading and the formation of lipid laden foam cells was examined by staining the intracellular lipid droplets with 60% Oil Red O (O0625, Sigma-Aldrich) in isopropanol at room temperature for 5 minutes. Cell nucleus was counter-stained with Mayer's hematoxylin (26043-06, Sigma-Aldrich) for 5 min. The stained coverslips were mounted on glass

slides and photographed using a Zeiss Axiovert 100 microscope. The formation of foam cells was quantified in at least 10 representative view fields in different areas of each coverslip using ImageJ 64 software (NIH, Bethesda, MD). The assay was performed in a genotype-blinded manner.

SDS-polyacrylamide gel electrophoresis (PAGE) and Western blotting

SDS-PAGE and Western blotting were carried out as previously described [1]. Samples of fresh or cultured macrophages were washed with phosphate-buffered saline (PBS) and lysed in SDS-PAGE sample buffer containing 2% SDS. Total protein was extracted by sonication and heated at 80°C for 5 min. *Urinary bladder tissues were examined to verify genotypes* and the SDS-PAGE samples were prepared similarly, in which the extraction of protein was done by mechanical homogenization.

The protein extracts were analyzed using 12% gel in Laemmli buffer system with an acrylamide: bisacrylamide ratio of 29:1. After electrophoresis, the gels were fixed and stained with Coomassie Blue R-250 to verify sample integrity and normalize protein input. Duplicated gels were electrically blotted on nitrocellulose membrane using a Bio-Rad semi-dry transfer apparatus for Western blot analysis. The membrane was incubated with a rabbit antiserum, RAH2, which was raised against mouse calponin 2 immunogen and has weaker cross-reaction to calponin 1 [95] or a mouse anti-calponin 1 monoclonal antibody (mAb) CP1 [26] in Tris-buffered saline containing 0.1% bovine serum albumin (BSA). The calponin bands recognized by the first antibody were revealed using alkaline phosphatase-labeled anti-rabbit IgG or anti-mouse IgG second antibody (Santa Cruz Biotechnology) and 5-bromo-4-chloro-3-indolyl phosphate/nitro blue tetrazolium chromogenic substrate reaction.

In vitro wound healing assay

Elicited mouse peritoneal macrophages were seeded in glass-bottom dishes (P35G-0-14-C, MatTek) at $1.5x10^6$ per microwell for adhesion at high-density. Foam cells were produced by incubating the adhered macrophages with 50 μg/mL acetylated LDL for 24 hours. The monolayers of confluent macrophages and foam cells were wounded by scratching using a thin pipette tip. Care was taken to produce uniformly sized wounds of approximately 300 μm in width. The detached cells were washed away with culture medium containing 10% FBS.

The scratch-wounded monolayer cultures were incubated in 5% CO_2 at 37°C in a stage top incubator (Model TC-124A, Warner Instruments) mounted on an inverted microscope (Zeiss Axiovert 100, Germany). Closure of the wound was monitored using an attached digital camera (AmScope). The wound area of each recorded field was measured using ImageJ64 MRI wound healing and ROI tools (NIH, Bethesda, MD). The assay was performed in a genotype-blinded manner.

Examination and quantification of aortic atherosclerotic lesions

6.5-month-old male and female mice were studied. Lesion development in the aortae was determined using the *en face* method [99]. The entire aorta was removed, cleaned for periadventitial fat and carefully cut open longitudinally. The opened aorta was then pinned on a dark color board and stained with 60% Oil Red O at room temperature for 50 minutes. The aorta tissue was examined under a dissection scope and photographed. The images were analysis with ImageJ64 software. The area examined covered both thoracic and abdominal regions defined as the segment from 0.8 mm before the branch point of the innominate artery to the iliac bifurcation, including

0.5 mm of the large branching vessels at the aortic arch.

Atherosclerosis lesion at the aortic root was studied in tissue cross-sections. Briefly, the base of the heart including the most proximal part of the ascending aorta was excised and embedded in O.C.T. compound (Tissue-Tek, 4583). The tissue piece was oriented to have all three aortic valves in the same geometric plane. The portion containing the aortic root was cut consecutively into 8 μm sections, starting from the commissures of the aortic cusps, using a Leica CM 1950 cryostat. Sections were collected on Fisher Superfrost Plus-coated slides following a scheme similar to that described previously [100], processed for Oil Red O, hematoxylin, and eosin stain after fixation in 3.7% formaldehyde. The slides were imaged and the aortic root lesion area was determined using ImageJ64 software.

Immunohistochemistry

Aortic root sections were fixed in 75% acetone with 25% ethanol for 10 min and blocked in PBS containing 0.05% Tween-20 and 1% BSA at room temperature for 30 min. Endogenous peroxidase was inactivated by incubation with 1% H_2O_2 in PBS at room temperature for 10 min. After wash with PBS, the sections were stained with a rat mAb against mouse CD68 (Bio-Rad MCA 1957) or normal rat serum control at room temperature for 2 hrs. After washing with PBS-Tween-20 to remove excess primary antibody, the sections were incubated with horseradish peroxidase-conjugated anti-rat secondary antibody (SouthernBiotech, 3050-05) at room temperature for 1 hr. Washed with PBS-Tween-20 again to remove excess secondary antibody, the labeling of CD68 was visualized via 3,3'-diaminobenzidine-H_2O_2 substrate reaction in a dark box for 1 min. The reaction was stopped by repeating washes with 20 mM Tris-HCl, pH 7.6.

Nuclei were then counterstained with Hematoxylin. Slides were mounted with cover slips and imaged. The areas of macrophage infiltration were determined using ImageJ64 software.

Multiplexed cytokine analysis

Peritoneal residential macrophages were isolated from WT and *Cnn2*$^{-/-}$ mice as above and seeded in 24-well plates at 2x10^6 per well in RPMI 1640 medium containing 10% FBS. The adherent cells were cultured at 37°C in RPMI 1640 medium containing 10% FBS. Foam cells were produced by replacing the culture medium with RPMI 1640 containing 10% FBS and 100 μg/ml acetylated LDL. After 48 hrs of culture, the cells were gently washed twice with PBS and total protein contents were extracted with a lysis buffer containing 50 mM Tris-HCl, 150 mM NaCl, 0.5% *IGEPAL CA-630 (Sigma I3021)*, 1 mM EDTA and protease inhibitor cocktail (13911, Sigma-Aldrich). After sitting on ice for 20 min, the cell lysates were transferred to centrifuge tubes and centrifuged in a microcentrifuge at 14,000 rpm, 4°C for 10 min. The clarified supernatant was collected and stored at -80°C. Cytokine/chemokine levels in the samples were quantified using bead-based multiplex immunoassays at a commercial service facility (Eve Technologies). The results were normalized to the level of total protein determined using SDS-PAGE densitometry.

Cell adhesion assay

Freshly isolated peritoneal residential cells from WT and *Cnn2*$^{-/-}$ mice were seeded in multiple 12-well plates at the density of 2.5x10^5 cells per well in 500 μl RPMI-1640 medium containing 10% FBS. The WT and *Cnn2*$^{-/-}$ cells were seeded on the same plate to ensure parallel washing conditions. At a series of time points, non-

adherent cells were removed by gentle washing with pre-warmed RPMI-1640 medium for three times. The adherent cells were then fixed immediately in the wells with 1% glutaraldehyde for 30 min. A seeding control plate of cells was fixed directly without washing by adding 50 μl 11% glutaraldehyde into each well (for a final concentration of glutaraldehyde of 1%).

The fixed plates were washed three times by submersion in deionized water, air-dried, and stained by adding 500 μL of 0.1% Crystal Violet in 20 mM MES buffer, pH 6.0. After shaking at room temperature for 20 min, the plates were washed with deionized water to remove excess crystal violet dye and air-dried prior to solubilizing the bound dye in 120 μL of 10% acetic acid. 100 μL of the dye extract was transferred from each well to a 96-well plate for quantification [101]. $A_{595\,nm}$ values were measured with a reference wavelength of 655 nm using a Bio-Rad Benchmark automated microplate reader. The experiments were done in triplicate wells and repeated.

Isolation and culture of mouse skin fibroblasts

Fibroblasts were isolated as described previously from the back skin of neonatal WT and *Cnn2*$^{-/-}$ mice [102]. Briefly, 3-4 days old mice were euthanized and soaked in 70% ethanol for 2 minutes before removing the skin around torso under sterile condition. In a 35 mm culture dish, the skin was incubated with 0.5% trypsin (9002-07-7 GIBCO) in DMEM at 37°C for 1 hr. After washing with DMEM, the tissue was minced into fine pieces using a sharp razor for digestion in 2 mL of 700 U/mL collagenase I (M3A14008A Worthington) in DMEM at 37°C for 2 hrs in a 15 mL centrifuge tube with agitation every 20 minutes by gentle shaking. 2 mL ice-cold DMEM containing 20% FBS was then added and the tube was vortex 5 seconds for 5 times. The tissue

suspension was pipetted up and down several times and the isolated cells were passed through a 100 μm nylon mesh. The cells were collected by centrifugation at 150 x g for 5 minutes and re-suspend in 8 mL DMEM containing 20% FBS for culture at 37°C in 5% CO_2. Soon after becoming confluent, the P_0 cells from each mouse were expanded into four 100 mm dishes to prepare 8-10 vials of frozen stock of P_1 cells (0.5 to 1 million cells per vial). Urinary bladder of each mouse was examined using Western blot as above to verify the $Cnn2^{-/-}$ and WT genotypes. The frozen cells were stored in liquid nitrogen before being thawed and passed one more time (P_2) for experiments.

Immunofluorescence microscopy

Mouse skin fibroblasts and peritoneal macrophages were cultured on pre-cleaned glass coverslips. After adherent culture for 24 hrs, pre-confluent cells on the coverslips were fixed with cold acetone or 4% paraformaldehyde for 15 min. After blocking with 1% BSA in PBS at room temperature for 30 min (paraformaldehyde fixed cover slips were penetrated with 0.5% Triton X-100 for 10 min prior to blocking), the coverslips were incubated with anti-calponin 2 mAb 1D11 [30], anti-calponin 2 rabbit polyclonal Ab RAH2 [95], anti-tropomyosin mAb CG3 [103], anti-paxillin mAb 5H11 (EMD Millipore 05-417), and an anti-non-muscle myosin IIA rabbit polyclonal Ab (Abcam, ab24762) at 4°C overnight. After washes with PBS containing 0.05% Tween-20, the coverslips were stained with corresponded secondary antibodies: Fluorescein isothiocyanate (FITC)-conjugated goat anti-mouse IgG (Sigma, F1010), FITC-conjugated sheep anti-rabbit IgG (Sigma, F7512), tetramethylrhodamine isothiocyanate (TRITC)-conjugated goat anti-rabbit IgG (Sigma, T6778) and TRITC-conjugated phalloidin (Sigma P1951) (for actin filaments) at room temperature for 1 hr. After final

washes with PBS containing 0.05% Tween-20, the coverslips were mounted on glass slides and examined using fluorescence confocal microscopy for the cellular localizations of calponin 2 in macrophages and fibroblasts in relationship to the other cytoskeleton proteins.

Data analysis

All quantitative data are presented as mean ± SEM. Statistical analysis was done with Student's test or two-way ANOVA using the Origin software (two-tailed assays unless noted in the figure legend).

Results

Cnn2$^{-/-}$ macrophages retain the ability of lipid uptake

Our previous studies demonstrated that *Cnn2*$^{-/-}$ macrophages have enhanced phagocytotic activity, which was assessed by the uptake of mouse serum-coated fluorescent latex beads [1]. Different from the non-specific phagocytosis of beads, the uptake of lipid complex by macrophages is a scavenger receptor-mediated engulfment, and also related to the intracellular cholesterol metabolism in macrophages. Therefore, here we first examined whether deletion of calponin 2 affects the lipid uptake ability of macrophages. Peritoneal residential macrophages from *Cnn2*$^{-/-}$ and WT mice were studies and the formation of foam cells were examined after 4, 8 and 24 hrs of incubation with acetylated LDL. The results showed that intracellular lipid droplets were significantly increased during the course of incubation in both WT and *Cnn2*$^{-/-}$ groups. No difference was detected at any of the time points studied (Figure 13).

Deletion of calponin 2 compensates for the impaired motility of lipid-laden foam cells

The intrinsic motility of calponin 2-null macrophages and foam cells were

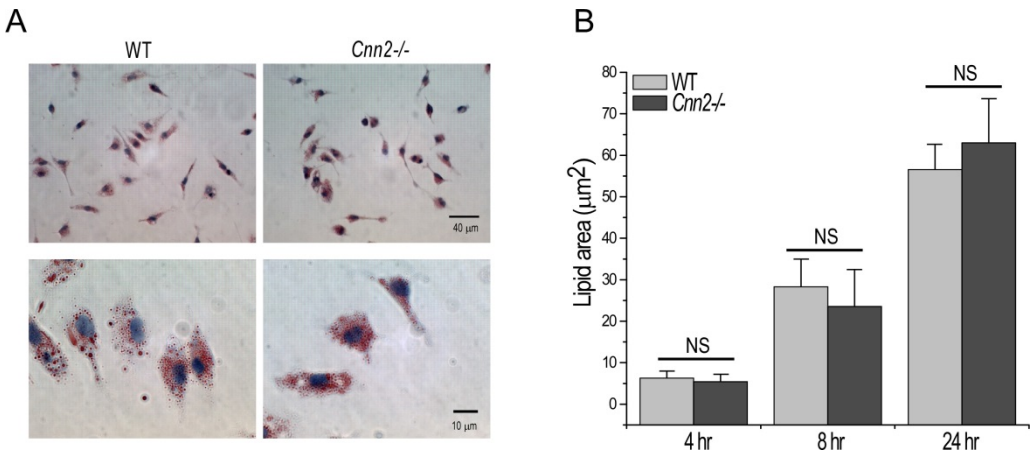

Figure 13. *Cnn2*$^{-/-}$ macrophages retained the ability of lipid engulfment and formation of foam cells. Peritoneal residential macrophages isolated from WT and *Cnn2*$^{-/-}$ mice were cultured on cover slips and incubated with 25 μg/ml acetylated LDL for 4, 8 and 24 hrs. Intracellular lipid droplets were stained with Oil Red O. A. Representative low (upper panels) and high (lower panels) magnification images at 24 of hrs incubation with LDL. B. Quantitative measurements during the incubation with LDL. The results showed that the area and intensity of lipid droplets were significantly increased during the course of LDL incubation but no significant difference (NS) was detected between WT and *Cnn2*$^{-/-}$ groups (n=3 mice for each group).

investigated in the absence of chemotactic stimulation. *In vitro* wound healing assay in monolayer cell cultures was used for measuring the rate of two-dimensional cell migration. To obtain confluent monolayer cultures, elicited peritoneal macrophages were used in the assay. The SDS-gel and Western blots in Figure 14A demonstrated similar levels of calponin 2 expressed in residential and elicited mouse peritoneal macrophages. Figure 14B further shows the effective lipid loading in the production of foam cells for use in the wound healing assays.

The wound healing studies showed a significantly faster closure of the scratch wound in *Cnn2*$^{-/-}$ macrophages versus the wild type control (Figure 15A). The migration velocity of WT and *Cnn2*$^{-/-}$ foam cells was both significantly hindered as compared to that of the genotype-matched macrophages. However, the migration velocity of WT foam cells was hindered significantly more than that of *Cnn2*$^{-/-}$ foam cells. As a

consequence, *Cnn2*$^{-/-}$ foam cells moved even faster than that of WT macrophages (Figure 15B).

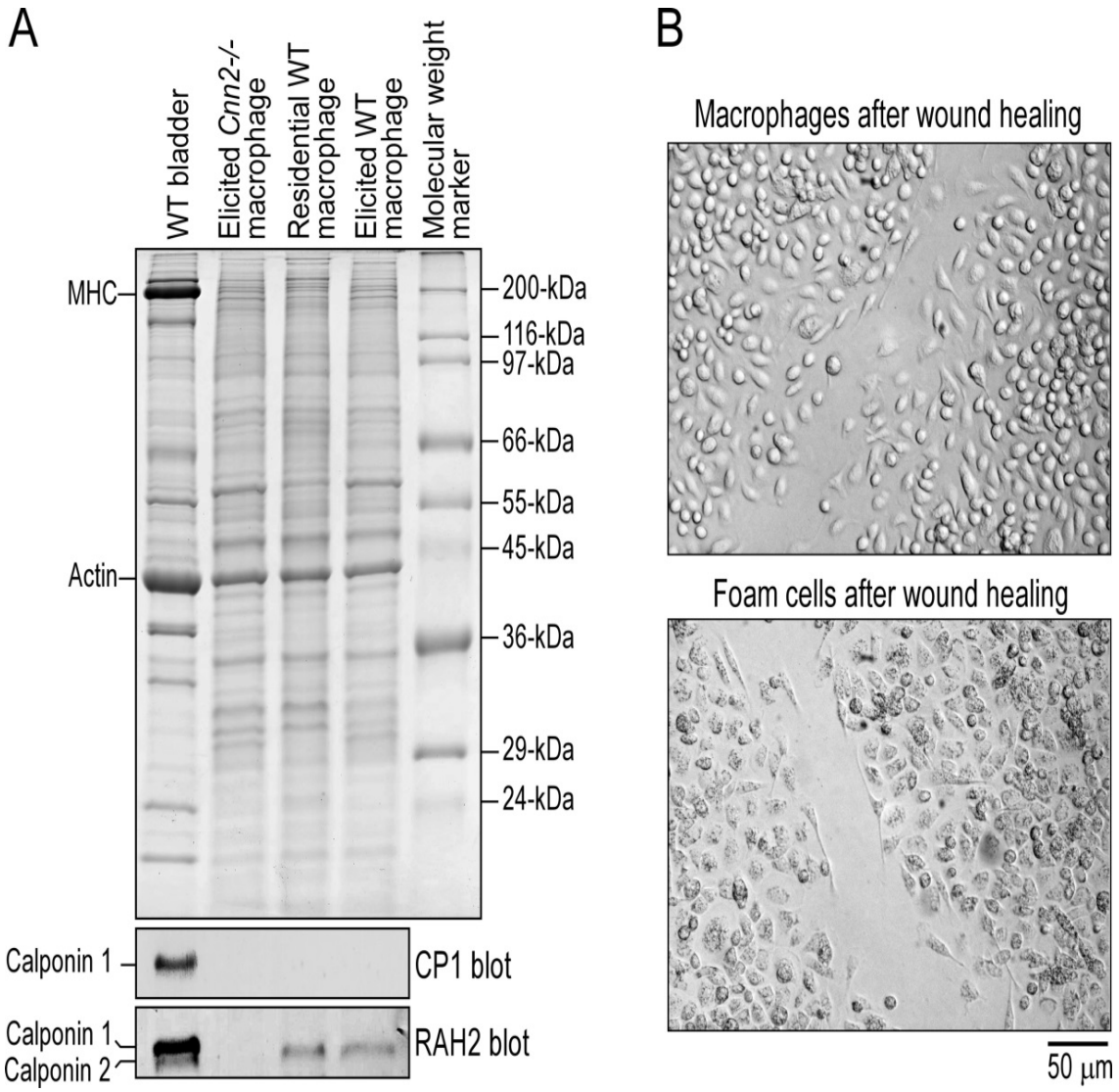

Figure 14. Similar levels of calponin 2 expression in residential and elicited mouse peritoneal macrophages and effective lipid loading to produce foam cells. SDS-PAGE and Western blots using mAb CP1 specifically against calponin 1 and polyclonal antibody RAH2 raised against calponin 2 showed similar levels of calponin 2 in residential and elicited mouse peritoneal macrophages. Wild type mouse urinary bladder that expresses both calponin 1 and calponin 2 was used as a positive control and *Cnn2*$^{-/-}$ macrophages as a negative control. No calponin 1 is detected in residential or elicited mouse peritoneal macrophages. B. The images *show a WT example for LDL-treatment in culture to effectively transform all macrophages into foam cells (Figure 13 showed that there is no difference in lipid ingestion between WT and Cnn2*$^{-/-}$ *macrophages)*, justifying their use in wound healing studies.

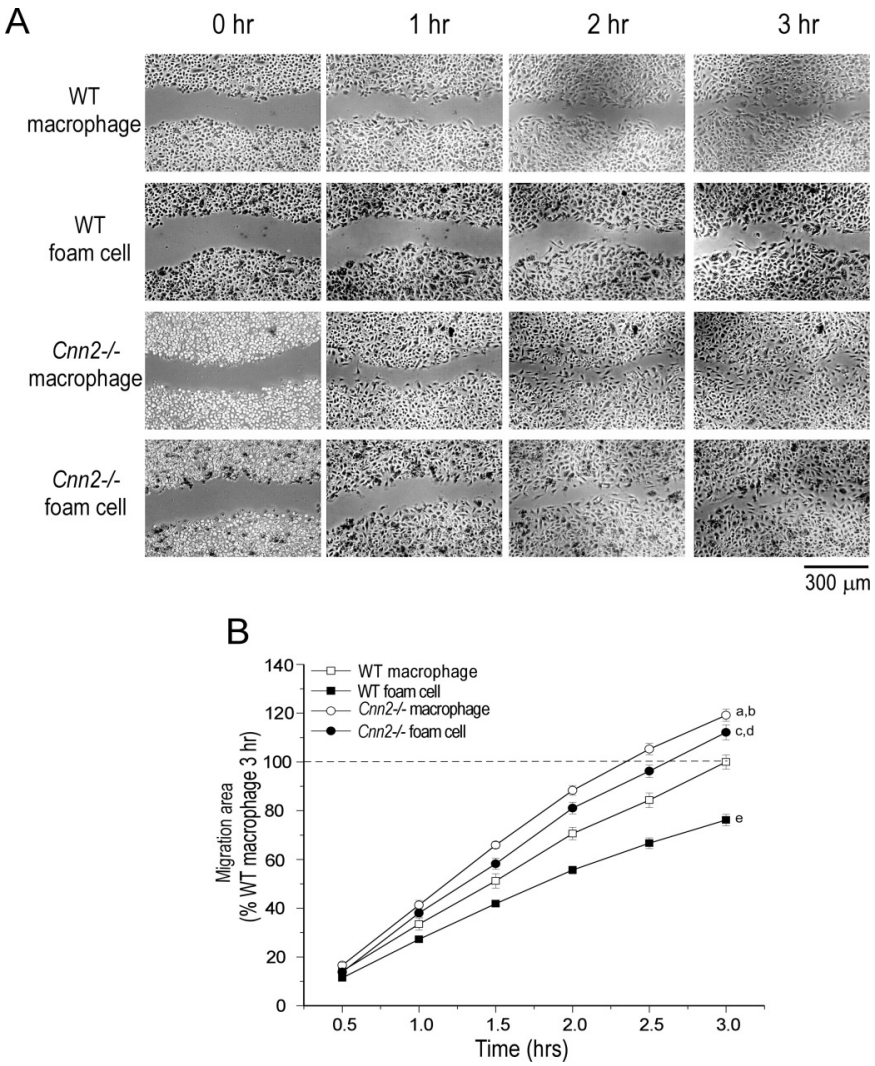

Figure 15. Faster migration of calponin 2-null macrophages than that of WT macrophages, compensating for the impaired migration of foam cells. Scratch wounds were made in monolayer cultures of mouse macrophages and foam cells. Healing of the wound by cell migration was monitored for 3 hrs. The micrographs (A) and densitometry quantification of the wound area (B) showed a faster closure of the wound in the *Cnn2*$^{-/-}$ macrophage culture than that of WT macrophage control. The migration velocity was hindered in both WT and *Cnn2*$^{-/-}$ foam cells as compared to that of genotype-matched macrophages, which was, however, significantly compensated in *Cnn2*$^{-/-}$ foam cells. Values are presented as Mean ± SEM. n equal to the experimental repeats (the number of wounds studied in each of the Cnn2-/- and WT groups). ^{a}P<0.05, Cnn2$^{-/-}$ macrophage vs. WT macrophage; ^{b}P<0.05, Cnn2$^{-/-}$ macrophage vs. Cnn2$^{-/-}$ foam cell; ^{c}P<0.05, Cnn2$^{-/-}$ foam cell vs. WT foam cell; ^{d}P<0.05, Cnn2$^{-/-}$ foam cell vs. WT macrophage; ^{e}P<0.05 WT foam cell vs. WT macrophage. Statistical analysis was performed using two-way ANOVA with mean comparison using Tukey test.

Deletion of calponin 2 attenuated the development of atherosclerosis in ApoE$^{-/-}$ *mice*

Apolipoprotein E (ApoE) is present on the surface of several lipoproteins and plays an important role in cholesterol transportation and metabolism. ApoE deficiency

in mice leads to hyperlipidemia and spontaneous atherosclerosis even when fed with a normal diet [104]. To focus our study on the effect of calponin 2 deletion on the function of macrophages in the pathogenesis of atherosclerosis under a relatively more physiological condition, ApoE$^{-/-}$ mice fed on a normal chow diet was used as the atherosclerosis model. *Apo*E$^{-/-}$; *Apo*E$^{-/-}$,*Cnn2*$^{-/-}$ double KO and *ApoE*$^{-/-}$,*Cnn2*$^{f/f}$,*lysM*$^{cre+}$ myeloid-specific *Cnn2* KO mice *were studied* at 6.5 month of age to examine aortic atherosclerotic lesions. A possible gender difference in the development of atherosclerosis in *Apo*E$^{-/-}$ mice has been suggested [105, 106] [107] [108]. Therefore, data of both male and female were collected in our study to consider gender-based variation. The aorta *en face* method was employed and atherosclerotic lesions were quantified.

While no difference was detected in the levels of total serum cholesterol between *ApoE*$^{-/-}$ and *ApoE*$^{-/-}$,*Cnn2*$^{-/-}$ groups (data not shown), the results in Figure 16 showed that in male mice, the area of *Apo*E deficiency-caused atherosclerotic plaques was reduced by *56.2%* with global deletion of calponin 2 and by *91.9%* with myeloid cell-specific deletion of calponin 2. In females, *ApoE*$^{-/-}$,*Cnn2*$^{-/-}$ and *ApoE*$^{-/-}$,*Cnn2*$^{f/f}$,*lysM*$^{cre+}$ mice also showed significantly reduced plaque areas (*51.9%* and *50.3%* less as compared with that in *ApoE*$^{-/-}$ controls, respectively). The fact that myeloid cell-specific KO of *Cnn2* has the same or stronger effect in comparison with that of global KO indicates that the therapeutic effect was primarily via the function of myeloid cells. This result is consistent with another finding in our lab that myeloid cell-specific Cnn2 knockouts have stronger effects on attenuating inflammatory arthritis than that in global Cnn2 knockouts [64]. These data indicate that loss of calponin 2 in some other cell

types may counteract the effect of calponin 2 deletion in myeloid cells on attenuating and resolution of inflammation. We further examined the atherosclerotic lesions at aortic roots of male *ApoE*$^{-/-}$,*Cnn2*$^{f/f}$,*lysM*$^{cre+}$ mice and *ApoE*$^{-/-}$ controls. The results in Figure 17 showed significantly less total lesion area and macrophage content in *ApoE*$^{-/-}$, *Cnn2*$^{f/f}$,*lysM*$^{cre+}$ mice.

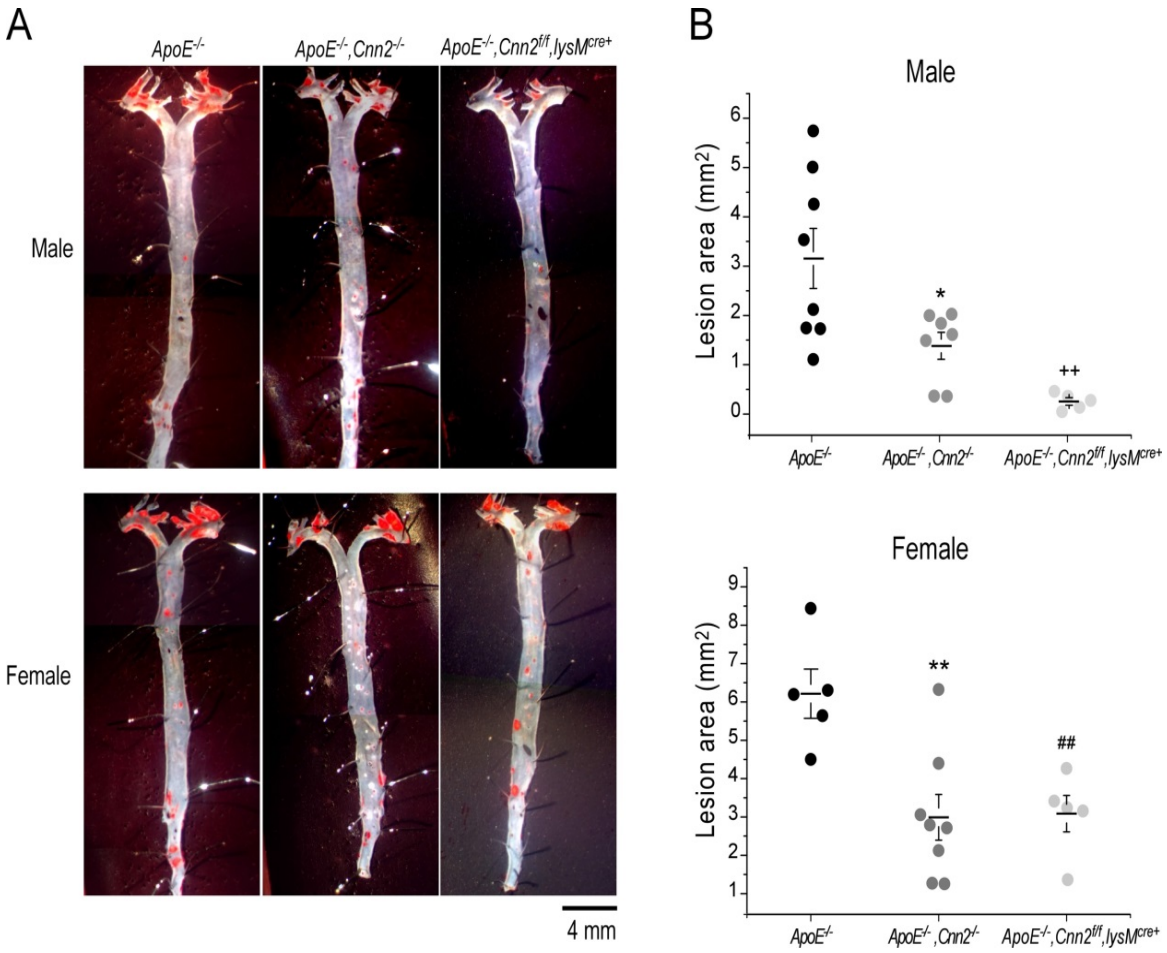

Figure 16. Atherosclerotic lesions in aorta *en face* of 6.5-month-old *ApoE*$^{-/-}$ *ApoE*$^{-/-}$, *Cnn2*$^{-/-}$ and *ApoE*$^{-/-}$, *Cnn2*$^{f/f}$, *lysM*$^{cre+}$ mice fed on standard chow diet. A. Representative Oil Red O staining of *en face* aorta. The results showed that *ApoE*$^{-/-}$,*Cnn2*$^{-/-}$ and *ApoE*$^{-/-}$,*Cnn2*$^{f/f}$, *lysM*$^{cre+}$ mice had significantly attenuated atherosclerotic lesions compared to that of the age- and sex-matched *ApoE*$^{-/-}$ mice. B. Lesion quantification of Oil Red O staining of *en face* aorta. **P*<0.05, *ApoE*$^{-/-}$,*Cnn2*$^{-/-}$ *vs. ApoE*$^{-/-}$; $^{\#}$*P*<0.05, *ApoE*$^{-/-}$,*Cnn2*$^{f/f}$,*lysM*$^{cre+}$ *vs. ApoE*$^{-/-}$; ***P*<0.01, *ApoE*$^{-/-}$,*Cnn2*$^{-/-}$ *vs. ApoE*$^{-/-}$; $^{\#\#}$*P*<0.01, *ApoE*$^{-/-}$,*Cnn2*$^{f/f}$,*lysM*$^{cre+}$ *vs. ApoE*$^{-/-}$.

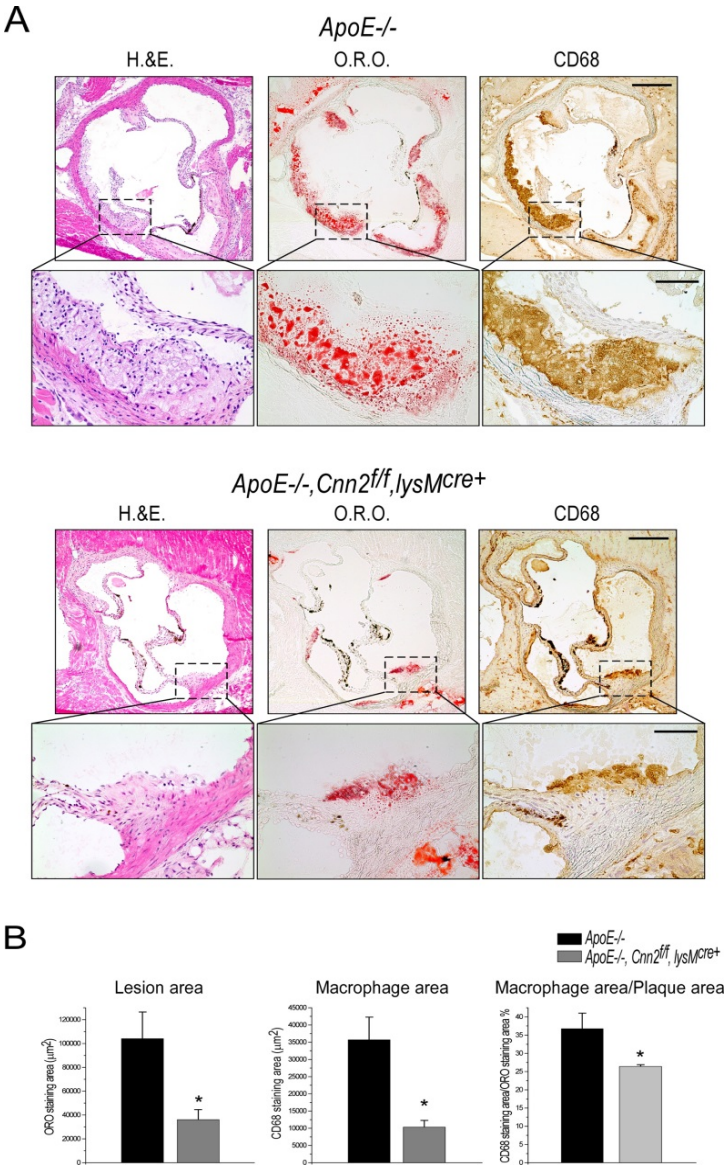

Figure 17. Atherosclerotic lesions in aortic root of 6.5-month-old ApoE$^{-/-}$ and ApoE$^{-/-}$, Cnn2$^{f/f}$, lysM^{cre+} mice fed on standard chow diet. A. Representative images of aortic sinus sections. Lesion morphology and lipid contents were evaluated with H & E and Oil Red O staining. Macrophage infiltration was detected via immunohistochemical staining for macrophage marker CD68. B. Quantification analysis of the lipid content and macrophage infiltration. The results showed that ApoE$^{-/-}$,Cnn2$^{f/f}$,lysM^{cre+} aortae had significantly attenuated atherosclerotic lesion and macrophage infiltration compared to that of age- and sex-matched ApoE$^{-/-}$ mice. *P<0.05.

It was reported that endogenous estrogen plays an atheroprotective role in female mice [109]. However, there are also data indicating that the lesions in *ApoE*$^{-/-}$ mice were severer in females [110] [108]. Our present study showed severer lesion development in female *ApoE*$^{-/-}$ mice and a likely more effective attenuation of atherosclerosis by calponin 2 deletion in male mice (Figure 16B). The significance of this observation merits investigation in future studies.

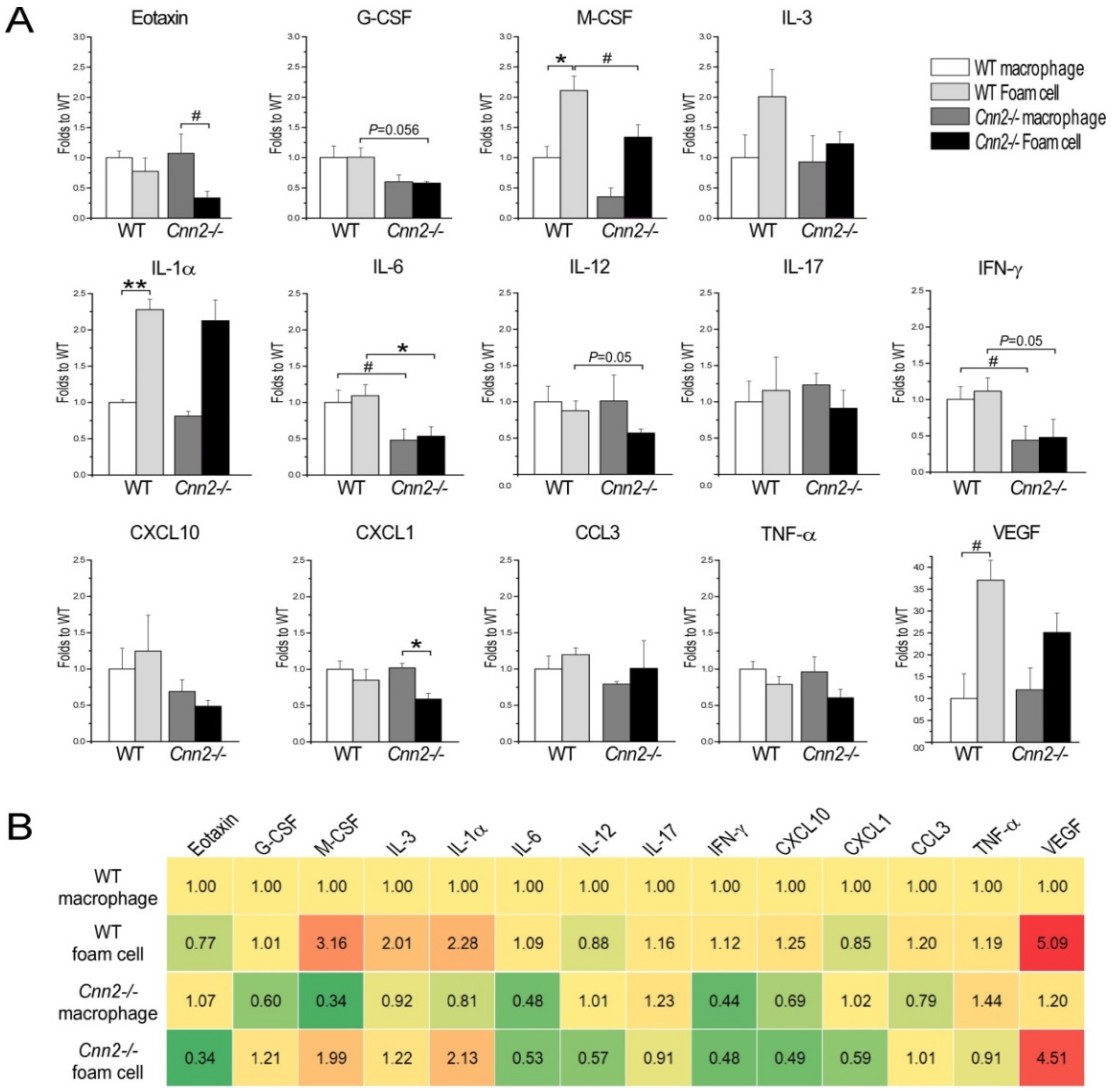

Figure 18. Cytokine production in WT and *Cnn2*$^{-/-}$ macrophages and foam cells. A. Levels of representative cytokines in WT and *Cnn2*$^{-/-}$ macrophages and foam cells. Values are presented as mean ± SEM (n=3 mice each for WT and *Cnn2*$^{-/-}$ groups). **P*<0.05, ***P*<0.01 (both two-tail *t*-test), and $^{\#}$*P*<0.05 (one-tail *t*-test). B. The heat map summarizes that WT foam cells had increases in cytokines associated with monocytosis (M-CSF and IL-3) and inflammation (IL-1α and VEGF) as compared with that of untreated WT macrophages. Untreated *Cnn2*$^{-/-}$ macrophages have decreased baseline levels of cytokines associated with monocytosis (G-CSF and M-CSF) and inflammation (IL-6, IFN-γ and CXCL10) in comparison with that of untreated WT macrophages. *Cnn2*$^{-/-}$ foam cells also had significantly lower levels of cytokines associated with monocytosis (Eotaxin, G-CSF, M-CSF and IL-3) and inflammation (IL-6, IL-12, IFN-γ, CXCL10, CXCL1, TNF-α and VEGF) is comparison with that of WT foam cells.

Deletion of calponin 2 alters cytokine productions of macrophages and foam cells

Cnn2$^{-/-}$ and WT mouse macrophages and *in vitro* lipid-loaded foam cells were

examined for their production of cytokines. The quantitative data in Figure 18A and the summary heat map in Figure 18B demonstrated that in comparison with untreated WT macrophages, WT foam cells increases in cytokines associated with monocytosis (M-CSF and IL-3) and inflammation (IL-1α and VEGF). On the other hand, untreated *Cnn2*$^{-/-}$ macrophages exhibited decreased baseline levels of cytokines associated with monocytosis (G-CSF and M-CSF) and inflammation (IL-6, IFN-γ and CXCL10) as compared with that of untreated WT macrophages. In comparison with that of WT foam cells, *Cnn2*$^{-/-}$ foam cells had significantly lower levels of cytokines associated with monocytosis (Eotaxin, G-CSF, M-CSF and IL-3) and inflammation (IL-6, IL-12, IFN-γ, CXCL10, CXCL1, TNF-α and VEGF).

Deletion of calponin 2 decreases adhesion of macrophages to culture substrate

It is known that calponin 2 plays a role in enhancing the adhesion of cells to

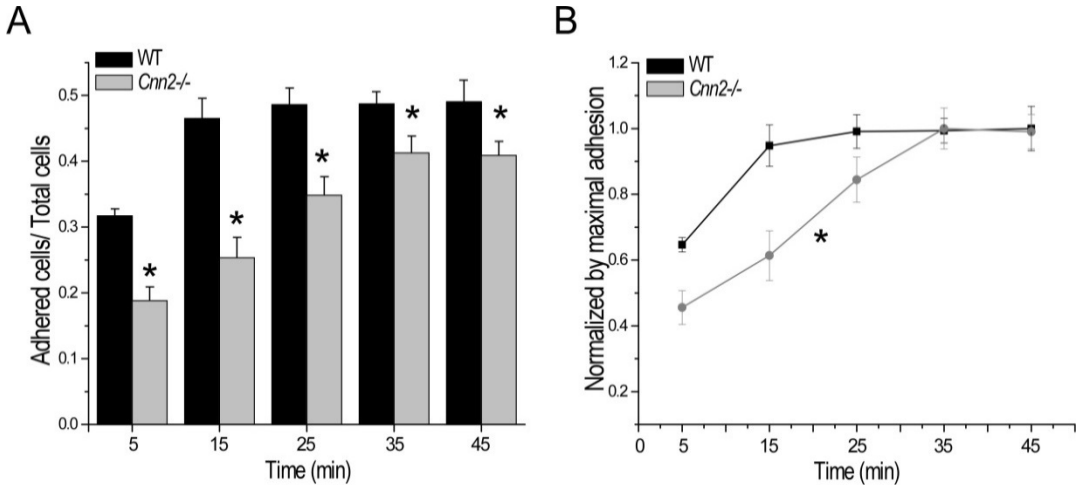

Figure 19. Decreased substrate adhesion of *Cnn2*$^{-/-}$ macrophages. Freshly isolated mouse peritoneal residential macrophages were studied for the velocity of substrate adhesion by quantification of the adherent cells at a series of time points. A. Normalized to the absorbance of the total seeded cells fixed in unwashed wells, the results showed that *Cnn2*$^{-/-}$ macrophages have a decreased substrate adhesion as compared with that of WT macrophages. B. Normalized to the maximum adherent cells of each group, the data further demonstrated that *Cnn2*$^{-/-}$ macrophages adhered to the culture substrate slower than that of WT macrophages, reaching the plateau of adhesion at 35 min vs. 15 min after seeding. *P<0.05 vs. WT group.

culture substrate [[2]. Substrate adhesion is a critical factor in macrophage differentiation and activation [111]. The results in Figure 19 showed that the deletion of calponin 2 significantly weakened and slowed adhesion of macrophages to the culture substrate, suggesting a possible mechanism for calponin 2 to regulate macrophage functions via altering cell adhesion.

To investigate the mechanism for calponin to regulate cell adhesion, primary skin fibroblasts were studied taking advantage of their extended spreading in culture, which permits more clear imaging of the cytoskeleton. Typical actin stress fibers were seen in

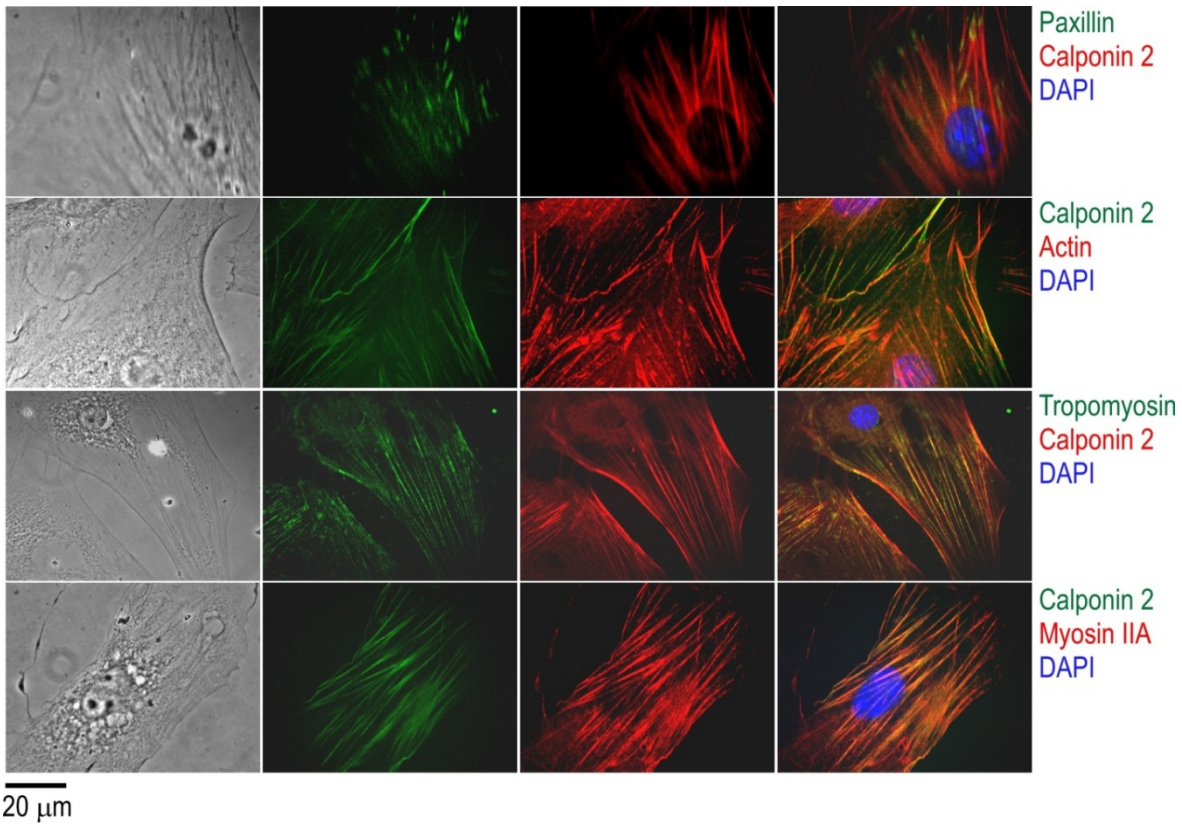

Figure 20. Association of calponin 2 with the actin-myosin cytoskeleton. Primary cultures of neonatal mouse skin fibroblasts on coverslips were examined. Confocal fluorescence microscopic images showed that calponin 2 co-localizes with tropomyosin-F-actin stress fibers (the distribution of tropomyosin detected using mAb CG3 is similar to that of F-actin stress fibers and co-localized with calponin 2) and myosin IIA, but not at the focal adhesion sites identified by anti-paxillin mAb 5H11 staining. Cell nucleus was stained with DAPI.

the cultured neonatal mouse skin fibroblasts (Figure 20). Immunofluorescence staining using anti-calponin 2 mAb 1D11 and rabbit polyclonal antibody RAH2 revealed co-localizations of calponin 2 with F-actin, tropomyosin and myosin IIA, but not with paxillin-stained focal adhesions [112]. The results suggest that calponin 2 enhances substrate adhesion of cells possibly by decreasing dynamics of the actin cytoskeleton through the inhibition of myosin motor function, which is a fundamental function of calponin [52] [53].

Intracellular distribution of calponin 2

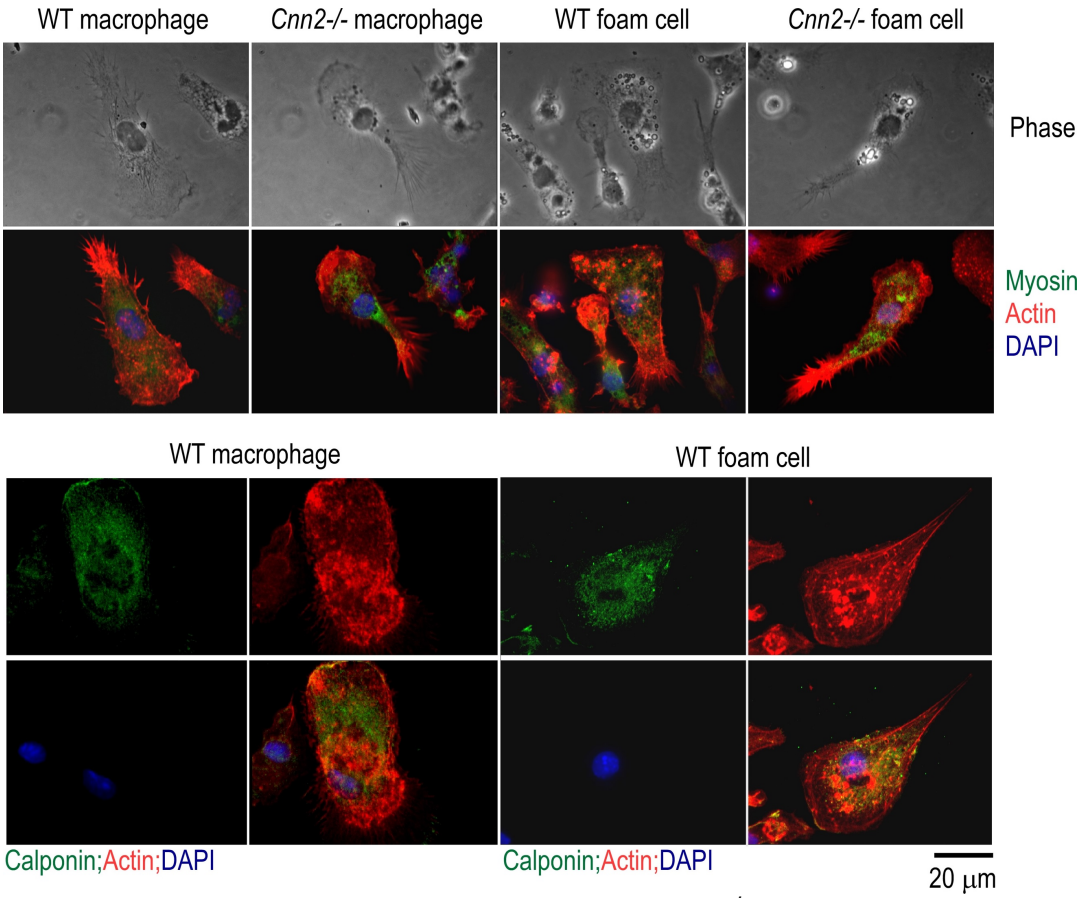

Figure 21. The actin-myosin cytoskeleton in WT and Cnn2$^{-/-}$ macrophages and foam cells. A. Confocal fluorescence microscopic images showed concentrated F-actin in the leading edge and the trailing tail of migrating macrophages, while myosin IIA mainly in the center of cell body and absent at the trailing tail. The distribution patterns of F-actin and myosin are similar in WT vs. Cnn2$^{-/-}$ macrophages and the foam cells. B. The cellular location of calponin 2 was investigated in WT macrophages and foam cells with F-actin as a reference. The results showed that calponin 2 is concentrated in the center of cell body and absent at the trailing tail, similar to that of myosin IIA. Cell nucleus was stained with DAPI.

We further examined the effect of calponin 2 deletion on the actin-myosin cytoskeleton in WT and *Cnn2*$^{-/-}$ macrophages and foam cells. The results in (Figure 21) showed that while F-actin is concentrated in the leading edge and the trailing tail of migrating macrophages, myosin mainly in the center of cell body. The distribution patterns of F-actin and myosin are similar in WT vs. *Cnn2*$^{-/-}$ macrophages and the foam cells. The cellular location of calponin 2 in WT macrophages and foam cells is similar to that of myosin IIA. A hypothesis is that calponin 2 enhances substrate adhesion of cells by inhibiting myosin motor function and decreasing dynamics of the cytoskeleton, which merits further investigation.

Discussion

Atherosclerosis is an inflammatory disease and the main cause of coronary heart disease and stroke [6]. Macrophages play a central role in the pathophysiology of atherosclerosis and the regulation of macrophage function is a promising therapeutic target for the disease [113]. In the present study, we investigated the role of calponin 2, an actin cytoskeleton-associated regulatory protein, in macrophages in the development of arterial atherosclerosis. The results demonstrated that deletion of calponin 2 enhances the motility of macrophages, compensates for the hindered motility of foam cells (Figure 15), and attenuates the development of ApoE deficiency-caused atherosclerosis in vivo (Figures 16 and 17). These novel findings have several impacts on our understanding of calponin regulation of macrophage function in inflammatory diseases.

Deletion of calponin 2 increases the motility of macrophages and compensates for the impaired motility of foam cells

Macrophages and foam cells are pivotal cell types in the development of

inflammatory lesion in arterial atherosclerosis, effecting on the progression and regression of plaques [114]. Although phagocytosis clearance of lipoproteins by macrophages is likely to be beneficial at the outset of this inflammatory response, dysregulation of lipid metabolism and accumulation of lipid-ingested macrophages in atherosclerotic plaques may alter immune phenotypes and cause apoptosis to exaggerate inflammatory response and aggravate the progression of atherosclerosis lesion. Therefore, promotions of cholesterol efflux from macrophages [115] and macrophage emigration from plaques [116] have been proposed as therapeutic approaches.

Cholesterol loading in macrophages results in significant reduction of migration ability [117] [118], accompanied by decreased capacity of force generation by cell locomotors [119]. Lipid-ingested macrophages have hindered migration and the retention of macrophages in atherosclerotic lesions contributes to the failure of resolving inflammation and plaque development [120] [114]. Reversal of cholesterol loading can restore the migration ability of macrophages [118]. Calponin 2 is a regulator of cell motility. Calponin binds to F-actin and inhibits the actin-activated MgATPase activity of myosin II [49] [50]. This function plays a role in modulating smooth muscle contractility and corresponds to the effect of calponin 2 on stabilizing the actin cytoskeleton in non-muscle cells and inhibiting cell motility [121]. Calponin 2 and myosin II are both concentrated in the center of the cell body of macrophages (Figure 21), supporting this hypothesis that deletion of calponin 2 removes an inhibition of myosin II motor and increases the dynamics of the cytoskeleton. This mechanism lays a foundation for calponin to regulate actin cytoskeleton-based functions, such as cell proliferation,

adhesion and migration [27] [2] [33] [34].

Previous studies have demonstrated that primary fibroblasts and peritoneal macrophages isolated from *Cnn2*$^{-/-}$ mice migrated faster than that of WT control cells [60] [1]. Our present study further showed that deletion of calponin 2 increases the motility of not only macrophages but also foam cells, overcoming the negative impact of lipid loading (Figure 15). Since *Cnn2*$^{-/-}$ and WT macrophages have similar amount of lipid loading (Figure 13), the less impaired motility of *Cnn2*$^{-/-}$ foam cells is likely based on higher intrinsic cytoskeleton dynamics other than increasing lipid efflux. This notion is supported by the fact that the motility of *Cnn2*$^{-/-}$ foam cells remained faster than that of WT macrophages (Figure 15).

This finding suggests that calponin 2 is a potential target for controlling the motility of macrophages and foam cells to attenuate the progression of atherosclerosis. Deleting calponin 2 to increase the motility of macrophages and compensate for the hindered motility of foam cells is a mechanism downstream of cellular signaling pathways, which may provide a specific treatment for atherosclerosis. Supporting this notion, the development of atherosclerosis in *ApoE*$^{-/-}$ mice was very effectively attenuated by deleting calponin 2 in macrophages (Figures 16 and 17).

Deletion of calponin 2 in macrophages attenuates the development of atherosclerosis with reduced production of inflammatory cytokines

Cytokine-mediated cell signaling plays dominant roles during the pathogenesis and progression of atherosclerosis [122]. As expected, our study found up-regulations of pro-inflammatory cytokines M-CSF, IL-3, IL-1α and VEGF were found in WT foam cells compared to that in WT macrophages (Figure 18). IL-1α is a prominent pro-inflammatory cytokine produced by macrophages following ingestion of oxidized LDL

[123, 124]. Atherosclerotic lesions in *ApoE*$^{-/-}$ mice transplanted with *IL-1*$\alpha^{-/-}$ bone marrow cells was 52% less than that in *IL-1*$\alpha^{+/+}$ transplanted controls (Kamari et al., 2011). Atherosclerosis development is also accompanied by the up-regulation of VEGF [125]. VEGF stimulates the proliferation and growth of endothelial cells, induces angiogenesis, and potentially promotes plaque formation and destabilization [126]. M-CSF and IL-3, cytokines that are associated with monocytosis, are induced by hypercholesterolemia and cause proliferation of hematopoietic stem cells and progenitor cells [127].

Our study further showed that the deletion of calponin 2 alters cytokine production profiles of macrophages and foam cells (Figure 18). Comparing with WT foam cells, *Cnn2*$^{-/-}$ foam cells have decreased productions of monocytosis associated cytokines G-CSF, M-CSF and IL-3 and pro-inflammatory cytokines IL-6, and IFN-γ. The decreased production of inflammatory cytokines was also found in *Cnn2*$^{-/-}$ macrophages as compared to that in WT macrophages, indicating a baseline anti-inflammatory phenotype that effectively overrides the pro-inflammatory stimulation of lipid ingestion. This mechanism provides a molecular basis for the attenuated development of atherosclerosis in *Apo*E$^{-/-}$,*Cnn2*$^{-/-}$ and *Apo*E$^{-/-}$,*Cnn2*$^{f/f}$,*lysM*$^{cre+}$ mice (Figures 16 and 17).

Deletion of calponin 2 decreases cell adhesion as a potential mechanism to reduce pro-inflammatory activity of macrophages

Calponin is an actin filament-associated regulatory protein and its function has been most extensively studied for the regulation of smooth muscle contractility (Liu & Jin, 2016). The smooth muscle-specific isoform calponin 1 functions as an inhibitory regulator of smooth muscle contraction through inhibiting actomyosin ATPase [21]. Calponin 2 is the isoform of calponin expressed in macrophages and functions in

decreasing the dynamics of actin cytoskeleton and regulating phagocytosis, migration and adhesion. The current knowledge regarding macrophage differentiation and functions in inflammatory diseases is mainly from studies of receptor-ligation based signaling pathways. Our present study showed that calponin 2, a cytoskeleton regulatory protein, effectively modifies the function of macrophages in the development of atherosclerosis, proposing a novel cell motility-based mechanism to attenuate inflammatory diseases.

Differentiation and phenotype polarization of macrophages could promote either resolution of inflammatory process and attenuation of atherogenesis [128] [129] or acceleration of atherosclerosis [130] [131]. It has been broadly observed that substrate adhesion is critical for macrophage differentiation [132] [111]. Macrophages cultured on stiffer substrate exhibited increased spreading area and enhanced adhesion, accompanied with elevated classical activation than that of macrophages cultured on softer substrate [133]. Macrophage grown on soft substrates produced less proinflammatory cytokines with decreased TLR4 activity than that of the macrophages grown on rigid substrates [134]. The modulation of macrophage function by substrate rigidity is dependent on actin polymerization and RhoGTPase activation [19].

Similar to the findings in other cell types [33, 60, 2], calponin 2 facilitates the adhesion of macrophages to the culture substrate (Figure 19). Calponin 2 is not located at the cell focal adhesions but concentrated in the center of the cell body as that of myosin II (Figures 20 and 21). This observation suggests that calponin 2 facilitates and stabilizes cell adhesion by inhibiting myosin II motor and reducing the dynamics of cytoskeleton. The deletion of calponin 2 to increase the dynamics of actin cytoskeleton

and weaken cell adhesion (Figure 19) could be responsible for the decreased baseline production of pro-inflammatory cytokines in *Cnn2*$^{-/-}$ macrophages and the attenuated up-regulation of pro-inflammatory cytokines in *Cnn2*$^{-/-}$ foam cells (Figure 18).

Summary

Our study demonstrated that calponin 2 regulates macrophage function in the development of atherosclerosis via modulating the function of actin cytoskeleton. Deletion of calponin 2 increases macrophage motility and compensates for the impaired motility of foam cells, reduces inflammatory cytokines in macrophages and foam cells, and reduces atherosclerosis lesions in *ApoE*$^{-/-}$ mice. The data provide evidence that changes in myosin motor-based cytoskeleton dynamics and cell adhesion alter macrophage activities, implicating a potentially novel therapeutic target for the treatment and prevention of atherosclerosis.

CHAPTER 4 - MECHANICAL REGULATION OF CYTOSKELETON FUNCTION IN BLOOD VESSELS: THE ROLE OF A CALPONIN-RELATED PROTEIN, SM22

Abstract

SM22, also named transgelin, encoded by the gene *TAGLN* is a calponin-related protein found in smooth muscle, fibroblast and cancer cells. SM22 was discovered three decades ago but its biological function remains unclear. In addition to an application as differentiation marker for smooth muscle cells, SM22 has been reported to regulate the structure and dynamics of actin cytoskeleton and cell motility in fibroblasts and cancer cells. Here we report a novel finding that the expression and degradation of SM22/transgelin are both regulated by mechanical tension. Mass spectrometry identification detected that SM22 was significantly decreased in mouse aortic rings after incubation under low mechanical tension. Using specific monoclonal antibodies developed against chicken gizzard SM22, we found high levels of SM22 in human fetal lung fibroblast cells line MRC-5 (ATCC CCL-177) and primary neonatal mouse skin fibroblasts. Similar to that of calponin 2, the level of SM22 is positively dependent on the mechanical tension in the cytoskeleton as determined by the stiffness of the culture substrate. Quantitative RT-PCR demonstrated a transcriptional regulation of *TAGLN* gene expression by mechanical tension in the cytoskeleton. The level of SM22 is decreased in skin fibroblasts isolated from calponin 2 knockout mice compared to that in calponin 2-positive wild type cells, suggesting their correlated functions. With the close phylogenetic relationship between *TAGLN* and the calponin genes, SM22 is identified as a calponin-like cytoskeleton regulatory protein. These findings laid a groundwork for understanding the physiological function of SM22/transgelin in the mechanoregulation of cytoskeleton and cell motility.

Introduction

SM22 is a globular 22-kDa protein with basic isoelectric point originally isolated from chicken gizzard smooth muscle [135] [136].It was then found in mammalian smooth muscles and has since been considered as a biomarker for smooth muscle differentiation [137]. SM22 was rediscovered in 1993 and named transgelin due to its apparent ability to induce gelation of actin filament *in vitro* [138]. Sequence analysis showed that SM22 and transgenlin represent the same protein [136] [139]. Subsequent studies have further identified a family of related proteins including SM22α/transgelin, SM22β, mp20, NP22, NP25, p27, and WS3-10 [140].

Based on sequencing data for vertebrate genomes, all these proteins are encoded by three homologous genes, *TAGLN*1, 2 and 3, located on chromosomes 11, 1 and 3, respectively, in the human genome. SM22α, transgelin and WS3-10 are identical proteins encoded by *TAGLN*1 gene, SM22β is the product of *TAGLN*2, and NP22 and NP25 found in neuronal tissues is the product of *TAGLN*3. The proteins encoded by *TAGLN*1 and *TAGLN*2 have been demonstrated with similar functions as actin-binding proteins abundantly expressed in contractile smooth muscle cells [141]. They are also expressed in fibroblasts with a role in modulating actin-cytoskeleton based functions such as shape changing, migration and cell type transformation [142].

SM22α has been identified with structural similarities to that of calponin [137]. Calponin is known to be a family of actin-filament associated regulatory proteins. Three isoforms of calponin encoded by three homologous genes have been found in vertebrate species: A basic calponin (calponin 1, isoelectric point (pI) = 9.4) encoded by *CNN1* [22], a neutral calponin (calponin 2, pI = 7.5) encoded by *CNN2* [23] [24] and an

acidic calponin (calponin 3, pI = 5.2) encoded by *CNN3* [25]. Extensive research in the past two decades has determined that calponin 1 is specifically expressed in mature smooth muscle tissue with a role in regulating smooth muscle contractility; calponin 2 is expressed developing and remodeling smooth muscle and many non-muscle cell types with a role in regulating actin cytoskeleton based functions such as proliferation, adhesion migration and phagocytosis; calponin 3 is found in neuronal cells, myoblasts and embryonic trophoblasts, where it may function in regulating the actin cytoskeleton with a proposed role in the plasticity of neural tissues and embryonic development [34].

Primary structures of the three calponin isoforms share a conserved N-terminal calponin homology (CH) domain and a conserved middle region containing two actin-binding sites, whereas their C-terminal segments are variable to constitute the main differences among the isoforms [34]. SM22α has structural similarities with calponin in the CH domain and the first actin-binding site, implicating a function of actin-binding. It has been reported that the expression pattern of SM22α in differentiated smooth muscle is similar to that of calponin 1 while its regulation of actin cytoskeleton in fibroblasts is similar to that of calponin 2 in non-muscle cells.

In this chapter, we demonstrate for the first time that the gene expression and degradation of SM22α are both regulated by cytoskeleton tension. Maintaining mechanical tension protected SM22α from degradation in mouse aorta *in vitro*. The levels of SM22α mRNA and protein in fibroblasts are both positively related to the stiffness of the culture substrate, similar to that of calponin 2. Interestingly, the level of SM22α is decreased in skin fibroblasts isolated from calponin 2 knockout (KO) mice compared to that in wild type (WT) control cells, indicating their related functions.

These findings lay the groundwork for understanding the physiological function of SM22/transgelin in mechanoregulation of the cytoskeleton.

Materials and Methods

Genetically modified mice

The generation and initial characterization of *Cnn2*-floxed (*Cnn2*$^{f/f}$) mice and induction of systemic *Cnn2* KO have been described previously [1]. The alleles have been transferred to full C57BL/6 background. All animal studies were carried out under protocols approved by the Institutional Animal Care and Use Committee of Wayne State University.

Examination of smooth muscle protein degradation in response to tissue tension

Adult mouse aortae were isolated immediately after euthanasia. One segment of the aorta was mounted on a pipet tip and secured with 6-0 suture to apply constant tension to the tissue. Another segment was left slack. Special care was taken to avoid stretching or other tissue damages. The aortic tissues were then incubated in phosphate buffered saline (PBS) at 37 °C for 6 hrs. The tension-applied portion and the slack portion were then processed in parallel to prepare SDS-gel samples by high speed mechanical homogenization in SDS-gel sample buffer containing 2% SDS and heated at 80 °C for 5 min to extract total protein while inactivating endogenous proteases. The samples were examined using SDS-polyacrylamide gel electrophoresis (PAGE) and Western blotting as described below.

SDS-PAGE and Western blotting

Representative tissues were obtained from 6-month old C57B/L6 mice immediately after euthanasia and rapidly frozen at -80 °C. Total protein was extracted

by homogenization in SDS-PAGE sample buffer as above. Total protein extracts from cell cultures were prepared by lysing phosphate-buffered saline (PBS)-washed monolayer cells in SDS-PAGE sample buffer and heating at 80 °C for 5 min.

The protein extracts were analyzed using 14% SDS-gel in a modified Laemmli buffer system with an acrylamide:bisacrylamide ratio of 180:1 and at pH 8.8 for stacking and resolving gels as well as for the sample buffer. After electrophoresis, the gels were fixed and stained with Coomassie Blue R-250 to assess sample integrity and to normalize the protein input. Duplicated gels were electrically blotted on nitrocellulose membrane using a Bio-Rad semi-dry transfer apparatus for Western blot analysis. The membrane was incubated with a mouse anti-SM22α mAb 3F6 (described below) or a rabbit antiserum, RAH2, previously raised against mouse calponin 2 [95] in Tris-buffered saline containing 0.1% bovine serum albumin (BSA). The calponin and SM22α bands recognized by the first antibody were revealed using alkaline phosphatase-labeled anti-rabbit IgG or anti-mouse IgG second antibody (Santa Cruz Biotechnology) and 5-bromo-4-chloro-3-indolyl phosphate/nitro blue tetrazolium chromogenic substrate reaction.

LC-MS/MS protein identification

Protein bands of interest were excised from SDS-gel. The gel slices were washed with 50 mM ammonium bicarbonate, reduced in 10 mM DTT at 37°C for 45 min and then alkylated with 55 mM iodoacetamide at room temperature for 30 min. 10 ng/μl each of Lys-C, trypsin, Glu-C, and chymotrypsin were added to four replicate reaction tubes for in gel protein digestion by incubation at 37 °C overnight except for chymotrypsin that was incubated at room temperature. The resulting peptides were

separated on a reversed-phase C18 column with a 90 min gradient using a Dionex Ultimate HPLC system. MS and MS/MS spectra were then acquired on an Applied Biosystems QSTAR XL mass analyzer using information dependent acquisition mode. MS scan was performed from m/z 400-1,500 for 1s followed by product ion scans on two most intense multiply charged ions. Peak lists were identified by submitting to Mascot server to search against the NCBInr database for all entries with carbamidomethyl (C) used as a fixed modification and oxidation (M), N-acetylation (protein N terminus) as variable modifications.

Cloning of mouse SM22α cDNA and expression in E. coli

Total RNA was extracted from adult mouse uterus (that is known expressing SM22α at a high level) using the TRIzol reagent (Invitrogen) as described the manufacture's protocol. Integrity of the isolated RNA was verified using agarose gel electrophoresis. cDNA encoding SM22α was obtained by reverse transcription-coupled polymerase chain reaction (RT-PCR). Reverse transcription was carried out using an anchored oligo(dT) primer TV20 and avian myeloblastosis virus reverse transcriptase (AMVRT) at 42 °C for 2 hrs. PCR amplification of the coding region of SM22α cDNA was carried out using primers synthesized containing unique *Nde*I and *Eco*RI restriction enzyme cutting sites (Forward primer: 5'-CTC***CATATG***GCCAACAAGGGTCCA-3'; Reverse primer: 5'-CTG***GAATTC***CCTTTCTAACTGATGAT-3', *N*deI and *E*coRI sites were indicated as bold italic font in primer sequence) for cloning into the T7 polymerase-based pAED4 expression plasmid vector [143].

The cDNA was ligated to *Nde*I and *Eco*RI cut pAED4 vector. The recombinant plasmids were used to transform JM109 *E. coli*. Positive plasmids were screened by

PCR and confirmed by sequencing of the cDNA insert. Competent BL21(DE3)pLysS *E. coli* cells were transformed with the SM22α expression plasmid. Freshly transformed colonies were used to inoculate LB media containing 100 μg/mL ampicillin and 12.5 μg/mL chloramphenicol. The cultures were incubated at 37 °C with vigorous shaking and induced at $O.D._{600nm}$ of ~0.3 by adding IPTG to a final concentration of 0.4 mM. The culture were continued for 3 hrs and harvested as previously described [143].

Mouse SM22α protein expressed in the bacterial culture was purified at 4 °C from the French pressed cell lysate with ammonium sulfate fractionation cation exchange chromatography using a CM52 column at pH 6, and size exclusion chromatography using a G75 column at pH 7.0 as adapted from the method for the purification of calponin 1 [144] SM22 protein was traced during the purification and the final product was verified using SDS-PAGE and Western blotting as described above.

Development of anti-SM22 monoclonal antibodies (mAb)

Chicken gizzard SM22α was purified as described previously [136] and used to immunize Balb/c mice. As described previously [30], spleen cells of a short-term immunized mouse were harvested for fusion with Sp2/0-MLK mouse myeloma cells. Hybridoma clones were screened by indirect enzyme-linked immunosorbent assay (ELISA) against the immunogen, verified by Western blotting against the immunogen, and subcloned three or more times to establish stable cell lines. Anti-SM22α mAbs were produced in the forms of hybridoma cultural supernatant and mouse ascites fluids. Specificity of the anti-SM22α mAbs was examined using Western blotting against various tissue extracts as described above.

Cell Cultures

NIH/3T3 mouse fibroblast line (ATCC CRL-1658) was cultured in Dulbecco's Modified Eagle Medium (DMEM) containing 10% fetal bovine serum (FBS). Human lung fibroblast line MRC-5 (ATCC CCL-171) was cultured in Eagle's Minimum Essential Medium (EMEM) containing 10% FBS. All culture media used contained 2 mM L-glutamine, penicillin (100 i.u./mL) and streptomycin (50 i.u./mL). The cell cultures were maintained in a humidified incubator at 37 °C in the presence of 5% CO_2.

Fibroblasts were isolated from the back skin of neonatal WT and *Cnn2*$^{-/-}$ mice for primary cultures as described previously [102]. Briefly, 3-4 days old mice were euthanized after PCR genotyping and soaked in 70% ethanol for 2 min before removing the skin around torso under sterile condition. In a 35 mm culture dish, the skin was incubated with 0.5% trypsin (9002-07-7 GIBCO) in DMEM at 37 °C for 1 hr. After washing with DMEM, the tissue was minced into fine pieces using a sharp razor for digestion in 2 mL of 700 U/mL collagenase I (M3A14008A Worthington) in DMEM at 37 °C for 2 hrs in a 15 mL centrifuge tube with agitation every 20 min by gentle shaking. 2 mL ice-cold DMEM containing 20% FBS was then added and the tube was vortex 5 sec for 5 times. The tissue suspension was pipetted up and down several times and the isolated cells were passed through a 100 μm nylon mesh. The cells were collected by centrifugation at 150x g for 5 min and re-suspend in 8 mL DMEM containing 20% FBS for culture at 37 °C in 5% CO_2. Soon after becoming confluent, the P_0 cells from each mouse were expanded into four 100 mm dishes to prepare 8-10 vials of frozen stock of P_1 cells (0.5 to 1 million cells per vial). Urinary bladder of each mouse was examined using Western blot as above to verify the *Cnn2*$^{-/-}$ and WT genotypes. The frozen cells were stored in liquid nitrogen before being thawed and passed one more time (P_2) for

experiments.

Examination of substrate stiffness-dependent expression of SM22α and calponin 2

A thin layer of polyacrylamide gel was prepared on glass cover slips to provide stiffness-tunable matrix for cell culture as described previously [145] [146]. 450 µL of 0.1 M NaOH was smeared on each 22 X 22 mm cover slip and heat with NaOH solution at 80°C until the lipid is evaporated. Thereafter, the cover slips were treated with 3-aminopropyltrimethoxysilane for 5 min and then with 0.5% glutaraldehyde for 30 min. Polyacrylamide gels of different stiffness were polymerized in between the treated cover slip at the bottom and a siliconized cover slip on the top. After polymerization, the untreated cover slip was removed to expose the ~100 µm thin layer of gel to be used as cell culture matrix.

To coat matrix protein for cell culture, the gels were first conjugated with a heterobifunctional protein cross-linker sulfo-SANPAH (1 mM buffered with 50 mM HEPES, pH 8.5) (Pierce, 22589), by photoactivation at wavelengths of 325 nm. Then 0.1 mg/mL Type I collagen (Sigma, C7661) was applied to the gel surface and incubated at 37 °C overnight. Gels were then washed with Minipore water and sterilized with UV irradiation for 3 hours. The gel was soaked in culture media at 37 °C for 1 hour before plating cells.

To examine the effect of the culture substrate stiffness on the expression of SM22α and calponin 2, NIH/3T3, MRC5 and primary WT or *Cnn2*$^{-/-}$ mouse fibroblasts were seeded on plastic culture dish or polyacrylamide gels of different stiffness. The cells were harvested after 24 hrs of culture by directly lysis in SDS-gel sample buffer after washes with prewarmed D-PBS. The levels of SM22 and calponin 2 proteins

normalized to actin in the cellular protein extracts were examined with Western blot analysis using an anti-SM22 mAb 3F6 and an anti-calponin 2 rabbit polycolonal Ab RAH2, respectively.

Quantitative RT-PCR

Total RNA was extracted from monolayer cell cultures on plastic or gel substrates of different stiffness using Trizol reagent (Invitrogen). Integrity of the isolated RNA was verified using agarose gel. One μg of each RNA sample was reverse transcribed using an anchored oligo(dT) primer (TV20) and at 42 °C for 2 hrs. Quantitative PCR was carried out with Power SYBR Green PCR master mix (Applied Biosystems) to determine the level of SM22 cDNA relative to the level of glyceraldehyde-3-phosphate dehydrogenase (GAPDH), using an Applied Biosystems 7300 real time PCR system (Applied Biosystems, Foster City, CA). The PCR primers (Table 2) of mouse SM22α, calponin 2 and GAPDH quantifications were designed crossing exons to avoid background signals from any genomic DNA contamination. The quantitative PCR was carried out in 20-μL volumes with 10 min preheating at 95 °C followed by 40 cycles of 15 sec at 95 °C and 60 sec at 60 °C. Melting curve analysis was performed at the end to verify that there was no significant formation of primer dimmers under the PCR conditions. The results were analyzed using the $2^{-\Delta\Delta Ct}$ method as per the Applied Biosystems user's instructions.

Data analysis

DNA and protein sequence analysis was performed using the DNAStar software (Lasergene). 2-D densitometry was done to quantify SDS-gel and Western blots on images scanned at 600 dpi. Statistical significance for quantitative data was determined

using Student's t test.

Table 2. Primers used for quantitative PCR.

Target Gene	Forward Primer	Reverse Primer
Mouse SM22	5'-GACATGTTCCAGACTGTTGACCTC-3'	5'-CCTCTTATGCTCCTGGGCTTTCTT-3'
Mouse Calponin 2	5'-AACAGGAGAGGAACTTTGACG-3'	5'-TCCATGGAGGCAGGATA-3'
Mouse GAPDH	5'-TCAACAGCAACTCCCACTCTTCCA-3'	5'-ACCCTGTTGCTGTAGCCTATTCA-3'

The forward primer of mouse SM22 is located in exon 3 and the reverse primer is across exon 4 and exon 5. The forward primer of mouse calponin 2 is located in exon 4 and the reverse primer in exon 5. The forward primer of mouse GAPDH is located in exon 6 and the reverse primer in exon 7.

Results

Development of specific anti-SM22α mAbs

Three anti-SM22α mAbs, 3F6, 2G4 and 3B9, were developed. Together with our successfully cloned and bacterially expressed mouse SM22α, the specificity of the anti-SM22α mAbs is shown in Figure 22. It is of interest to note that 3F6 demonstrates the equally high affinity and specificity against purified mouse SM22α and SM22α in

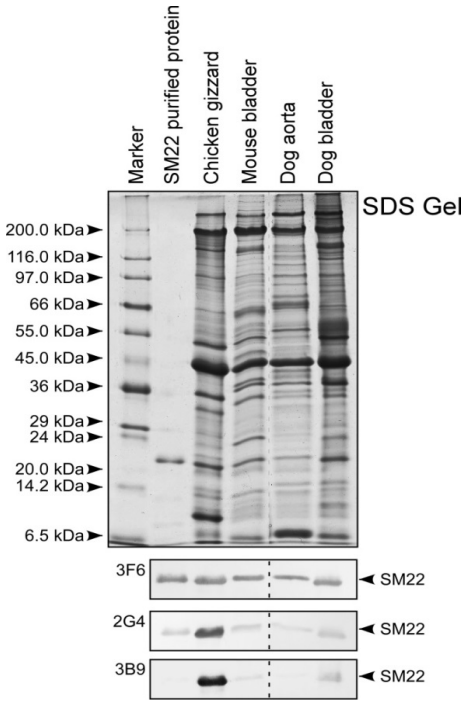

Figure 22. The specificity of SM22α mAbs. mAbs 3F6, 2G4 and 3B9 were screened by immunoblotting against purified mouse SM22α and smooth muscles from avian and mammalians. 3F6 demonstrates the equally high affinities against purified mouse SM22α and SM22α in smooth muscles of avian and mammalian species. 2G4 and 3B9 have stronger affinity against chicken SM22α than SM22α of mouse and dog.

smooth muscles from different species, whereas 2G4 and 3B9 have particularly strong affinity against chicken gizzard SM22α (the immunogen) but weak reactions against SM22α from other species. Thus mAb 3F6 that recognizes SM22α in both avian and mammalian species was used in the present study as a tool to quantitatively assess the expression of SM22α.

Reduced mechanical tension causes a degradation of SM22 in mouse aortic rings Protein profiles of the aortic rings after 6 hrs incubation at 37 °C in the presence or absence of external mechanical load were examined using SDS-PAGE (Figure 23). The results showed that as normalized to actin, almost all proteins were preserved at same degrees in the loaded and unloaded portions of mouse aorta after 6

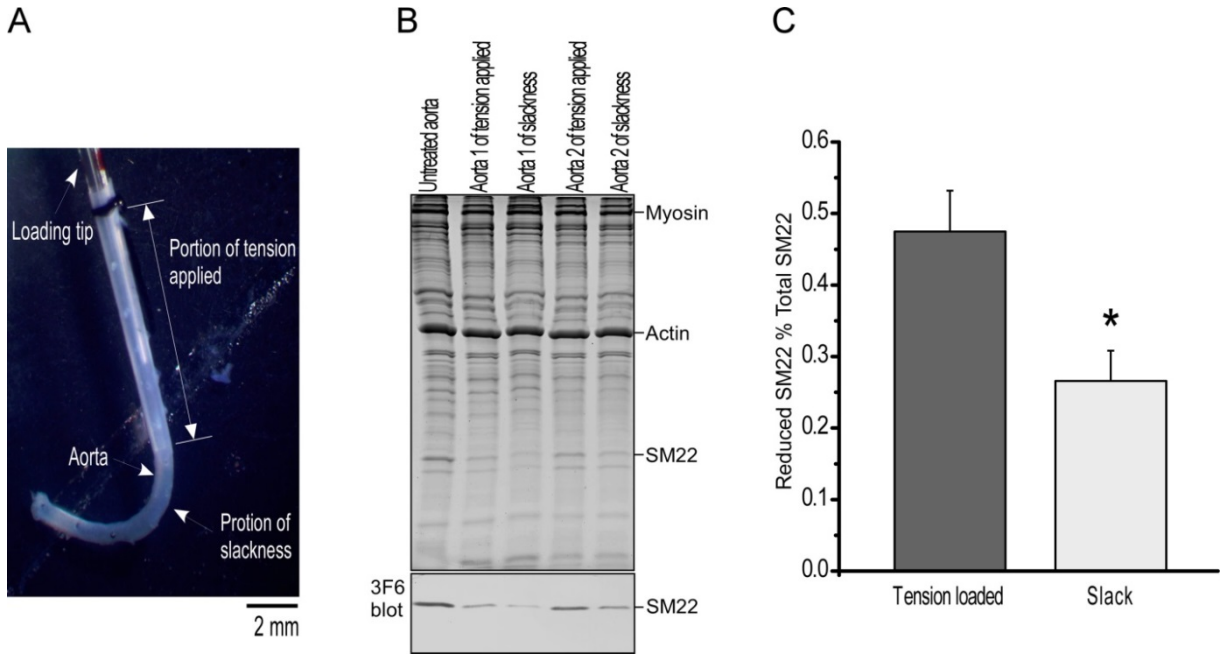

Figure 23. Mechanical load prevented the degradation of SM22α in mouse aortic rings. (A) A portion of the aorta was applied with a mechanical load by the insertion of a pipet tip. The other portion of the aorta was left slack. (B) After incubation in PBS at 37 °C for 6 hrs, total protein was extracted respectively from the loaded and unloaded portions of the aorta and examined using SDS-PAGE. A visible load-protected protein band was identified by mass spectrometry to be SM22α, that was confirmed with the mAb 3F6 Western blot. (C) Densitometry quantification of mAb 3F6 Western blots normalized to the actin band in the Coomassie blue-stained SDS-gel and untreated samples showed an effective prevention of SM22α degradation in the tension-loaded aortic ring (*P<0.05). The results are summarized from three individual experiments.

hrs incubation at 37°C except for a specific protein band that was preserved significantly better in the loaded tissue sample. This band was isolated from the SDS-gel of the loaded aortic tissue lane and mass spectrometry identified it to be SM22α, which was confirmed with Western blotting using SM22α -specific mAb 3F6 (Figure 23B).

Expression of SM22α, calponin 1 and calponin 2 in representative mouse tissues

Total protein extracts from representative organs and tissues of adult mice were analyzed by Western blotting using anti-SM22α mAb 3F6, an anti-calponin 1 mAb CP1 [26] and anti-calponin 2 polyclonal antibody RAH2 [95]. Actin was used as an internal control for the sample loading. The blots showed that SM22α and calponin 1 are

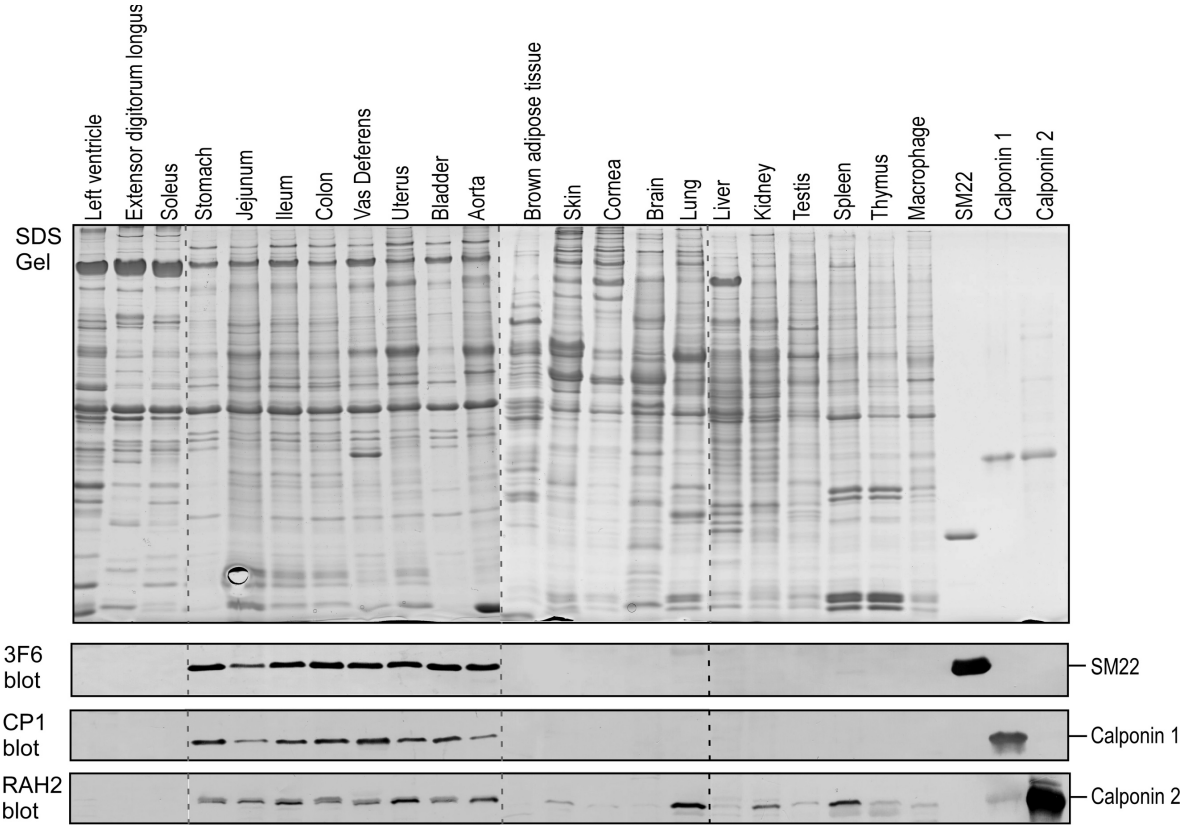

Figure 24. Tissue expression profiles of SM22α, calponin 1 and calponin 2. Total protein extracts from representative organs and tissues of adult mice were analyzed with SDS-gel and Western blots using anti-SM22α mAb 3F6, anti-calponin1 mAb CP1 and anti-calponin 2 polyclonal Ab RAH2, with slight cross reaction to calponin 1. Purified mouse SM22α, calponin 1 and calponin 2 were used as a controls. The sample loading was normalized to the level of actin. The Western blots detected SM22α and calponin 1 in all the types of smooth muscle organs, while calponin 2 in smooth muscle and in multiple non-muscle tissues

present at significant levels in mature smooth muscle tissues, while calponin 2 is seen in smooth muscle as well as multiple non-muscle tissues (Figure 24).

The levels of SM22α and calponin 2 in fibroblast cell lines and neonatal mouse fibroblasts are regulated by the stiffness of culture substrate

A novel finding in our study is that the expression level of SM22α in non-muscle cells is positively regulated by the stiffness of culture substrate (Figures 25 and 26). The cell images in Figure 25A and 26A showed that human fetal lung fibroblast MRC5 and mouse fibroblast 3T3 cell lines and neonatal mouse primary skin fibroblasts cultured on polyacrylamide gels of lower stiffness produced lower tension in the cytoskeleton as reflected by the smaller spreading area, whereas cells cultured on stiffer substrates had higher tension and larger spreading area. Moreover, calponin 2-null mouse fibroblasts produced smaller spreading area reflecting weaker adhesion in comparison with that of WT fibroblasts cultured on the stiffness-matched polyacrylamide gel (Figure 26A). The

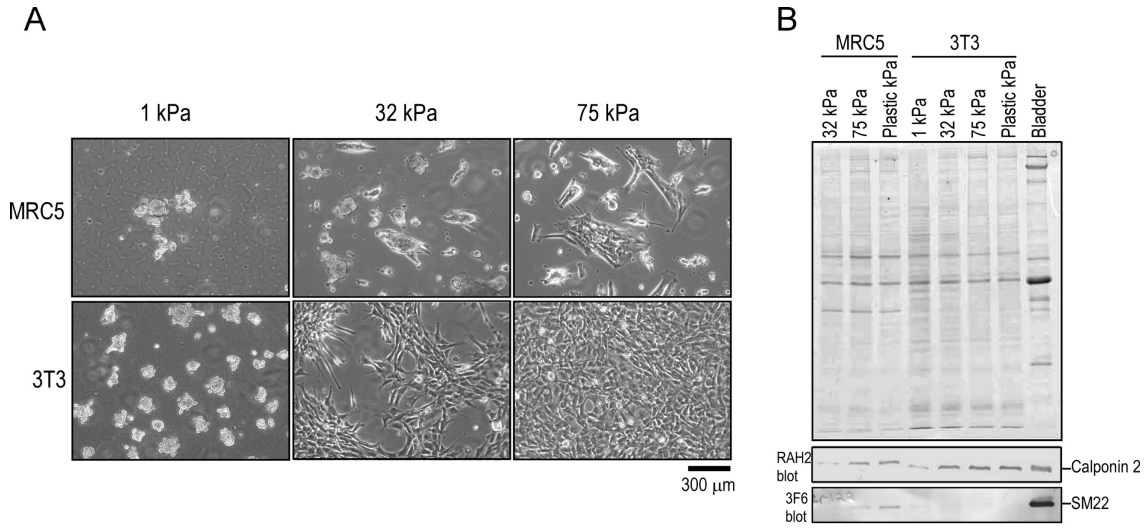

Figure 25. Substrate stiffness-upregulated the level of SM22 and calponin 2 in 3T3 and MRC5 cell lines. (A) Microscopic images of mouse fibroblast cell line 3T3 and human fetal lung fibroblast cell line MRC5 cultured on gel substrate of various stiffness showed that soft gels of low stiffness rendered low tension in the cytoskeleton as reflected by the small cell spreading area, whereas stiff substrates produce higher cytoskeleton tension and large cell spreading area. (B) With protein inputs normalized to the actin band, SDS-PAGE and Western blots showed that the levels of SM22 and calponin 2 in 3T3 and MRC5 were positively related to the stiffness of culture substrate.

Western blots in Figure 25B demonstrate that the expression of calponin 2 in MRC5 and NIH/3T3 fibroblasts is positively related to the stiffness of culture substrate and cytoskeleton tension. The same trend was observed in the expression of SM22α in MRC5 cells. No expression of SM22α was detected in NIH/3T3 cells.

It is of interest to note that the mechanical tension sensing range for the expression of calponin 2 is between 1 kPa and 32 kPa, and the sensing was saturated in higher stiffness in both MRC5 and NIH/3T3, whereas the stiffness-sensing range for SM22α is higher than that for calponin 2: The expression of SM22α in MRC5 cells remains non-detectable at 1 kPa and 32 kPa, but increased in the higher stiffness (75 kPa) of the culture substrates. The Western blots in Figure 26B exhibit that the expression of SM22α in primary fibroblasts isolated from WT and *Cnn2-/-* neonatal

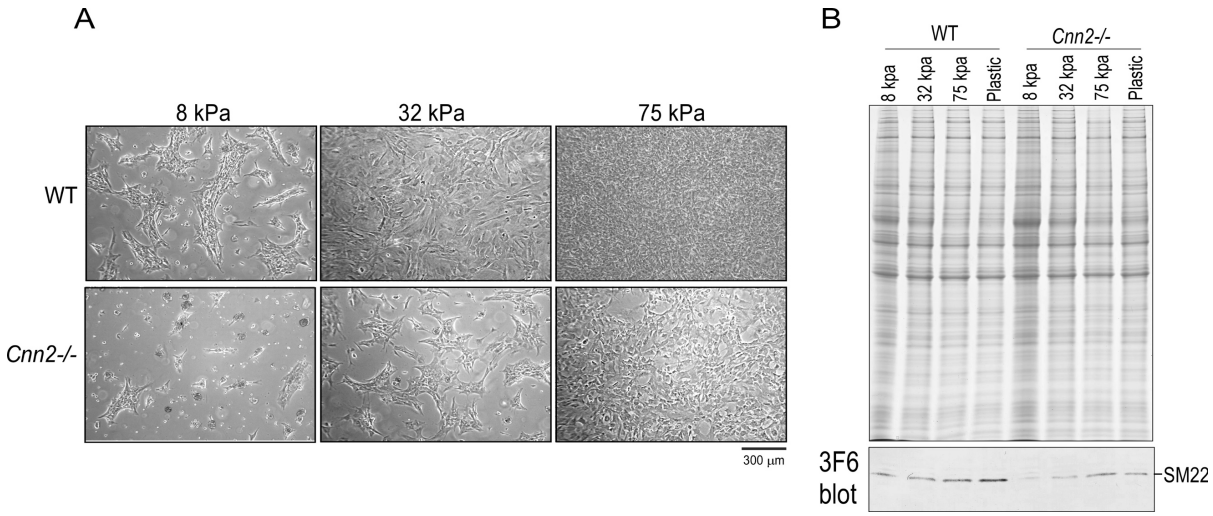

Figure 26. Substrate stiffness-upregulated the level of SM22α in WT and *Cnn2-/-* fibroblasts. (A) Microscopic images of neonatal mouse skin fibroblasts cultured on gel substrate of various stiffness showed that soft gels of low stiffness rendered low tension in the cytoskeleton as reflected by the small cell spreading area, whereas stiff substrates produce higher cytoskeleton tension and large cell spreading area. As previously observed [1] [2], calponin 2-null fibroblasts exhibited smaller spreading area and weaker adhesion in comparison with that of WT fibroblasts cultured on the stiffness-matched polyacrylamide gel. (B) With protein inputs normalized to the actin band, SDS-PAGE and Western blots showed that the levels of SM22α in mouse skin fibroblasts were positively related to the stiffness of culture substrate. Calponin 2-null fibroblasts exhibited decreased expression of SM22α, especially in cells cultured on low stiffness gel substrates.

mouse is also positively related to the stiffness of culture substrate that builds the tension in the cytoskeleton. Interestingly, calponin 2-null fibroblasts showed overall decreases in the level of SM22α, especially in cultures on low stiffness substrates (Figure 26B).

Cytoskeleton tension regulates SM22α expression at transcriptional level

Our previous Northern blotting [30] and promoter analysis [32] demonstrated that the expression of calponin 2 gene is regulated by the stiffness of culture substrate at the

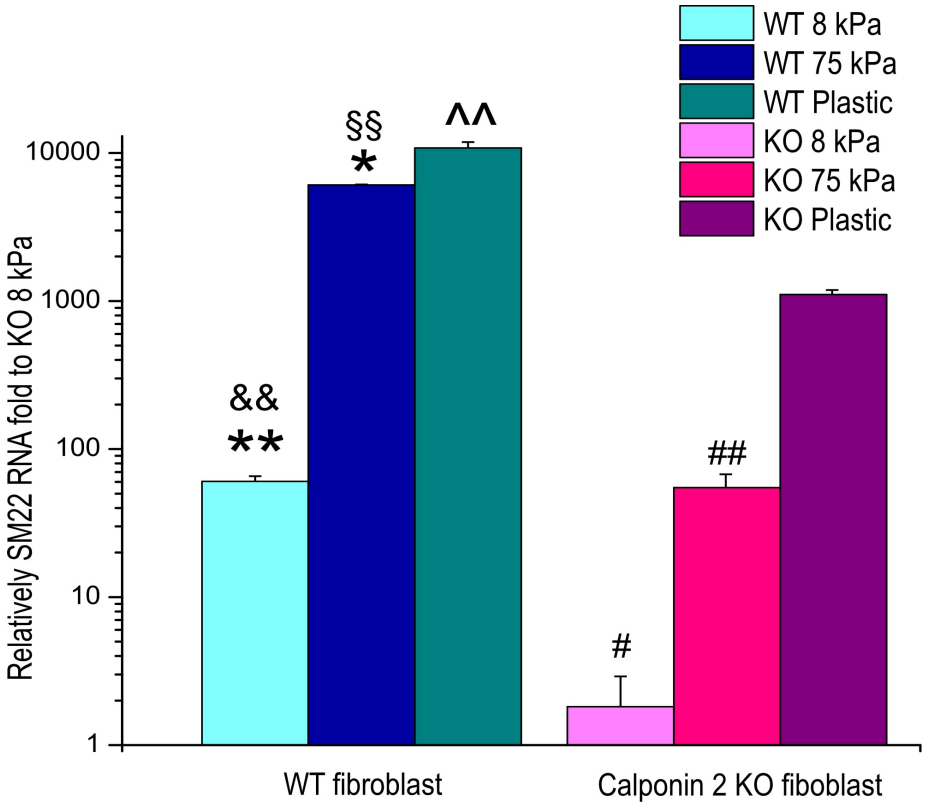

Figure 27. Quantitative RT-PCR examination of SM22α expression at transcriptional level. qPCR was carried out with Power SYBR Green PCR master mix to determine the level of SM22α cDNA relative to the level of GAPDH. The fold changes of gene expression are normalized to the that of calponin 2-null fibroblasts cultured on gel substrate of 8 kPa stiffness. The results show that the levels of SM22α cDNA expression in mouse skin fibroblasts were positively related to the stiffness of culture substrate. Calponin 2-null fibroblasts exhibited overall decreased gene expression of SM22α, especially in cells cultured on low stiffness gel substrates. The results further indicated an increase in the dependence SM22α gene expression on substrate stiffness in calponin 2 KO cells. ***P*<0.01, WT 75kPa vs. WT 8 kPa; **P*<0.05, WT Plastic vs. WT 75 kPa; # *P*<0.05, KO 75kPa vs. KO 8 kPa; ##*P*<0.01, KO Plastic vs. KO 75 kPa; && *P*<0.01, KO 8 kPa vs. WT 8 kPa; §§ *P*<0.01, KO 75 kPa vs. WT 75 kPa; ^^*P*<0.01, KO Plastic vs. WT Plastic.

transcriptional level. The results of our present study further demonstrated with quantitative RT-PCR that the expression of SM22α is regulated by the cytoskeleton tension produced by the stiffness of culture substrate. The qPCR data in Figure 27 show that the mRNA level of SM22α is up-regulated as the stiffness of culture substrate increased. Consistent with the protein expression level in Figure 26, Calponin 2-null fibroblasts exhibited decreased gene expression of SM22α, especially in cells cultured on low stiffness gel substrates. The expression of SM22α mRNA reached a plateau in wild type neonatal mouse skin fibroblasts on 75-kPa substrate, but did not in *Cnn2*-/- cells as compared with that in control cells cultured on the near rigid plastic substrate (Figure 27). This observation indicates that the deletion of calponin 2 resulted in an increase in the dependence SM22α gene expression on substrate stiffness.

Similarity of primary structures of SM22α and calponin isoforms

It has been previously noticed that SM22α has a sequence similarity to that of calponin [137]. To further assess their evolutionary homology and lineage, DotPlot pairwise alignment with amino acid sequences of mouse SM22α and mouse calponin 1 using MegAlign program (Lasergene; DNASTAR, Inc, Madison, WI) showed that SM22α has significant sequence similarity to that of the N-terminal and middle regions of calponin 1 which is conserved regions in all three calponin isoforms. The result further showed that the greatest similarity between SM22α and calponin 1 is in the segment of amino acids 75 to 150 of both proteins, which corresponds to the CH domain and the first actin binding site in calponin 1 (Figure 28A).

The phylogenetic tree of SM22α and calponin isoforms of representative avian

and mammalian species constructed from amino acid sequences with J Hein method using the MegAlign computer program (Figure 28B upper panel) showed a clear evolutionary relation between SM22α and calponin. Considering SM22α's sequence similarity matches to the N-terminal and middle regions of calponin 1 (Figure 28A), we also constructed a phylogenetic tree after removing the C-terminal variable region of the three calponin isoforms (Figure 28B lower panel). The results show that the evolutionary diversity between SM22α and calponins with C-terminal deletion became significantly less as compared with that between SM22α and intact calponin isoforms

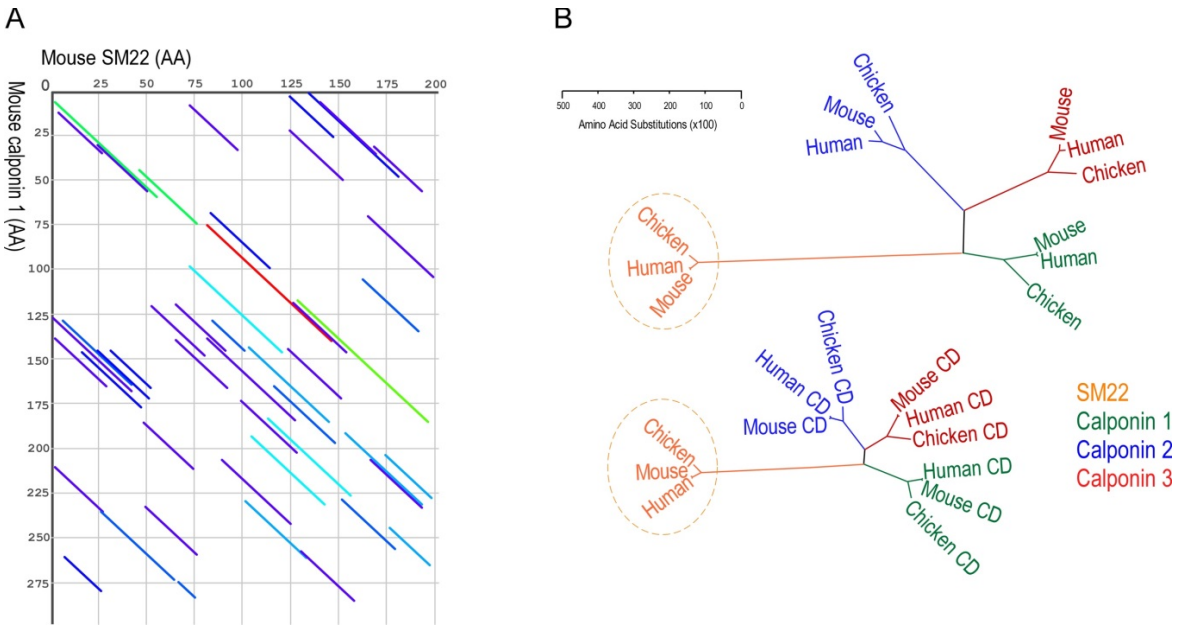

Figure 28. Sequence similarity and evolutionary lineage between SM22α and calponin isoforms. (A) DotPlot pairwise alignment of the amino acid sequences of mouse SM22α and mouse calponin 1. The diagonal lines indicate regions of sequence similarities with the color codes indicating degree of matching as specified in the software parameters. Dark blue indicates lower similarities, with progressively higher similarities indicated by pale blue, green, yellow, orange and red. The results show that the highest similarity between SM22α and calponin 1 is present in the region of amino acid 75 to 150 in both proteins, which attributes to the CH domain and the first actin binding site in calponin 1. (B) Upper panel: Phylogenetic tree of SM22α and calponin isoforms. The results showed a clear evolutionary relationship between SM22α and calponin. Lower panel: Phylogenetic tree of SM22α and calponin isoforms with their C-terminal variable region removed (CD). Removal of the C-terminal variable region of calponin significantly decreased the structural diversity between SM22α and calponin as well as that among the three calponin isoforms. (See Appendix C for NCBI database for sequence analyzed)

(Figure 28B upper panel). The C-terminal segment of calponin is a variable region that constitutes the main diversity among calponin isoform [34]. This established feature is consistent with our phylogenetic analysis results showing that the structural diversity among the three calponin isoforms was also significantly decreased by removing the C-terminal variable region (Figure 28B). Therefore, the results demonstrate that SM22α is a protein closely related to the core structure of calponin, which is conserved among the calponin isoforms.

Discussions

SM22α was discovered three decades ago but its biological function remains unclear. In addition to possible roles in smooth muscle contraction, it has been proposed with functions in regulating the structure and dynamics of actin cytoskeleton and cell motility in fibroblasts. Down-regulation of SM22α has been correlated to cell type transformation and tumorigenesis. In the present study, we report for the first time that the expression and degradation of SM22α is regulated by mechanical tension. SM22α has a high degree of structural similarity and potentially close evolutionary homology to calponin that is known to be regulated and function in the mechanoregulation of the cytoskeleton. Therefore, SM22α may be a member of the calponin family of proteins and involved in the regulation of contractile actin filaments and non-contractile actin cytoskeleton. By comprehensively investigating its tissue distribution and regulation by mechanical tension, our present study provides novel data with the following significances.

SM22α is expressed at significant levels in smooth muscle and some non-muscle cells in culture

SM22α is known to be abundantly expressed in adult smooth muscles and has

been applied as a biomarker of differentiated smooth muscle cells [137]. However, SM22α has also been detected in primary fibroblasts and some tumor cell lines. Our broad tissue survey and analysis of several non-muscle cell lines in culture using a highly specific mAb developed against SM22α (Figure 24, 25 and 26) clearly showed that the expression of SM22α is not exclusively specific to smooth muscle cells. Therefore, the use of SM22α as a biomarker for smooth muscle cells or the application of SM22α promoter-driven Cre transgene allele in inducing smooth muscle-specific gene targeting requires more careful consideration and some clear precautions.

On the other hand, the high levels of SM22α expressed in differentiated smooth muscle cells is together with calponin 1 [141] that is a more specific marker for mature and contractile smooth muscle cells [27] Based on numerus studies from multiple laboratories, no calponin 1 expression has been reported in any non-smooth muscle cell types, or dedifferentiated smooth muscle cells in culture. The highly specific expression of calponin 1 in smooth muscle cells demonstrates its value as a more specific biomarker for differentiated smooth muscle cells and the use of the *Cnn1* gene promoter [22] to drive smooth muscle specific gene delivery and Cre recombinase expression.

Mechanoregulation of SM22 protein degradation and gene transcription

In the present study, we report for the first time that the expression and degradation of SM22α is regulated by cytoskeleton tension. Shown in Figure 23, we first detected an effective preservation of SM22α protein in mouse aortic rings by simply maintaining a load of mechanical tension whereas a significant decrease of SM22α occurred in the unloaded control after 6 hrs of incubation at 37 °C. This rapid degradation indicated a role of cytoskeleton tension dependent stability of SM22α.

Previous studies observed that three-day organ culture of rat portal vein in the absence of distension caused lower SM22α synthesis compared with culture under a mechanical load [147] [148]. To test the effect of cytoskeleton tension on the expression of SM22α in non-muscle cells, we demonstrated that the stiffness of culture substrate positively regulates the expression SM22α in primary neonatal mouse skin fibroblasts and representative fibroblast cell lines (Figures 25 and 26).

The results from quantitative RT-PCR on RNA extracted from mouse primary fibroblasts cultured on high and low stiffness substrates further showed that the levels of SM22α mRNA are also positively responsive to the stiffness of culture substrate (Figure 27). Altogether, the results demonstrate that similar to that of calponin 2 regulation, the gene expression and protein degradation of SM22α are both regulated by mechanical tension in the cytoskeleton.

Interrelated regulation and function of SM22α and calponin 2 in fibroblasts

SM22α [149] and calponin are both actin-binding proteins. An interesting result of our study is that the level of SM22α in fibroblasts is related to the presence or absence of calponin 2 (Figure 26). SM22α is decreased in *Cnn2-/-* fibroblasts as compared with that in WT fibroblasts expressing significant amounts of calponin 2. Whereas the significance of the interdependent expressions of SM22α and calponin 2 remains to be investigated, previous studies have reported in smooth muscle cells, SM22α and calponin 1 undergo different mechanisms in modulating actin filaments. Upon PKC phosphorylation, calponin 1-decorated actin stress fibers remain stable in the center of cells, while SM22α-decorated actin fibers undergo rapid reorganization into podosomes [137]. This observation suggests that calponin 1 is more specifically

associated with contractile actin filaments than SM22α, whereas SM22α may function in the non-contractile actin cytoskeleton that is known to be regulated by calponin 2.

Previous studies in our lab have demonstrated in multiple cell types that cytoskeleton tension regulates both expression and degradation of calponin 2 [29] [30]. The promoter of *Cnn2* gene contains a low tension-activated suppressor element that is responsible for the regulation of calponin 2 gene expression by tension built in the cytoskeleton [32]. The mechanoregulation of calponin 2 in cells and stabilization of actin cytoskeleton by calponin 2 suggest that calponin 2 may play dual functions in mediating cell sensing of external forces as well as cellular responses to maintain a physiological equilibrium between cytoskeleton tension and the mechanical environment. Our new finding of the interrelated regulation of SM22α and calponin 2 in responses to cytoskeleton tension suggests a crosstalk between these two actin filament-associated proteins, which is worth further investigating.

Consideration of SM22α as a prototype member of the calponin family

Our present study demonstrated that the protein degradation and gene expression of SM22α is regulated by mechanical tension in the cytoskeleton, suggesting that is may have calponin 2-like regulation and function. This notion is strongly supported by the fact that SM22α, and calponin have similar structures, especially in the regions conserved among the three calponin isoforms (Figure 28). Although the mechanoregulations of SM22α and calponin appear not completely parallel and they may modulate different cellular structure and functions, the excellent alignment of SM22α sequence with the conserved N-terminal and middle regions of calponin suggest not only their common ancestry but also a possibility that SM22α

represents a “mini-calponin” that lacks only the isoform-specific, possibly evolutionarily added, C-terminal variable domain. This structural difference between SM22α and calponin may allow them to provide specific as well as complementary functions. As a mini-calponin, SM22α may represent a prototype member of the calponin family and the absence of the diversity-driven C-terminal variable region may provide an informative experimental system to understand the fundamental core functions as well as the structure-function relationships of calponin and the three isoforms.

CHAPTER 5 - PHYSIOLOGICAL CONTRACTILITY OF CARDIOMYOCYTES IN THE WALL OF MOUSE AND RAT AZYGOS VEIN

(This chapter contains previously published material. See Appendix D)

Abstract

We previously demonstrated the abundant presence of cardiomyocytes in the wall of thoracic veins of adult mouse and rat. The highly differentiated morphology and myofilament protein contents of the venous cardiomyocytes suggested contractile functions. Here we further investigated the contractility of mouse and rat azygos venous rings in comparison with that of atrial strips and ventricular papillary muscle. X-gal staining of transgenic mouse vessels expressing *lacZ* under a cloned cardiac troponin T promoter demonstrated that the venous cardiomyocytes are discontinuous from atrial myocardium and aligned in the wall of thoracic veins perpendicular to the vessel axis. Histology study displayed sarcomeric striations in the venous cardiomyocytes, which indicate an encirclement orientation of myofibrils in the vessel wall. Mechanical studies found that the rings of mouse and rat azygos vein produce strong cardiac type twitch contractions when stimulated with electrical pacing in contrast to the weak and slow smooth muscle contractions induced using 90 mM KCl. The twitch contraction and relaxation of mouse azygos veins further exhibited cardiac type of β-adrenergic responses. Quantitative comparison showed that the contractions of venous cardiomyocytes are slightly slower than that of atrium muscle but significantly faster than that of ventricular papillary muscle. These novel findings indicate that the cardiomyocytes abundant in the wall of rodent thoracic veins possess fully differentiated cardiac muscle phenotype despite their anatomical and functional segregations from the heart.

Introduction

Cardiomyocytes in adult hearts are post-mitotic cells and cannot be recalled into cell cycle [150-153]. Therefore mammalian heart is considered as terminally differentiated organ without self-renewal potential [154]. A general consensus is that the proper differentiation of cardiomyocytes from progenitor cells requires a specific tissue environment, physiological activity, and mechanical load [155-158]. Understanding the requirements for cardiomyocyte differentiation is of major medical importance in exploring myocardial regeneration for the treatment of ischemic heart disease and other terminal heart failures resulting from losses of cardiomyocytes and cardiac muscle.

Twitch-like contractions of thoracic venous vessels have been observed in mammalian species for two centuries, occurring independently of and asynchronously to the heart beats. Later it was demonstrated these contractions are attributed to the presence of striated muscle in the venous wall [159, 160]. Recent publications described more observations in large mammals, including humans, that the atrial myocardium extends into the vena cavae and pulmonary veins to form short 'sleeves' [161], which is considered as a possible source of atrial fibrillation [162-165]. Different in small rodents, myocardium-like tissue was also found as far as in distal regions of extra- and intra-pulmonary veins [166, 167]. However, the physiological feature and function of the venous cardiomyocytes remain to be established.

We recently examined the tissue distribution, ultrastructural features, expression and developmental regulation of myofilament protein isoforms of rodent thoracic venous cardiomyocytes [166]. The results showed that the venous cardiomyocytes are present

in clusters discontinuous and located far from the atrial muscle mass. They exhibit highly differentiated ultrastructure of cardiac muscle characterized by mature sarcomere structures and intercellular connection by intercalated discs. Cardiac-specific isoforms of myofilament proteins are expressed in venous cardiomyocytes and the expression patterns of troponin I (TnI) and troponin T (TnT) isoforms are synchronized with that in the heart during postnatal development.

The apparently fully differentiated morphology and myofilament protein contents of the cardiomyocytes in rodent thoracic veins suggested contractile functions. In the present study, we further investigated the contractility of mouse and rat azygos venous rings. X-gal staining of transgenic mouse vessels expressing *lacZ* under a cloned cardiac TnT promoter demonstrated that the venous cardiomyocytes are aligned in the wall of thoracic veins perpendicular to the vessel axis. Histology study showed sarcomeric striations in the venous cardiomyocytes, which indicate encirclement orientation of myofibrils in the vessel wall. Selective measurements of cardiac and smooth muscle contractions found that the rings of rat azygos veins produce strong cardiac type twitch contractions when stimulated with electrical pacing in contrast to the weak and slow smooth muscle contractions induced using 90 mM KCl. Stimulation with isoproterenol *ex vivo* and *in vivo* demonstrated cardiac-type β-adrenergic responses of the venous cardiomyocytes. Quantitative comparison showed that the twitch contractions of venous cardiomyocytes are slightly slower than that of atrium muscle but significantly faster than that of ventricular papillary muscle. These novel findings indicate that the cardiomyocytes in the wall of rodent thoracic veins possess fully differentiated cardiac muscle phenotype in terms of physiological contractility despite

their anatomical and functional segregations from the heart.

Materials and Methods

All animal procedures were approved by the Institutional Animal Care and Use Committee and were conducted in accordance with the Guiding Principles in the Care and Use of Animals, as approved by the Council of the American Physiological Society.

X-gal staining of transgenic mouse tissues

An *in situ* perfusion protocol was used as described previously [166]. Two- to 3-month-old *cTnT-LacZ* transgenic mice [168] were heparinized for 30 min and anesthetized with intraperitoneal injection of pentobarbital (100 $mg \cdot kg^{-1}$). After opening the thorax cavity, the left ventricle were cannulated to perfuse the circulatory system with filtered Krebs-Henseleit solution (118 mM NaCl, 25 mM $NaHCO_3$, 4.7 mM KCl, 12 mM KH_2PO_4, 2.25 mM $MgSO_4$, 2.25 mM $CaCl_2$, 0.32 mM EGTA, 15 mM D-glucose, 2 mM sodium pyruvate, oxygenated with 5%CO_2 and 95% O_2 at 37°C, pH7.4) using a peristaltic pump (Bio-Rad, Hercules, CA) at a flow rate of 4 $mL \cdot min^{-1}$. Blood was flushed out from incisions made in the lung. Perfusion pre-fixation was followed using filtered 3.7% formaldehyde in Phosphate-buffered saline (PBS) until the visceral tissues hardened. Krebs-Henseleit solution was briefly perfused to remove excess fixative before perfusion with X-gal substrate solution (0.1% 5-bromo-4-chloro-indolyl-galactopyranoside, 5 mM potassium ferrocyanide, 0.02% IGEPAL (Sigma-Aldrich, St. Louis, MO, USA), 0.01% sodium deoxycholate in PBS) at 37°C. Color development was monitored, and when necessary, permitted to progress further by dissecting out the heart/lung-aorta/azygos vein tissue block and incubating with gentle agitation in X-gal substrate solution at 37°C. After three 5 min rinses in PBS at room temperature, the

tissue block was post-fixed in 3.7% formaldehyde at 4°C overnight. Whole-mount tissue samples were imaged under a dissection scope and photographed.

Hematoxylin and Eosin Staining

Systemic *in situ* perfusion fixation of adult wild-type mice was performed for 1 hour as described above. A tissue block containing aorta and azygos vein was dissected out and further fixed in 3.7% formaldehyde overnight to obtain better preservation of the venous structure. After dehydration in 30% sucrose for 48 hours, the tissue block was embedded in optimum cooling temperature (O.C.T.) compound and rapidly frozen in liquid nitrogen for cryo-sectioning. Cross-sections of 10 μm thickness were cut using a Leica CM 1950 cryostat. The sections were stained with hematoxylin and eosin [169], examined using a Zeiss Axiovert 100 microscope, and photographed.

SDS-polyacrylamide gel electrophoresis (PAGE) and Western blotting

Adult mouse azygos vein and heart tissues were collected immediately postmortem and processed for SDS-PAGE or frozen at -80°C until use. Using a high-speed mechanical homogenizer, the tissues were rapidly homogenized in Laemmli SDS-PAGE sample buffer containing 2% SDS to prevent enzymatic degradation of proteins, heated at 80°C for 5min, and clarified by centrifugation in a microcentrifuge at top speed for 5 min. The protein extracts were resolved on 14% Laemmli gel with an acrylamide:bisacrylamide ratio of 180:1. Atrial and ventricular proteins were loaded at 40 μg/ well, vessel rings all dissolved in 25 μl SDS sample buffer and 3 μl loaded. Loading volume of every sample was later adjusted by densitometry measurement of actin. The gels were stained with Coomassie Brilliant Blue R250 to reveal the protein

bands. Duplicate gels were electrically blotted to nitrocellulose membranes using a semidry transfer apparatus (Bio-Rad, Hercules, CA).

After blocking in Tris-buffered saline (TBS) containing 1% bovine serum albumin (BSA), the membranes were incubated with monoclonal antibodies (mAbs) CG1 (from University of Iowa, 1:2000 dilution) against smooth-muscle α-tropomyosin, CGβ6 (from University of Iowa, 1:4000 dilution) against smooth-muscle β-tropomyosin, CT3 (1:4000 dilution) against cardiac TnT and TnI-1 (1:1000 dilution) against cardiac TnI at 4°C overnight [170, 171]. After high stringency washes in TBS containing 0.5% Triton X-100 and 0.05% SDS, the membranes were incubated with alkaline phosphatase-conjugated anti-mouse IgG second antibody (Santa Cruz Biotechnology, Inc., Santa Cruz, CA) at room temperature for 1 hr, washed again and developed in 5-bromo-4-chloro-3-indolylphosphate/nitro blue tetrazolium substrate solution to visualize the protein bands recognized by the mAbs.

Phosphoprotein staining

To examine protein phosphorylation, SDS-PAGE gels were stained using Pro-Q Diamond reagents (Invitrogen) following the manufacturer's instruction. Phosphoprotein markers (PeppermintStick^{TM}, Invitrogen) were used as control. Florescence imaging was performed using a Typhoon 9210 scanner (GE Healthcare) with excitation at 532 nm and recording of emission at 580 nm to detect and quantify the phosphoprotein bands.

In vivo treatment with isoproterenol was carried out in adult mice to maximize protein kinase A-catalyzed phosphorylation of cardiac myofilament proteins [172]. Intraperitoneal injection of isoproterenol (0.2 mg·kg^{-1}) was applied under light

anesthesia using isoflurane while the heart rate was monitored via surface EKG. As soon as the increase in heart rate reached a plateau, the mouse was euthanize and the heart and thoracic veins were isolated immediately and rapidly processed into SDS-PAGE samples as above to minimize the effect of endogenous phosphatases.

Tissue preparation for contractility measurements

C57BL/6 mice and Sprague Dawley rats were used in this study. Thirty minutes after intraperitoneal injection of 100 units (mice) or 300 units (rats) of heparin, the animal was anesthetized with intraperitoneal injection of pentobarbital sodium (100 $mg \cdot kg^{-1}$ body weight). The heart and azygos vein were rapidly isolated and placed in Krebs-Henseleit buffer continuously gassed with 95% O_2 and 5% CO_2 at room temperature.

Atrial muscle strips from mice were prepared by clamping the top and tying up the bottom of the left atrium with 6-0 sutures for mounting to force measurement apparatus.

The anterior papillary muscle of the left ventricle from mice was prepared by dissecting together with the tendon at one end and a small portion of the ventricular wall tissue at the other end [173]. Both the tendon and ventricular-wall ends were tied with 6-0 sutures for mounting to force measurement apparatus.

Azygos vein was trimmed to remove connective tissues and cut into 1 mm rings for mounting to force measurement apparatus using steel wire hooks. Special care was taken to avoid stretch or tissue damage. Rings from the proximal and distal portions of 4-week rat azygos vein were used for comparison of smooth muscle and cardiac-like contractility patterns. Rings from the proximal portion of mouse azygos vein were used

for contractility measurement in comparison with mouse atrial strips and ventricular papillary muscles. 3-week old mice were chosen for comparison of contractility pattern, for the advantage of more effective superfusion than adult thicker tissue. We have previously shown that the expression of cardiac muscle proteins in venous cardiomyocytes is synchronized with that in the atrial and ventricular muscles during development [166], justifying the use of tissues from young mice at the same age for contractility comparisons. However, adult mice were preferred in *ex vivo* isoproterenol treatment, in consideration of the mature development of β receptors.

Selective measurements of cardiac muscle and smooth muscle contractions

Ring of rat azygos vein was mounted in a thermostatically controlled chamber with continuous perfusion of oxygenated Krebs-Henseleit buffer at 3 $mL \cdot min^{-1}$. The tissues were allowed to equilibrate for 20 min with electrical pulse stimulations at 0.1 Hz. The assays were carried out at 27°C. Isometric contractile force was measured using Aurora Scientific force transducer Model 403A and recorded using Chart 5 software (ASI, Aurora Scientific).

Rings from proximal and distal portions of rat azygos vein were electrically paced at 0.1 Hz in physiological Kreb's solution to induce cardiac muscle contractions. The buffer was then switched to a modified Kreb's buffer containing 90 mM KCl [174, 175] for 2 min to generate smooth muscle contraction while the cardiomyocytes were paralyzed despite continuing electrical pacing at 0.1 Hz. Perfusion was then returned to normal Kreb's buffer and the recovery of electrically stimulated cardiac muscle contraction was recorded.

Comparison of contractility of azygos vein and cardiac muscle preparations

Comparison of the contractility of azygos ring, atrial strip and papillary muscle was performed at 27°C under 0.1 Hz pacing. The left atrial strip and papillary muscle were vertically mounted and azygos ring was horizontally mounted in three different organ baths with continuous perfusion oxygenated Kreb's buffer. Isometric contractile force was measured using Aurora Scientific force transducers: Model 403A for azygos ring and Model 300B for atrial strip and papillary muscle. The stimulating voltage was set at 2X threshold voltage for each tissue tested [173].

The mounted muscle tissues were adjusted to optimal length after 20 min equilibration under 0.1 Hz electrical pacing. The muscles were then paced at 1 Hz and tested for the effects of 3 nM, 10 nM and 50 nM isoproterenol on the development of isometric force and contractile velocities. The isoproterenol tests were performed under dimed light at 32 ˚C. Each assay was completed in 1 hour to ensure tissue viability.

Data analysis

Densitometry analysis of SDS-PAGE gel, Pro-Q stained gel and Western blot images scanned at 600 dpi was performed using NIH Image software version 1.61. Quantitative data were documented as mean ± SEM. The statistical significance of difference between the mean values was analyzed using paired Student's t-test or two-way ANOVA.

RESULTS

Abundant cardiomyocytes in the wall of mouse thoracic veins aligned perpendicular to the vessel axis

Reported previously [166], in the *cTnT-LacZ* transgenic mice, the *LacZ* reporter gene is driven by a cloned promoter of rat cardiac TnT gene, a cardiac muscle-specific

gene, to indicate differentiated cardiomyocytes. The X-gal staining results in Figure 29A revealed abundant cardiomyocytes in the wall of thoracic veins including superior vena cava (SVC) and azygos vein, but not arteries such as the aorta. The X-gal-stained cardiomyocytes are distributed discontinuously from the heart and aligned perpendicular to the vessel axis longitudinally encircling the vessel wall.

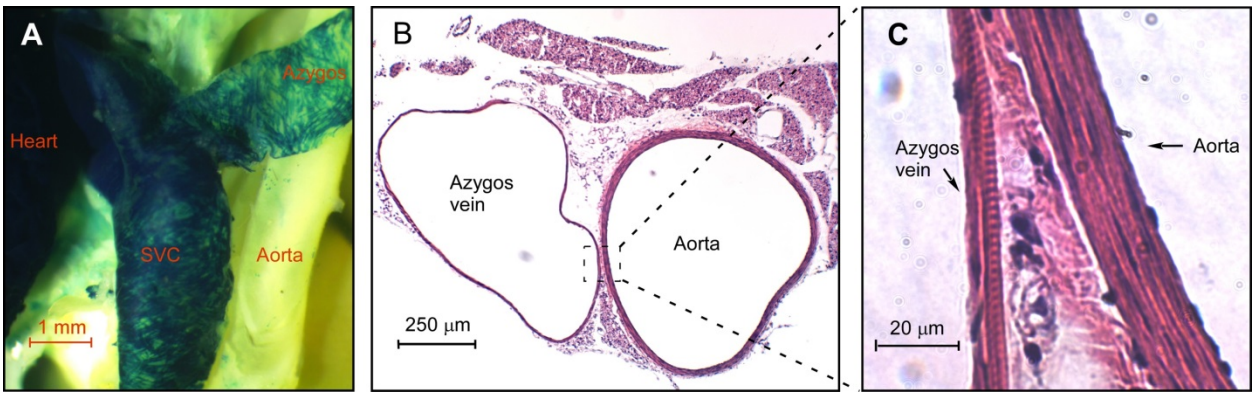

Figure 29. Abundant cardiomyocytes in the wall of mouse thoracic veins aligned perpendicular to the vessel axis. *A*: X-gal staining of thoracic vessels of adult transgenic mouse bearing a β-galactosidase reporter gene driven by a cloned cardiac TnT promoter demonstrated abundant LacZ-expressing cells in the wall of superior vena cava (SVC) and azygos vein, but not aorta. The venous cardiomyocytes are distributed discontinuously from the heart. The venous cardiomyocytes are aligned perpendicular to the vessel axis longitudinally encircling the vessels. *B* and *C*: Low and high-magnification images of H.E. staining of cross section of adult mouse azygos vein and aorta. The high-magnification micrograph demonstrated clear striation in the venous cardiomyocytes, reflecting sarcomeric structures, in clear contrast to the smooth muscle cells in the aortic wall. The striation pattern also indicates the longitudinal alignment of venous cardiomyocytes encircling the vessel.

To further examine the histological structure of the vessel walls, H.E. staining of cross-sections of azygos vein and aorta from wild-type adult mice was performed (Figures 29B and 29C). The high-magnification micrograph in Figure 29C showed clear sarcomeric striations in the venous cardiomyocytes, reflecting a mature myofibrils structure that is in sharp contrast to the smooth muscle layers in the aortic wall. The direction of the striations further indicated the orientation of myofibrils and the longitudinal alignment of venous cardiomyocytes encircling the vessel wall.

The orientation of venous cardiomyocytes encircling the vessels implicated a

correlation to the lumen pressure and wall tension, and supports the approach of investigating physiological contractility using vessel rings.

Abundant presence of cardiomyocytes in the proximal portion but absent in the distal portion of azygos vein

Using mAbs recognizing cardiac TnT (CT3 [176]) and cardiac TnI (TnI-1 [73]), two cardiac myofilament-specific protein [55], SDS-PAGE and Western blots in Figure 30 detected high levels of cardiac TnT and cardiac TnI in the proximal portion of mouse azygos vein, similar to that in atrial and ventricular muscles. In contrast, the distal portion of mouse azygos vein and aorta express high levels of smooth muscle tropomyosins without a detectable level of cardiac troponin (Figure 30). The results indicate the distribution of cardiomyocytes in the proximal portion of azygos vein and the anticipated smooth muscle contents in the distal portion of azygos vein.

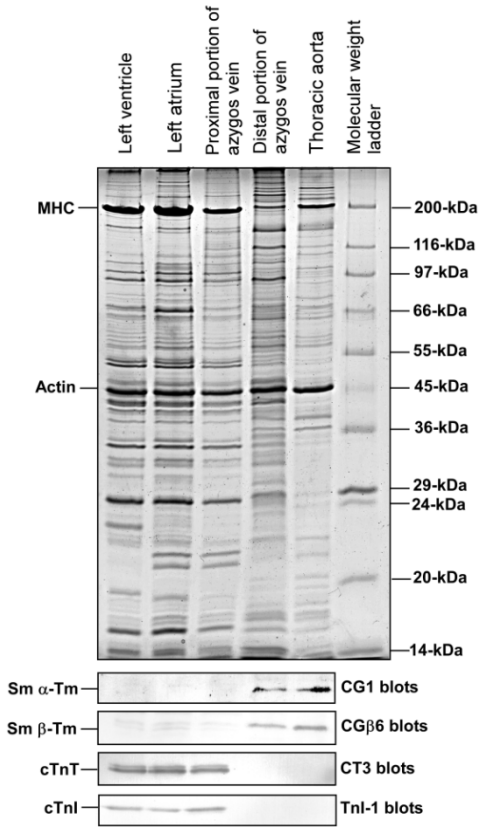

Figure 30. Cardiac myofilament proteins are highly expressed in the proximal but not the distal portion of adult mouse azygos vein. SDS-PAGE and Western blots using mAbs CG1 against smooth-muscle α-tropomyosin (Sm α-Tm), CGβ6 against smooth-muscle β-tropomyosin (Sm β Tm), CT3 against cardiac TnT (cTnT) and TnI-1 against cardiac TnI (cTnI) detected high levels of cardiac TnT and cardiac TnI in the proximal portion of mouse azygos vein, in sharp contrast with the distal portion of azygos vein and thoracic aorta that express high levels of smooth muscle tropomyosin with no cardiac troponin was detectable. Ventricular and atrial muscle samples were examined as control.

Consistent with the biochemical analysis of muscle type-specific protein contents, contractility measurement of rat azygos rings from proximal and distal portion showed different contractile properties. Azygos ring from proximal portion was able to produce cardiac-type twitch contraction upon electrical pacing (Figure 31A). Switching to superfusion buffer containing 90 mM KCl paralyzed the twitch contraction of the cardiomyocytes as expected while generated a weak and slow smooth muscle type of contraction. Once the superfusion was switched back to physiological Kreb's solution, the cardiac type of contractility resumed (Figure 31A).

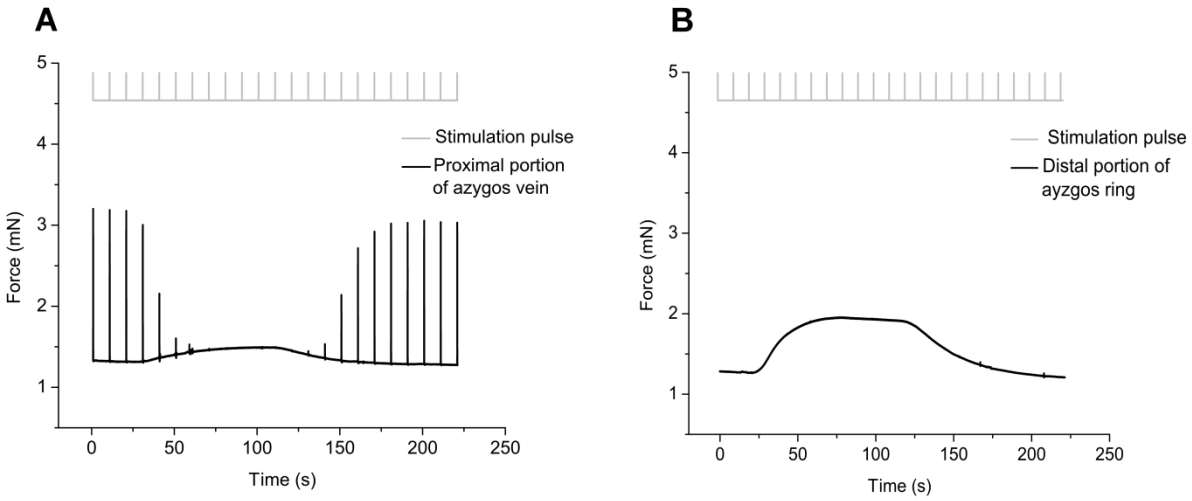

Figure. 31 Distinct contractile properties of the proximal and distal portions of rat azygos vein. *A*: The proximal portion of rat azygos vein produced strong cardiac type twitch contractions when stimulated with electrical pacing. Switching to superfusion buffer containing 90 mM KCl inhibited the twitch contraction of the cardiomyocytes while a weak and slow smooth muscle contraction was induced. Returning to normal Kreb's buffer resumed the cardiac type contractility. *B*: In contrast, the distal portion of rat azygos vein did not respond to electrical pacing but generates a typical smooth-muscle type contraction when superfused with buffer containing 90 mM KCl, which ceased after returning to normal Kreb's buffer.

In contrast, the distal portion of rat azygos vein did not respond to electrical pacing but produced a typical smooth-muscle type contraction when superfused with buffer containing 90 mM KCl, which ceased after the superfusion was returned to normal Kreb's buffer (Figure 31B). The data of selective activation of cardiac and

smooth muscle contractions clearly demonstrate the presence of physiologically functional cardiomyocytes in the proximal portion of azygos vein.

Heart-like β-adrenergic response of cardiomyocytes in mouse azygos vein.

When stimulated with increment concentrations of isoproterenol, the force development (Figure 32A), contractile (+dF/dt, Fig. 32B) and relaxation (–dF/dt, Figure 32C) velocities of azygos ring, atrium strip and ventricular papillary muscle were all positively responsive with significant increases. The increasing amplitudes of azygos ring and atrial strip groups were significantly higher than that of papillary muscle group, possibly reflecting more effective superfusion of thinner tissue preparations.

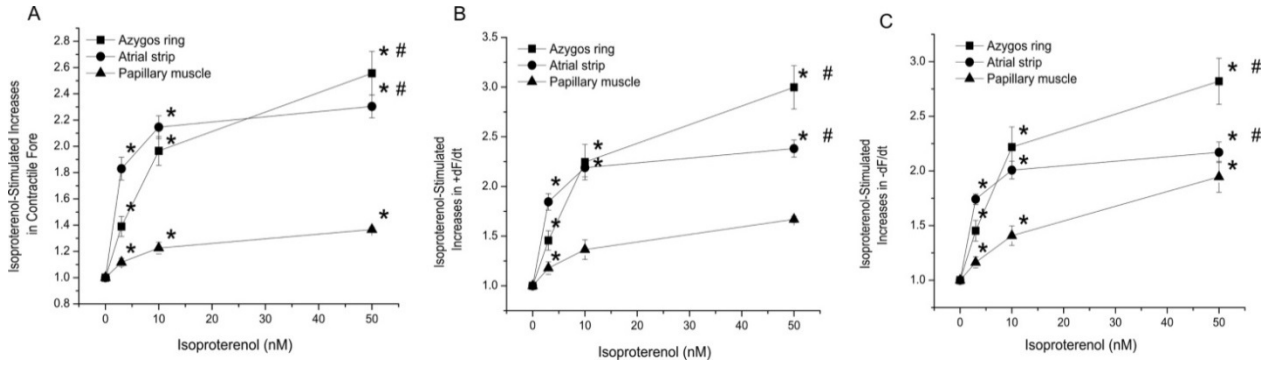

Figure 32. Heart-like β-adrenergic response of cardiomyocytes in mouse azygos vein. Force development (*A*), contractile (+dF/dt, *B*) and relaxation (–dF/dt, *C*) velocities of azygos ring, atrium strip and ventricular papillary muscle all exhibited positive responses upon the treatment of increment concentrations of isoproterenol. **P<0.05 versus* the value at the immediate lower concentration of isoproterenol; *#P<0.05 versus* the papillary muscle group; n = 8 for azygos veins, n = 3 each for atrium and papillary muscle groups.

Pro-Q Diamond stained SDS-gel demonstrated significantly increased phosphorylation of myosin binding protein C and cardiac TnI *in vivo* upon isoproterenol treatment (Figure 33). The results support the *ex vivo* contractility study that showed positive responses of force development and contractile and relaxation velocities to isoproterenol stimulation. The phosphorylation of myosin binding protein C and cardiac TnI did not show significant difference between azygos vein, atrium and ventricle groups

(Figures 33B and 33C). These results indicate heart-like β-adrenergic-protein kinase A signaling in the venous cardiomyocytes.

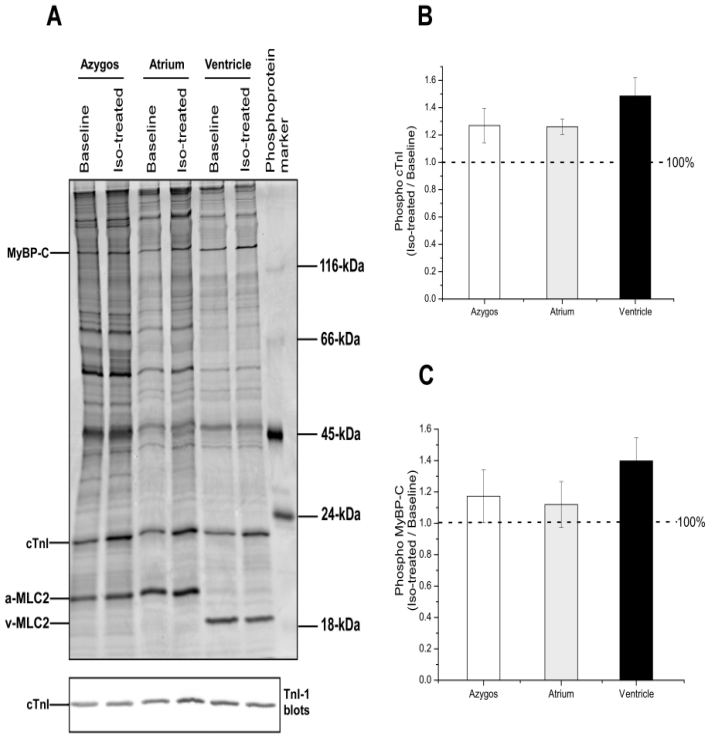

Figure 33. Similar isoproterenol-induced *in vivo* phosphorylation of myosin binding protein C and cardiac TnI in adult mouse azygos vein, atrial and ventricular muscles. *A*: Pro-Q Diamond stained SDS-gel showed that phosphorylation of myosin binding protein C (MyBP-C) and cardiac TnI (cTnI) was significantly increased upon isoproterenol treatment *in vivo*. Total cardiac TnI was quantified from Western blot using mAb TnI-1 as protein input control. *B* and *C*: Densitometry quantification of the Pro-Q gel for phosphorylated MyBP-C and cTnI. Normalized to the cardiac TnI Western blot, there was no significant difference in the levels of isoproterenol-stimulated phosphorylation of MyBP-C and cTnI in the azygos vein, atrium and ventricle samples. n = 3 each for azygos vein, atrium and ventricle groups.

Contraction and relaxation of azygos cardiomyocytes are slightly slower than that of atrial muscle but significantly faster than ventricular papillary muscle

The comparison between representative twitch contractions of azygos ring, atrium strip and ventricular papillary muscle demonstrated that the atrium muscle contracts and relaxes the fastest, papillary muscle the slowest, and the azygos cardiomyocytes is in between (Figure 34A). Quantitative study of the time parameters demonstrated that azygos cardiomyocytes contracted slightly slower than that of atrial muscle but significantly faster than ventricular papillary muscle (Figure 34B). The results suggest that the venous cardiomyocytes are similar but not identical to atrial muscle in contractile properties.

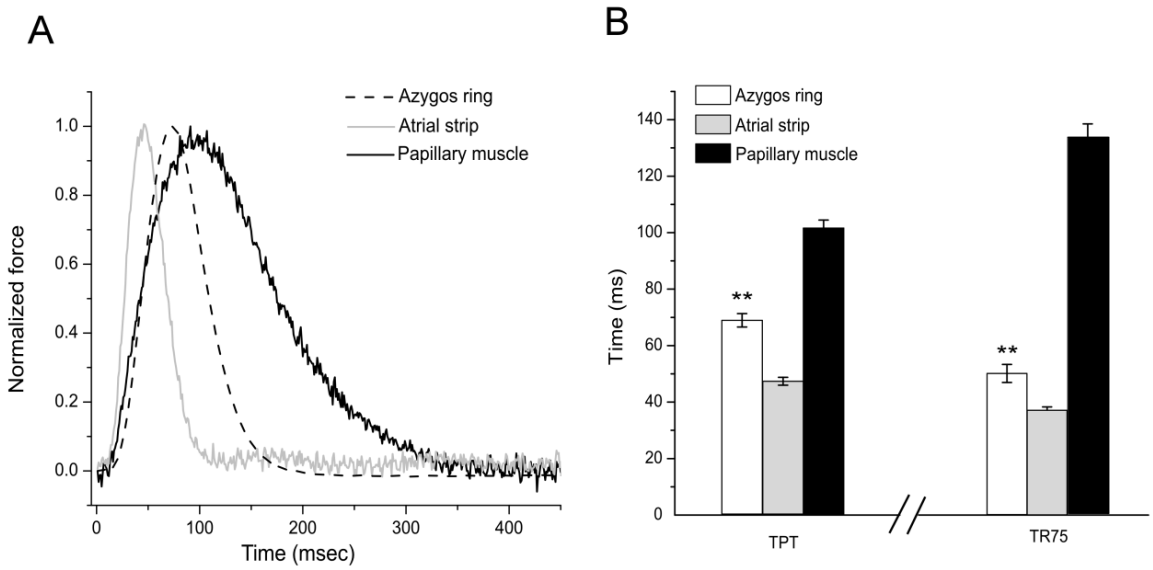

Figure. 34. Time parameters of twitch contractions of azygos vein, atrium strips and ventricular papillary muscle from 3-week mice. *A*: Comparison of representative twitch traces of azygos ring, atrium strip and papillary muscle. *B*: Time parameters of contraction and relaxation of azygos ring, atrium strip and papillary muscle showed that the azygos ring contracted slightly slower than that of atrial muscle but significantly faster than ventricular papillary muscle. TPT: time to peak tension; TR75: time to 75% relaxation. ***P<0.01 versus* papillary muscle and atrium strip.

Discussion

We recently demonstrated the abundant presence of cardiomyocytes in the wall of thoracic veins of adult mouse and rat. Despite many revisits, the developmental origin of the thoracic venous cardiomyocytes, their differentiation state and their physiological function are not yet understood. The highly differentiated morphology and myofilament protein contents of the venous cardiomyocytes [166] suggested contractile functions. We further investigated in the present study the contractility of mouse and rat azygos venous rings in comparison with that of atrial strips and ventricular papillary muscle. The results contributed several interesting observations.

Distribution and orientation of the venous cardiomyocytes suggest a potential function in regulating vessel diameter

Ectopic beats originated from the atrial sleeves are implicated as a possible source of atrial fibrillation [162] [163] [164] [165]. However, the anatomical discontinuity

of the venous cardiomyocyte from the heart mass (Figure 29A) distinguishes the venous cardiomyocytes studied here from the extension of cardiac muscle in true atrial sleeves and does not support a role in generating arrhythmia.

A few hypotheses have been proposed for the physiological function of the venous cardiomyocytes, one of which is that these muscle cells may function as a "throttle valve" action to prevent backflow of blood during atrial systole and play a role in regulation of pulmonary blood flow [177]. Some observations, including the encirclement orientation of myofibrils in the cardiomyocytes in vessel wall (Figure 29), are in favor of this hypothesis. Other supports include that the electrical propagation of cardiomyocytes in rat pulmonary veins is toward the lung [178]; and the occurrence of intercalated discs between venous cardiomyocytes enables them to contract in synchronization [166, 178]. If this mechanism exists, it would be more necessary for the rodents rather than the larger mammals, that have abundant cardiomyocytes in the pulmonary vein [166, 167], possibly due to their very high heart rate that requires assistance with filling of the heart during the short diastoles.

Venous cardiomyocytes are physiologically responsive to β-adrenergic regulation

The β-adrenergic signaling pathway plays a critical role in the regulation of myocardial contractility and heart function. Activation of β-adrenoceptors on the plasma membrane of cardiomyocytes by catecholamines stimulates adenylyl cyclase and cAMP production, which in turn leads to activation of cAMP-dependent protein kinase (PKA) and phosphorylation of a multitude of intracellular substrates in the Ca^{2+} handling system and myofilaments, such as cardiac TnI and myosin-binding protein C [179]. In the present study we showed that stimulation with isoproterenol *in vivo* and *ex vivo*

produced cardiac-like β-adrenergic responses in the venous cardiomyocytes, indicating a physiological regulation.

Our *ex vivo* contractility study shows that azygos ring, atrial strip and papillary muscle groups are all responsive to the increment concentration of isoproterenol, producing increasing contraction force and velocity. Nevertheless, the increasing amplitudes of azygos ring and atrial strip groups were similar and significantly higher than that of the papillary muscle group (Figure 32). This difference may be attributed to the efficiency of superfusion in the *ex vivo* contractility study. A sufficient nutrient and oxygen supply is critical for the function of *ex vivo* myocardial muscle preparations [173]. β-Adrenergic stimulation of the muscle preparations increases the energy expenditure and demand of the contractile machineries in cardiomyocytes. Papillary muscles are the thickest and most compact in comparison with venous rings and atrial strips, thus the energy shortage under superfusion conditions would be more apparent, especially at the treatment of higher concentration of isoproterenol. Supporting this hypothesis other than intrinsic difference among the three types of cardiomyocytes in β-adrenergic responsiveness, *in vivo* isoproterenol treatment produced similar responses as shown by the similarly increased levels of phosphorylation of myofilament proteins (Figure 33) in azygos vein, atrial and ventricular muscles.

The results of both *ex vivo* and *in vivo* isoproterenol treatment demonstrate the fully developed β-adrenergic signaling in the venous cardiomyocytes, supporting their functional state of physiological maturity.

Venous cardiomyocytes are similar to atrial cardiac muscle in contractility and myosin content

Comparison of representative twitch traces showed that the contractions of venous cardiomyocytes are slightly slower than that of atrium muscle strips but significantly faster than that of ventricular papillary muscle (Figure 34). Our previous study demonstrated identical patterns of troponin and myosin heavy chain isoform expressions in mouse and rat thoracic vein cardiomyocytes and atrial and ventricular cardiac muscles, but suggested an expression of atrial specific isoform of myosin light chain (MLC) 2 in venous cardiomyocytes [166], which might contribute to the similar contractile features of azygos rings and atrial strips.

In cardiomyocytes, sarcomeric contraction results from the Ca^{2+}-regulated cross-bridge interactions between the myosin motor and actin filament. Ca^{2+}-binding to troponin allows myosin heads to form strong cross-bridges with the actin filament and activating the myosin ATPase. The energy from ATP hydrolysis displaces the thin filaments relative to the thick filaments and leads to sarcomere shortening and muscle contraction [180]. Myosin light chain 1 and MLC2 are key components of the myosin motor [181]. The expression of atrial and ventricular isoforms of MLC2 is regulated in a muscle type specific manner in the heart. The expression of same MLC2 in atria and venous cardiomyocytes may represent their similarity in the cellular backgrounds for contractility.

The different isoforms as well as phosphorylation levels of MLC2 play critical roles in modulating cross-bridge cycling and Ca^{2+} sensitivity of the myofilament in force development [182, 183]. Our phosphoprotein staining data in Figure 33 showed that MLC2 phosphorylation was similar in all of the three muscle types and positively

responded to isoproterenol treatment. This observation further supports that the MLC isoforms may be a key contributor to the similarity between azygos cardiomyocytes and atrial muscle as well as the difference from ventricular muscle.

Origin, differentiated phenotype, and maintenance of venous cardiomyocytes

Plausible findings in the present study demonstrate that the abundant cardiomyocytes in the wall of rodent thoracic veins possess fully differentiated cardiac muscle phenotype despite their anatomical and functional segregation from the heart. Cell lineage tracing studies demonstrated in mice that the cardiomyocytes in pulmonary veins are not originated from atrial cells but formed by differentiation of pulmonary mesenchymal cells [184]. The cardiomyocyte content in the thoracic veins is prominent in the embryo and recedes progressively after birth [178]. We have previously showed that the developmental regulation of myofilament protein expression is synchronized in the venous cardiomyocytes and the heart [166]. These facts indicate that the differentiation of the cardiac phenotype in the adult venous cardiomyocytes is pre-determined by intrinsic lineage commitment of progenitor cells. On the other hand, the effective maintenance of fully differentiated phenotype of the cardiomyocytes in the venous walls of adult mouse and rat indicates the feasibility of supporting the physiologically differentiated cardiomyocyte in a non-heart tissue environment. Such environmental determinants deserve more future studies that would lead to a better understanding of myocardial regeneration and repair.

CHAPTER 6 - CONCLUSIONS

For the first time, this work has demonstrated that the development of atherosclerosis in *ApoE-/-* mice can be attenuated via modulating the motility and other actin cytoskeleton-based functions in macrophages.

The results in Chapter 2 revealed that ApoE has weak immunogenicity possibly due to predicted immune tolerance of B lymphocytes to plasma proteins. However, ApoE can potentially serve as an effective carrier for delivering other immunogens such as the Tx segment. Although the combination of ApoE with another weak immunogen, *i.e.*, the C-terminal segment of calponin 2 did not increase the immunogenicity of either of the two components, the fact that mouse ApoE can be recognized by the immune system of mouse as an effective carrier intrigued us to test a novel approach to generating useful antibodies by immunizing *ApoE*-KO mice to avoid the intrinsic issue of immune tolerance in developing antibody tools against plasma proteins like ApoE, especially from the species same as the host to be immunized.

ApoE-/- mice spontaneously develop atherosclerotic lesions on regular diet due to disorders of cholesterol metabolism and dramatically increased plasma cholesterol level. The study in Chapter 3 demonstrated that either global or myeloid-cell specific deletion of calponin 2 from *ApoE-/-* mice can significantly attenuated the development of atherosclerosis. The fact that myeloid cell-specific KO of *Cnn2* has the same or stronger effect in comparison with that of global KO indicates that the therapeutic effect was primarily via the function of myeloid cells. More *in vitro* experiments revealed the underlying cellular and molecular mechanisms: Deletion of calponin 2 significantly increased the motility of macrophages and compensated for the impaired motility of

foam cells, while there is no difference between WT and *Cnn2* KO macrophages in regard of lipid ingestion. Immunohistochemistry study on the sections at aortic root further found that attenuated atherosclerotic lesions is associated with reduced macrophage infiltration, indicating the enhanced motility by calponin 2 deletion facilitates macrophages and the derived foam cells to migrate out the atherosclerotic lesions and diminish inflammatory response. The investigation of cytokine profiles showed that calponin 2-null macrophages produced less pro-inflammatory cytokines than that of WT macrophages, and the up-regulation of pro-inflammatory cytokines in foam cells was also attenuated by the deletion of calponin 2. The less activation of *Cnn2-/-* macrophages and foam cells is likely related to the weakened adhesion by deletion of calponin 2. Calponin 2 is an actin-binding protein and regulates the dynamics of actin cytoskeleton. Deletion of calponin 2 from macrophages results macrophage less adhesive and less activated in inflammatory responses along with elevated motility. These functional changes of macrophages play a therapeutic role in treatment and prevention of atherosclerosis. These data provide evidence that changes in myosin motor-based cytoskeleton dynamics and cell adhesion alter macrophage activation, implicating a potentially novel therapeutic target for the treatment and prevention of atherosclerosis and other inflammatory diseases.

Based on the data presented in Chapter 3, the regulation of cytoskeleton is known to play a critical role in cell functions. The studies in Chapter 4 further addressed another calponin family related protein: SM22α, in the mechanoregulation of actin cytoskeleton. We report for the first time that the expression and degradation of SM22α is regulated by the mechanical tension of cytoskeleton. SM22α is abundantly

expressed in mature smooth muscle, and thus was considered as a biomarker for smooth muscle differentiation. However, recent research publications suggested that SM22α is also associated with non-contractile actin filaments. Consistently, our data demonstrated that SM22α may play a critical role in mechanical force transduction of actin cytoskeleton in fibroblasts. Chapter 3 and Chapter 4 together demonstrated that the calponin family proteins interactively regulate the contractile and non-contractile actin filaments in smooth muscle and non-muscle cells with impacts on many cell motility-based functions.

Chapter 5 documented the physiological contractility of cardiomyocytes in the wall of mouse and rat azygos vein. We found that there is abundant presence of mature cardiomyocytes in the wall of thoracic veins of adult mouse and rat. The venous cardiomyocytes demonstrated cardiac muscle type of twitch contractions similar to that in the heart, indicating a fully differentiated phenotype. The co-existence of cardiac muscle and smooth muscle in these vessel walls provides a novel model to study the differentiation of cardiac myocytes and the impact of the mechanical tissue environment.

In conclusion, my Ph.D. dissertation research extensively studied the mechanical force and actin cytoskeleton-based regulation of cell functions, especially the regulation of macrophage's function in the pathogenesis of atherosclerosis. These experimental data have made valuable contributions to the understanding of cell-mechanical force regulation and motility with many applications in future cardiovascular and cell physiological research as well as the development of new treatment for human diseases.

APPENDIX A

IACUC Protocol Approval Letter

WAYNE STATE UNIVERSITY

INSTITUTIONAL ANIMAL
CARE AND USE COMMITTEE
87 E. Canfield, Second Floor
Detroit, MI 48201-2011
Telephone: (313) 577-1629
Fax Number: (313) 577-1941

ANIMAL WELFARE ASSURANCE # A3310-01

PROTOCOL # A 09-02-13

Protocol Effective Period: October 29, 2013 – September 30, 2016

TO: Dr. J.-P. Jin
Physiology
5374 Scott Hall

FROM: Lisa Anne Polin, Ph.D. Lisa Anne Polin
Chairperson
Institutional Animal Care and Use Committee

SUBJECT: Approval of Protocol # A 09-02-13

"Role of calponin in the pathogenesis of atherosclerosis"

DATE: October 29, 2013

Your animal research protocol has been reviewed by the Wayne State University Institutional Animal Care and Use Committee, and given final approval for the period effective **October 29, 2013** through **September 30, 2016**. The listed source of funding for the protocol is **WSU-SOM Start up funds**. The species and number of animals approved for the duration of this protocol are listed below.

Species	Strain	Qty.	USDA Cat.
MICE	C57BL/6, both sexes, 20-30 mg	60	B
MICE	C57BL/6, both sexes, 20-30 mg	60	C
MICE	ApoE-KO gene targeted, C57BL/6 background, male and female 20-30 g	2	B
To be purchased			
MICE	H2-KO gene targeted, C57BL/6 background (to be bred), both sexes	180	B
MICE	H2-KO gene targeted, C57BL/6 background (to be bred), both sexes	180	C
MICE	ApoE-KO gene targeted, C57BL/6 background, both sexes	180	B
MICE	ApoE-KO gene targeted, C57BL/6 background, both sexes	180	C
MICE	H2/ApoE double KO gene targeted, C57BL/6 background both sexes	180	B
MICE	H2/ApoE double KO gene targeted, C57BL/6 background both sexes	180	C
MICE	Wild type littermates, both sexes	180	C
MICE	Wild type littermates, both sexes	180	B
To be bred in-house			

Be advised that this protocol must be reviewed by the IACUC on an annual basis to remain active. Any change in procedures, change in lab personnel, change in species, or additional numbers of animals requires prior approval by the IACUC. Any animal work on this research protocol beyond the expiration date will require the submission of a new IACUC protocol form and full committee review.

The Guide for the Care and Use of Laboratory Animals is the primary reference used for standards of animal care at Wayne State University. The University has submitted an appropriate assurance statement to the Office for Laboratory Animal Welfare (OLAW) of the National Institutes of Health. The animal care program at Wayne State University is accredited by the Association for Assessment and Accreditation of Laboratory Animal Care International (AAALAC).

APPENDIX B

NCBI database for calponin isoforms analyzed (Figure 2)

The NCBI database accession numbers of the sequences analyzed are: African clawed frog calponin 1, NP_001080753.1; African clawed frog calponin 2, NP_001085014.1; African clawed frog calponin 3, NP_001080482.1; Black flying fox calponin 1, ELK17809. 1; Black flying fox calponin 2, ELK19295.1; Black flying fox calponin 3, ELK05808.1; Brandt's bat calponin 1, EPQ04681.1; Brandt's bat calponin 2, EPQ08061.1; Brown tree snake calponin 2, JAG68493.1; Cattle calponin 1, NP_001039844.1; Cattle calponin 2, AAI03381.1; Cattle calponin 3, NP_001033268.1; Channel catfish, AHH43034.1 ; Chicken calponin 1, NP_990847.1; Chicken calponin 2, NP_001135728.1; Chimpanzee calponin 1, NP_001267033.1; Chimpanzee calponin 2, JAA13388.1; Chimpanzee calponin 3, JAA44470.1; Chinese hamster calponin 1, EGV96164.1; Chinese hamster calponin 2, EGV99480.1; Chinese hamster calponin 3, EGW11625.1; Croaker calponin 1, KKF32470.1; Croaker calponin 2, KKF29575.1; Croaker calponin 3, KKF23334.1; Damara mole calponin 1, KFO28782.1; Damara mole calponin 2, KFO28912.1; Damara mole calponin 3, KFO26533.1; Eastern diamondback rattlesnake calponin 2, AFJ49586.1; Ferret calponin 1, NP_001297140.1; Green turtle calponin 1, EMP37252.1; Green turtle calponin 3, EMP30806.1; Human calponin 1, NP_001290.2; Human calponin 2, AAI48265.1; Human calponin 3, AAB35752.1; King cobra calponin 3, ETE62831.1; Marmoset calponin 3, JAB48100.1; Mouse calponin 1, AAI38864.1; Mouse calponin 2, EDL31614.1; Mouse calponin 3, AAH85268.1; Mouse-eared bat calponin 1, ELK28732.1; Mouse-eared bat calponin 2, ELK29427.1; Mouse-eared bat calponin 3, ELK30701.1; Naked mole calponin 1, EHA97296.1; Naked mole calponin 2, EHB16944.1; Naked mole calponin 3, EHB05382.1; Orangutan calponin 2, NP_001124601.1; Rat calponin 1, NP_113935.1; Rat calponin 3, NP_062232.1; Rhesus macaque calponin 3, NP_001248738.1; Salmon calponin 1, NP_001139857.1; Salmon calponin 2, NP_001133873.1; Salmon calponin 3, NP_001133337.1; Sheep, calponin 1, NP_001009456.1; Snakehead calponin 2, AFJ79963.1; Timber rattlesnake calponin 2, JAG45504.1; Western clawed frog calponin 1, NP_001015796.1; NP_998841.1; Western clawed frog calponin 2, Western clawed frog calponin 3, NP_989257.1; Wild swine calponin 1, NP_999043.1; Yak calponin 1, ELR59973.1; Yak calponin 2, ELR60222.1; Yak calponin 3, ELR46902.1; Zebrafish calponin 2, NP_998514.1; Zebrafish calponin 3, NP_956047.1.

APPENDIX C

NCBI database for calponin and SM22 isoforms analyzed (Figure 28)

The NCBI database accession numbers of the sequences analyzed are: Chicken calponin 1, NP_990847.1; Chicken calponin 2, NP_001135728.1; Chicken calponin 3, XP_422326.3; Chicken SM22, AAA48782.1; Human calponin 1, NP_001290.2; Human calponin 2, AAI48265.1; Human calponin 3, AAB35752.1; Human SM22, NP_001001522.1; Mouse calponin 1, AAI38864.1; Mouse calponin 2, EDL31614.1; Mouse calponin 3, AAH85268.1; Mouse SM22, CAA92941.1.

APPENDIX D

Copyright License Agreement for Chapter 3

Title:	Deletion of calponin 2 in macrophages alters cytoskeleton -based functions and attenuates the development of atherosclerosis
Author:	Rong Liu,J.-P. Jin
Publication:	Journal of Molecular and Cellular Cardiology
Publisher:	Elsevier
Date:	October 2016

Review Order

Please review the order details and the associated terms and conditions.

No royalties will be charged for this reuse request although you are required to obtain a license and comply with the license terms and conditions. To obtain the license, click the Accept button below.

Licensed Content Publisher	Elsevier
Licensed Content Publication	Journal of Molecular and Cellular Cardiology
Licensed Content Title	Deletion of calponin 2 in macrophages alters cytoskeleton-based functions and attenuates the development of atherosclerosis
Licensed Content Author	Rong Liu,J.-P. Jin
Licensed Content Date	October 2016
Licensed Content Volume	99
Licensed Content Issue	n/a
Licensed Content Pages	13
Type of Use	reuse in a thesis/dissertation
Portion	full article
Format	both print and electronic
Are you the author of this Elsevier article?	Yes
Will you be translating?	No
Order reference number	
Title of your thesis/dissertation	Calponin and Cytoskeleton Dynamics in Macrophage Functions and the Pathogenesis of Atherosclerosis
Expected completion date	Oct 2016
Estimated size (number of pages)	146
Elsevier VAT number	GB 494 6272 12
Requestor Location	Juan M Gonzalez 5374 Scott Hall 540 E. Canfield DETROIT, MI 48201 United States Attn: Juan M Gonzalez
Total	0.00 USD

APPENDIX E

Copyright License Agreement for Chapter 5

Copyright Clearance Center RightsLink®

Home | Create Account | Help | Live Chat

Title: Physiological contractility of cardiomyocytes in the wall of mouse and rat azygos vein

Author: Rong Liu,Han-Zhong Feng,J.-P. Jin

Publication: Am J Physiol-Cell Physiology

Publisher: The American Physiological Society

Date: Apr 1, 2014

Copyright © 2014, Copyright © 2014 the American Physiological Society

LOGIN

If you're a copyright.com user, you can login to RightsLink using your copyright.com credentials. Already a RightsLink user or want to learn more?

Permission Not Required

Permission is not required for this type of use.

BACK | CLOSE WINDOW

Copyright © 2016 Copyright Clearance Center, Inc. All Rights Reserved. Privacy statement. Terms and Conditions.
Comments? We would like to hear from you. E-mail us at customercare@copyright.com

REFERENCES

1. Q.Q. Huang, M.M. Hossain, K. Wu, K. Parai, R.M. Pope, J.P. Jin, Role of H2-calponin in regulating macrophage motility and phagocytosis, The Journal of biological chemistry 283 (2008) 25887-25899.
2. M. Moazzem Hossain, X. Wang, R.C. Bergan, J.P. Jin, Diminished expression of h2-calponin in prostate cancer cells promotes cell proliferation, migration and the dependence of cell adhesion on substrate stiffness, FEBS open bio 4 (2014) 627-636.
3. E.N. Marieb, Human anatomy and physiology, 2nd ed., Benjamin/Cummings Pub. Co., Redwood City, Calif., 1992.
4. R. Ross, L. Harker, Hyperlipidemia and atherosclerosis, Science 193 (1976) 1094-1100.
5. R. Ross, Atherosclerosis is an inflammatory disease, American heart journal 138 (1999) S419-420.
6. P. Libby, Inflammation in atherosclerosis, Arteriosclerosis, thrombosis, and vascular biology 32 (2012) 2045-2051.
7. M. Nahrendorf, F.K. Swirski, Immunology. Neutrophil-macrophage communication in inflammation and atherosclerosis, Science 349 (2015) 237-238.
8. K.J. Moore, I. Tabas, Macrophages in the pathogenesis of atherosclerosis, Cell 145 (2011) 341-355.
9. A. Tedgui, Z. Mallat, Cytokines in atherosclerosis: pathogenic and regulatory pathways, Physiological reviews 86 (2006) 515-581.

10. C. Weber, A. Zernecke, P. Libby, The multifaceted contributions of leukocyte subsets to atherosclerosis: lessons from mouse models, Nature reviews. Immunology 8 (2008) 802-815.

11. C.K. Glass, J.L. Witztum, Atherosclerosis. the road ahead, Cell 104 (2001) 503-516.

12. G.K. Hansson, Immune mechanisms in atherosclerosis, Arteriosclerosis, thrombosis, and vascular biology 21 (2001) 1876-1890.

13. J.D. Smith, E. Trogan, M. Ginsberg, C. Grigaux, J. Tian, M. Miyata, Decreased atherosclerosis in mice deficient in both macrophage colony-stimulating factor (op) and apolipoprotein E, Proceedings of the National Academy of Sciences of the United States of America 92 (1995) 8264-8268.

14. H.M. Dansky, S.A. Charlton, M.M. Harper, J.D. Smith, T and B lymphocytes play a minor role in atherosclerotic plaque formation in the apolipoprotein E-deficient mouse, Proceedings of the National Academy of Sciences of the United States of America 94 (1997) 4642-4646.

15. A. Daugherty, E. Pure, D. Delfel-Butteiger, S. Chen, J. Leferovich, S.E. Roselaar, D.J. Rader, The effects of total lymphocyte deficiency on the extent of atherosclerosis in apolipoprotein E-/- mice, The Journal of clinical investigation 100 (1997) 1575-1580.

16. R.R. Packard, A.H. Lichtman, P. Libby, Innate and adaptive immunity in atherosclerosis, Semin Immunopathol 31 (2009) 5-22.

17. T.B. Rajavashisth, A. Andalibi, M.C. Territo, J.A. Berliner, M. Navab, A.M. Fogelman, A.J. Lusis, Induction of endothelial cell expression of granulocyte and

macrophage colony-stimulating factors by modified low-density lipoproteins, Nature 344 (1990) 254-257.

18. G.J. Randolph, Emigration of monocyte-derived cells to lymph nodes during resolution of inflammation and its failure in atherosclerosis, Curr Opin Lipidol 19 (2008) 462-468.

19. N.R. Patel, M. Bole, C. Chen, C.C. Hardin, A.T. Kho, J. Mih, L. Deng, J. Butler, D. Tschumperlin, J.J. Fredberg, R. Krishnan, H. Koziel, Cell elasticity determines macrophage function, PloS one 7 (2012) e41024.

20. N.G. Sosale, K.R. Spinler, C. Alvey, D.E. Discher, Macrophage engulfment of a cell or nanoparticle is regulated by unavoidable opsonization, a species-specific 'Marker of Self' CD47, and target physical properties, Curr Opin Immunol 35 (2015) 107-112.

21. K. Takahashi, M. Abe, K. Hiwada, T. Kokubu, A novel troponin T-like protein (calponin) in vascular smooth muscle: interaction with tropomyosin paracrystals, Journal of hypertension. Supplement : official journal of the International Society of Hypertension 6 (1988) S40-43.

22. J. Gao, J.M. Hwang, J.P. Jin, Complete nucleotide sequence, structural organization, and an alternatively spliced exon of mouse h1-calponin gene, Biochemical and biophysical research communications 218 (1996) 292-297.

23. P. Strasser, M. Gimona, H. Moessler, M. Herzog, J.V. Small, Mammalian calponin. Identification and expression of genetic variants, FEBS letters 330 (1993) 13-18.

24. H. Masuda, K. Tanaka, M. Takagi, K. Ohgami, T. Sakamaki, N. Shibata, K. Takahashi, Molecular cloning and characterization of human non-smooth muscle calponin, Journal of biochemistry 120 (1996) 415-424.

25. D. Applegate, W. Feng, R.S. Green, M.B. Taubman, Cloning and expression of a novel acidic calponin isoform from rat aortic vascular smooth muscle, The Journal of biological chemistry 269 (1994) 10683-10690.

26. J.P. Jin, M.P. Walsh, M.E. Resek, G.A. McMartin, Expression and epitopic conservation of calponin in different smooth muscles and during development, Biochemistry and cell biology = Biochimie et biologie cellulaire 74 (1996) 187-196.

27. M.M. Hossain, D.Y. Hwang, Q.Q. Huang, Y. Sasaki, J.P. Jin, Developmentally regulated expression of calponin isoforms and the effect of h2-calponin on cell proliferation, Am J Physiol Cell Physiol 284 (2003) C156-167.

28. Y. Fukui, H. Masuda, M. Takagi, K. Takahashi, K. Kiyokane, The presence of h2-calponin in human keratinocyte, Journal of dermatological science 14 (1997) 29-36.

29. M.M. Hossain, J.F. Crish, R.L. Eckert, J.J. Lin, J.P. Jin, h2-Calponin is regulated by mechanical tension and modifies the function of actin cytoskeleton, The Journal of biological chemistry 280 (2005) 42442-42453.

30. M.M. Hossain, P.G. Smith, K. Wu, J.P. Jin, Cytoskeletal tension regulates both expression and degradation of h2-calponin in lung alveolar cells, Biochemistry 45 (2006) 15670-15683.

31. J. Tang, G. Hu, J. Hanai, G. Yadlapalli, Y. Lin, B. Zhang, J. Galloway, N. Bahary, S. Sinha, B. Thisse, C. Thisse, J.P. Jin, L.I. Zon, V.P. Sukhatme, A critical role for calponin 2 in vascular development, The Journal of biological chemistry 281 (2006) 6664-6672.

32. W.R. Jiang, G. Cady, M.M. Hossain, Q.Q. Huang, X. Wang, J.P. Jin, Mechanoregulation of h2-calponin gene expression and the role of Notch signaling, The Journal of biological chemistry 289 (2014) 1617-1628.

33. P.C. Hines, X. Gao, J.C. White, A. D'Agostino, J.P. Jin, A novel role of h2-calponin in regulating whole blood thrombosis and platelet adhesion during physiologic flow, Physiol Rep 2 (2014).

34. R. Liu, J.P. Jin, Calponin isoforms CNN1, CNN2 and CNN3: Regulators for actin cytoskeleton functions in smooth muscle and non-muscle cells, Gene 585 (2016) 143-153.

35. H. Trabelsi-Terzidis, A. Fattoum, A. Represa, F. Dessi, Y. Ben-Ari, E. der Terrossian, Expression of an acidic isoform of calponin in rat brain: western blots on one- or two-dimensional gels and immunolocalization in cultured cells, The Biochemical journal 306 (Pt 1) (1995) 211-215.

36. C. Agassandian, M. Plantier, A. Fattoum, A. Represa, E. der Terrossian, Subcellular distribution of calponin and caldesmon in rat hippocampus, Brain research 887 (2000) 444-449.

37. L. Ferhat, G. Charton, A. Represa, Y. Ben-Ari, E. der Terrossian, M. Khrestchatisky, Acidic calponin cloned from neural cells is differentially

expressed during rat brain development, The European journal of neuroscience 8 (1996) 1501-1509.

38. L. Ferhat, M. Esclapez, A. Represa, A. Fattoum, T. Shirao, Y. Ben-Ari, Increased levels of acidic calponin during dendritic spine plasticity after pilocarpine-induced seizures, Hippocampus 13 (2003) 845-858.

39. M. Plantier, A. Fattoum, B. Menn, Y. Ben-Ari, E. Der Terrossian, A. Represa, Acidic calponin immunoreactivity in postnatal rat brain and cultures: subcellular localization in growth cones, under the plasma membrane and along actin and glial filaments, The European journal of neuroscience 11 (1999) 2801-2812.

40. Y. Shibukawa, N. Yamazaki, E. Daimon, Y. Wada, Rock-dependent calponin 3 phosphorylation regulates myoblast fusion, Experimental cell research 319 (2013) 633-648.

41. Y. Shibukawa, N. Yamazaki, K. Kumasawa, E. Daimon, M. Tajiri, Y. Okada, M. Ikawa, Y. Wada, Calponin 3 regulates actin cytoskeleton rearrangement in trophoblastic cell fusion, Molecular biology of the cell 21 (2010) 3973-3984.

42. K. Takahashi, R. Yoshimoto, K. Fuchibe, A. Fujishige, M. Mitsui-Saito, M. Hori, H. Ozaki, H. Yamamura, N. Awata, S. Taniguchi, M. Katsuki, T. Tsuchiya, H. Karaki, Regulation of shortening velocity by calponin in intact contracting smooth muscles, Biochemical and biophysical research communications 279 (2000) 150-157.

43. A. Flemming, Q.Q. Huang, J.P. Jin, H. Jumaa, S. Herzog, A Conditional Knockout Mouse Model Reveals That Calponin-3 Is Dispensable for Early B Cell Development, PloS one 10 (2015) e0128385.

44. M. Gimona, K. Djinovic-Carugo, W.J. Kranewitter, S.J. Winder, Functional plasticity of CH domains, FEBS letters 513 (2002) 98-106.

45. L. Fontao, D. Geerts, I. Kuikman, J. Koster, D. Kramer, A. Sonnenberg, The interaction of plectin with actin: evidence for cross-linking of actin filaments by dimerization of the actin-binding domain of plectin, Journal of cell science 114 (2001) 2065-2076.

46. V.E. Galkin, A. Orlova, A. Fattoum, M.P. Walsh, E.H. Egelman, The CH-domain of calponin does not determine the modes of calponin binding to F-actin, Journal of molecular biology 359 (2006) 478-485.

47. B.D. Leinweber, P.C. Leavis, Z. Grabarek, C.L. Wang, K.G. Morgan, Extracellular regulated kinase (ERK) interaction with actin and the calponin homology (CH) domain of actin-binding proteins, The Biochemical journal 344 Pt 1 (1999) 117-123.

48. M. Mezgueldi, A. Fattoum, J. Derancourt, R. Kassab, Mapping of the functional domains in the amino-terminal region of calponin, The Journal of biological chemistry 267 (1992) 15943-15951.

49. [49] S.J. Winder, M.P. Walsh, Smooth muscle calponin. Inhibition of actomyosin MgATPase and regulation by phosphorylation, The Journal of biological chemistry 265 (1990) 10148-10155.

50. M. Abe, K. Takahashi, K. Hiwada, Effect of calponin on actin-activated myosin ATPase activity, Journal of biochemistry 108 (1990) 835-838.

51. S.J. Winder, M.P. Walsh, C. Vasulka, J.D. Johnson, Calponin-calmodulin interaction: properties and effects on smooth and skeletal muscle actin binding and actomyosin ATPases, Biochemistry 32 (1993) 13327-13333.

52. V.P. Shirinsky, K.G. Biryukov, J.M. Hettasch, J.R. Sellers, Inhibition of the relative movement of actin and myosin by caldesmon and calponin, The Journal of biological chemistry 267 (1992) 15886-15892.

53. J.R. Haeberle, Calponin decreases the rate of cross-bridge cycling and increases maximum force production by smooth muscle myosin in an in vitro motility assay, The Journal of biological chemistry 269 (1994) 12424-12431.

54. T. Kake, S. Kimura, K. Takahashi, K. Maruyama, Calponin induces actin polymerization at low ionic strength and inhibits depolymerization of actin filaments, The Biochemical journal 312 (Pt 2) (1995) 587-592.

55. J.P. Jin, Z. Zhang, J.A. Bautista, Isoform diversity, regulation, and functional adaptation of troponin and calponin, Critical reviews in eukaryotic gene expression 18 (2008) 93-124.

56. K.C. Wu, J.P. Jin, Calponin in non-muscle cells, Cell biochemistry and biophysics 52 (2008) 139-148.

57. A. Bartegi, C. Roustan, R. Kassab, A. Fattoum, Fluorescence studies of the carboxyl-terminal domain of smooth muscle calponin effects of F-actin and salts, European journal of biochemistry / FEBS 262 (1999) 335-341.

58. C. Danninger, M. Gimona, Live dynamics of GFP-calponin: isoform-specific modulation of the actin cytoskeleton and autoregulation by C-terminal sequences, Journal of cell science 113 Pt 21 (2000) 3725-3736.

59. G. Burgstaller, W.J. Kranewitter, M. Gimona, The molecular basis for the autoregulation of calponin by isoform-specific C-terminal tail sequences, Journal of cell science 115 (2002) 2021-2029.

60. M.M. Hossain, G. Zhao, M.-S. Woo, J.H.C. Wang, J.P. Jin, h2-calponin Gene Knockout Increases Traction Force of Mouse Fibroblasts in vitro, Biophysical journal 108 143a.

61. M.M. Hossain, G. Zhao, M.S. Woo, J.H. Wang, J.P. Jin, Deletion of calponin 2 in mouse fibroblasts increases myosin II-dependent cell traction force, Biochemistry (2016).

62. M.P. Walsh, The Ayerst Award Lecture 1990. Calcium-dependent mechanisms of regulation of smooth muscle contraction, Biochemistry and cell biology = Biochimie et biologie cellulaire 69 (1991) 771-800.

63. G.E. Jones, Cellular signaling in macrophage migration and chemotaxis, Journal of leukocyte biology 68 (2000) 593-602.

64. Q.Q. Huang, M.M. Hossain, W. Sun, L. Xing, R.M. Pope, J.P. Jin, Deletion of calponin 2 in macrophages attenuates the severity of inflammatory arthritis in mice, Am J Physiol Cell Physiol (2016) ajpcell 00331 02015.

65. J.L. Goldstein, M.S. Brown, The low-density lipoprotein pathway and its relation to atherosclerosis, Annu Rev Biochem 46 (1977) 897-930.

66. R.L. Reddick, S.H. Zhang, N. Maeda, Atherosclerosis in mice lacking apo E. Evaluation of lesional development and progression, Arteriosclerosis and thrombosis : a journal of vascular biology / American Heart Association 14 (1994) 141-147.

67. A. Daugherty, Atherosclerosis: cell biology and lipoproteins, Curr Opin Lipidol 13 (2002) 453-455.

68. J.P. Jin, L.B. Smillie, An unusual metal-binding cluster found exclusively in the avian breast muscle troponin T of Galliformes and Craciformes, FEBS letters 341 (1994) 135-140.

69. O. Ogut, J.P. Jin, Expression, zinc-affinity purification, and characterization of a novel metal-binding cluster in troponin T: metal-stabilized alpha-helical structure and effects of the NH2-terminal variable region on the conformation of intact troponin T and its association with tropomyosin, Biochemistry 35 (1996) 16581-16590.

70. F.W. Studier, A.H. Rosenberg, J.J. Dunn, J.W. Dubendorff, Use of T7 RNA polymerase to direct expression of cloned genes, Methods in enzymology 185 (1990) 60-89.

71. J.P. Jin, M.L. Malik, J.J. Lin, Monoclonal antibodies against cardiac myosin heavy chain, Hybridoma 9 (1990) 597-608.

72. M. Little, S.M. Kipriyanov, F. Le Gall, G. Moldenhauer, Of mice and men: hybridoma and recombinant antibodies, Immunol Today 21 (2000) 364-370.

73. J.P. Jin, R.A. Samanez, Evolution of a metal-binding cluster in the NH(2)-terminal variable region of avian fast skeletal muscle troponin T: functional divergence on the basis of tolerance to structural drifting, Journal of molecular evolution 52 (2001) 103-116.

74. P.C. Leavis, J. Gergely, Thin filament proteins and thin filament-linked regulation of vertebrate muscle contraction, CRC critical reviews in biochemistry 16 (1984) 235-305.

75. T.A. Cooper, C.P. Ordahl, A single cardiac troponin T gene generates embryonic and adult isoforms via developmentally regulated alternate splicing, The Journal of biological chemistry 260 (1985) 11140-11148.

76. R.E. Breitbart, B. Nadal-Ginard, Complete nucleotide sequence of the fast skeletal troponin T gene. Alternatively spliced exons exhibit unusual interspecies divergence, Journal of molecular biology 188 (1986) 313-324.

77. J.P. Jin, Q.Q. Huang, H.I. Yeh, J.J. Lin, Complete nucleotide sequence and structural organization of rat cardiac troponin T gene. A single gene generates embryonic and adult isoforms via developmentally regulated alternative splicing, Journal of molecular biology 227 (1992) 1269-1276.

78. E.A. Bucher, G.K. Dhoot, M.M. Emerson, M. Ober, C.P. Emerson, Jr., Structure and evolution of the alternatively spliced fast troponin T isoform gene, The Journal of biological chemistry 274 (1999) 17661-17670.

79. L.B. Smillie, K. Golosinska, F.C. Reinach, Sequences of complete cDNAs encoding four variants of chicken skeletal muscle troponin T, The Journal of biological chemistry 263 (1988) 18816-18820.

80. F. Schachat, J.M. Schmidt, M. Maready, M.M. Briggs, Chicken perinatal troponin Ts are generated by a combination of novel and phylogenetically conserved alternative splicing pathways, Developmental biology 171 (1995) 233-239.

81. F.H. Arnold, B.L. Haymore, Engineered metal-binding proteins: purification to protein folding, Science 252 (1991) 1796-1797.

82. O. Ogut, J.P. Jin, Developmentally regulated, alternative RNA splicing-generated pectoral muscle-specific troponin T isoforms and role of the NH2-terminal hypervariable region in the tolerance to acidosis, The Journal of biological chemistry 273 (1998) 27858-27866.

83. J. Wang, J.P. Jin, Conformational modulation of troponin T by configuration of the NH2-terminal variable region and functional effects, Biochemistry 37 (1998) 14519-14528.

84. R.J. Solaro, J.A. Lee, J.C. Kentish, D.G. Allen, Effects of acidosis on ventricular muscle from adult and neonatal rats, Circulation research 63 (1988) 779-787.

85. O. Ogut, H. Granzier, J.P. Jin, Acidic and basic troponin T isoforms in mature fast-twitch skeletal muscle and effect on contractility, The American journal of physiology 276 (1999) C1162-1170.

86. K.H. Weisgraber, Apolipoprotein E: structure-function relationships, Adv Protein Chem 45 (1994) 249-302.

87. M.A. Perugini, P. Schuck, G.J. Howlett, Differences in the binding capacity of human apolipoprotein E3 and E4 to size-fractionated lipid emulsions, European journal of biochemistry / FEBS 269 (2002) 5939-5949.

88. S. Yokoyama, Y. Kawai, S. Tajima, A. Yamamoto, Behavior of human apolipoprotein E in aqueous solutions and at interfaces, The Journal of biological chemistry 260 (1985) 16375-16382.

89. P.E. Wright, H.J. Dyson, Intrinsically unstructured proteins: re-assessing the protein structure-function paradigm, Journal of molecular biology 293 (1999) 321-331.

90. D.M. Hatters, G.J. Howlett, The structural basis for amyloid formation by plasma apolipoproteins: a review, Eur Biophys J 31 (2002) 2-8.

91. D.M. Hatters, C.A. Peters-Libeu, K.H. Weisgraber, Apolipoprotein E structure: insights into function, Trends in biochemical sciences 31 (2006) 445-454.

92. A.J. Lusis, Atherosclerosis, Nature 407 (2000) 233-241.

93. G. Chinetti-Gbaguidi, S. Colin, B. Staels, Macrophage subsets in atherosclerosis, Nat Rev Cardiol 12 (2015) 10-17.

94. K. Takahashi, K. Hiwada, T. Kokubu, Isolation and characterization of a 34,000-dalton calmodulin- and F-actin-binding protein from chicken gizzard smooth muscle, Biochemical and biophysical research communications 141 (1986) 20-26.

95. R. Nigam, C.R. Triggle, J.P. Jin, h1- and h2-calponins are not essential for norepinephrine- or sodium fluoride-induced contraction of rat aortic smooth muscle, Journal of muscle research and cell motility 19 (1998) 695-703.

96. B.E. Clausen, C. Burkhardt, W. Reith, R. Renkawitz, I. Forster, Conditional gene targeting in macrophages and granulocytes using LysMcre mice, Transgenic Res 8 (1999) 265-277.

97. J.A. Piedrahita, S.H. Zhang, J.R. Hagaman, P.M. Oliver, N. Maeda, Generation of mice carrying a mutant apolipoprotein E gene inactivated by gene targeting in

embryonic stem cells, Proceedings of the National Academy of Sciences of the United States of America 89 (1992) 4471-4475.

98. X. Zhang, R. Goncalves, D.M. Mosser, The isolation and characterization of murine macrophages, Curr Protoc Immunol Chapter 14 (2008) Unit 14 11.

99. M.M. Bjorklund, A.K. Hollensen, M.K. Hagensen, F. Dagnaes-Hansen, C. Christoffersen, J.G. Mikkelsen, J.F. Bentzon, Induction of atherosclerosis in mice and hamsters without germline genetic engineering, Circulation research 114 (2014) 1684-1689.

100. A. Daugherty, S.C. Whitman, Quantification of atherosclerosis in mice, Methods in molecular biology 209 (2003) 293-309.

101. W. Kueng, E. Silber, U. Eppenberger, Quantification of cells cultured on 96-well plates, Anal Biochem 182 (1989) 16-19.

102. K.K. Sanford, W.R. Earle, G.D. Likely, The growth in vitro of single isolated tissue cells, Journal of the National Cancer Institute 9 (1948) 229-246.

103. J.J. Lin, T.E. Hegmann, J.L. Lin, Differential localization of tropomyosin isoforms in cultured nonmuscle cells, The Journal of cell biology 107 (1988) 563-572.

104. A. Daugherty, Mouse models of atherosclerosis, Am J Med Sci 323 (2002) 3-10.

105. R. Coleman, T. Hayek, S. Keidar, M. Aviram, A mouse model for human atherosclerosis: long-term histopathological study of lesion development in the aortic arch of apolipoprotein E-deficient (E0) mice, Acta Histochem 108 (2006) 415-424.

106. R.K. Tangirala, E.M. Rubin, W. Palinski, Quantitation of atherosclerosis in murine models: correlation between lesions in the aortic origin and in the entire aorta,

and differences in the extent of lesions between sexes in LDL receptor-deficient and apolipoprotein E-deficient mice, J Lipid Res 36 (1995) 2320-2328.

107. T. Chiba, M. Ikeda, K. Umegaki, T. Tomita, Estrogen-dependent activation of neutral cholesterol ester hydrolase underlying gender difference of atherogenesis in apoE-/- mice, Atherosclerosis 219 (2011) 545-551.

108. S.S. Meyrelles, V.A. Peotta, T.M. Pereira, E.C. Vasquez, Endothelial dysfunction in the apolipoprotein E-deficient mouse: insights into the influence of diet, gender and aging, Lipids Health Dis 10 (2011) 211.

109. C.M. Thomas, E.J. Smart, Gender as a regulator of atherosclerosis in murine models, Curr Drug Targets 8 (2007) 1172-1180.

110. G. Caligiuri, A. Nicoletti, X. Zhou, I. Tornberg, G.K. Hansson, Effects of sex and age on atherosclerosis and autoimmunity in apoE-deficient mice, Atherosclerosis 145 (1999) 301-308.

111. H. Liu, B. Shi, C.C. Huang, P. Eksarko, R.M. Pope, Transcriptional diversity during monocyte to macrophage differentiation, Immunology letters 117 (2008) 70-80.

112. C.E. Turner, Paxillin and focal adhesion signalling, Nature cell biology 2 (2000) E231-236.

113. J.G. Dickhout, S. Basseri, R.C. Austin, Macrophage function and its impact on atherosclerotic lesion composition, progression, and stability: the good, the bad, and the ugly, Arteriosclerosis, thrombosis, and vascular biology 28 (2008) 1413-1415.

114. K.J. Moore, F.J. Sheedy, E.A. Fisher, Macrophages in atherosclerosis: a dynamic balance, Nature reviews. Immunology 13 (2013) 709-721.

115. R. Ohashi, H. Mu, X. Wang, Q. Yao, C. Chen, Reverse cholesterol transport and cholesterol efflux in atherosclerosis, QJM 98 (2005) 845-856.

116. J.M. van Gils, M.C. Derby, L.R. Fernandes, B. Ramkhelawon, T.D. Ray, K.J. Rayner, S. Parathath, E. Distel, J.L. Feig, J.I. Alvarez-Leite, A.J. Rayner, T.O. McDonald, K.D. O'Brien, L.M. Stuart, E.A. Fisher, A. Lacy-Hulbert, K.J. Moore, The neuroimmune guidance cue netrin-1 promotes atherosclerosis by inhibiting the emigration of macrophages from plaques, Nature immunology 13 (2012) 136-143.

117. M. Pataki, G. Lusztig, H. Robenek, Endocytosis of oxidized LDL and reversibility of migration inhibition in macrophage-derived foam cells in vitro. A mechanism for atherosclerosis regression?, Arteriosclerosis and thrombosis : a journal of vascular biology / American Heart Association 12 (1992) 936-944.

118. C. Qin, T. Nagao, I. Grosheva, F.R. Maxfield, L.M. Pierini, Elevated plasma membrane cholesterol content alters macrophage signaling and function, Arteriosclerosis, thrombosis, and vascular biology 26 (2006) 372-378.

119. C.V. Zerbinatti, R.W. Gore, Uptake of modified low-density lipoproteins alters actin distribution and locomotor forces in macrophages, Am J Physiol Cell Physiol 284 (2003) C555-561.

120. B. Ludewig, J.D. Laman, The in and out of monocytes in atherosclerotic plaques: Balancing inflammation through migration, Proceedings of the National Academy of Sciences of the United States of America 101 (2004) 11529-11530.

121. R. Liu, J.P. Jin, Deletion of calponin 2 in macrophages alters cytoskeleton-based functions and attenuates the development of atherosclerosis, Journal of molecular and cellular cardiology 99 (2016) 87-99.

122. D.P. Ramji, T.S. Davies, Cytokines in atherosclerosis: Key players in all stages of disease and promising therapeutic targets, Cytokine Growth Factor Rev 26 (2015) 673-685.

123. S. Freigang, F. Ampenberger, A. Weiss, T.D. Kanneganti, Y. Iwakura, M. Hersberger, M. Kopf, Fatty acid-induced mitochondrial uncoupling elicits inflammasome-independent IL-1alpha and sterile vascular inflammation in atherosclerosis, Nature immunology 14 (2013) 1045-1053.

124. Y. Kamari, A. Shaish, S. Shemesh, E. Vax, I. Grosskopf, S. Dotan, M. White, E. Voronov, C.A. Dinarello, R.N. Apte, D. Harats, Reduced atherosclerosis and inflammatory cytokines in apolipoprotein-E-deficient mice lacking bone marrow-derived interleukin-1alpha, Biochemical and biophysical research communications 405 (2011) 197-203.

125. K. Kimura, T. Hashiguchi, T. Deguchi, S. Horinouchi, T. Uto, H. Oku, S. Setoyama, I. Maruyama, M. Osame, K. Arimura, Serum VEGF--as a prognostic factor of atherosclerosis, Atherosclerosis 194 (2007) 182-188.

126. P.W. Holm, R.H. Slart, C.J. Zeebregts, J.L. Hillebrands, R.A. Tio, Atherosclerotic plaque development and instability: a dual role for VEGF, Ann Med 41 (2009) 257-264.

127. L. Yvan-Charvet, J. Kling, T. Pagler, H. Li, B. Hubbard, T. Fisher, C.P. Sparrow, A.K. Taggart, A.R. Tall, Cholesterol efflux potential and antiinflammatory

properties of high-density lipoprotein after treatment with niacin or anacetrapib, Arteriosclerosis, thrombosis, and vascular biology 30 (2010) 1430-1438.

128. N. Sharma, Y. Lu, G. Zhou, X. Liao, P. Kapil, P. Anand, G.H. Mahabeleshwar, J.S. Stamler, M.K. Jain, Myeloid Kruppel-like factor 4 deficiency augments atherogenesis in ApoE-/- mice--brief report, Arteriosclerosis, thrombosis, and vascular biology 32 (2012) 2836-2838.

129. L. Cardilo-Reis, S. Gruber, S.M. Schreier, M. Drechsler, N. Papac-Milicevic, C. Weber, O. Wagner, H. Stangl, O. Soehnlein, C.J. Binder, Interleukin-13 protects from atherosclerosis and modulates plaque composition by skewing the macrophage phenotype, EMBO Mol Med 4 (2012) 1072-1086.

130. R.N. Hanna, I. Shaked, H.G. Hubbeling, J.A. Punt, R. Wu, E. Herrley, C. Zaugg, H. Pei, F. Geissmann, K. Ley, C.C. Hedrick, NR4A1 (Nur77) deletion polarizes macrophages toward an inflammatory phenotype and increases atherosclerosis, Circulation research 110 (2012) 416-427.

131. A.A. Hamers, M. Vos, F. Rassam, G. Marinkovic, K. Kurakula, P.J. van Gorp, M.P. de Winther, M.J. Gijbels, V. de Waard, C.J. de Vries, Bone marrow-specific deficiency of nuclear receptor Nur77 enhances atherosclerosis, Circulation research 110 (2012) 428-438.

132. Z. Szekanecz, A.E. Koch, Macrophages and their products in rheumatoid arthritis, Current opinion in rheumatology 19 (2007) 289-295.

133. A.K. Blakney, M.D. Swartzlander, S.J. Bryant, The effects of substrate stiffness on the in vitro activation of macrophages and in vivo host response to

poly(ethylene glycol)-based hydrogels, J Biomed Mater Res A 100 (2012) 1375-1386.

134. M.L. Previtera, A. Sengupta, Substrate Stiffness Regulates Proinflammatory Mediator Production through TLR4 Activity in Macrophages, PloS one 10 (2015) e0145813.

135. M.V. Smillie, L.A. Griffiths, P.J. Male, M.M. Wermeille, The disposition and metabolism of (+)-cyanidanol-3 in patients with alcoholic cirrhosis, Eur J Clin Pharmacol 33 (1987) 255-259.

136. J.R. Pearlstone, M. Weber, J.P. Lees-Miller, M.R. Carpenter, L.B. Smillie, Amino acid sequence of chicken gizzard smooth muscle SM22 alpha, The Journal of biological chemistry 262 (1987) 5985-5991.

137. M. Gimona, I. Kaverina, G.P. Resch, E. Vignal, G. Burgstaller, Calponin repeats regulate actin filament stability and formation of podosomes in smooth muscle cells, Molecular biology of the cell 14 (2003) 2482-2491.

138. C. Shapland, J.J. Hsuan, N.F. Totty, D. Lawson, Purification and properties of transgelin: a transformation and shape change sensitive actin-gelling protein, The Journal of cell biology 121 (1993) 1065-1073.

139. D. Lawson, M. Harrison, C. Shapland, Fibroblast transgelin and smooth muscle SM22alpha are the same protein, the expression of which is down-regulated in many cell lines, Cell Motil Cytoskeleton 38 (1997) 250-257.

140. S.J. Assinder, J.A. Stanton, P.D. Prasad, Transgelin: an actin-binding protein and tumour suppressor, The international journal of biochemistry & cell biology 41 (2009) 482-486.

141. G.K. Owens, Molecular control of vascular smooth muscle cell differentiation, Acta physiologica Scandinavica 164 (1998) 623-635.

142. O. Thompson, J.S. Moghraby, K.R. Ayscough, S.J. Winder, Depletion of the actin bundling protein SM22/transgelin increases actin dynamics and enhances the tumourigenic phenotypes of cells, BMC Cell Biol 13 (2012) 1.

143. J.P. Jin, S.M. Chong, Localization of the two tropomyosin-binding sites of troponin T, Arch Biochem Biophys 500 (2010) 144-150.

144. J.P. Jin, D. Wu, J. Gao, R. Nigam, S. Kwong, Expression and purification of the h1 and h2 isoforms of calponin, Protein expression and purification 31 (2003) 231-239.

145. R.J. Pelham, Jr., Y. Wang, Cell locomotion and focal adhesions are regulated by substrate flexibility, Proceedings of the National Academy of Sciences of the United States of America 94 (1997) 13661-13665.

146. J.R. Tse, A.J. Engler, Preparation of hydrogel substrates with tunable mechanical properties, Curr Protoc Cell Biol Chapter 10 (2010) Unit 10 16.

147. A. Zeidan, I. Nordstrom, S. Albinsson, U. Malmqvist, K. Sward, P. Hellstrand, Stretch-induced contractile differentiation of vascular smooth muscle: sensitivity to actin polymerization inhibitors, Am J Physiol Cell Physiol 284 (2003) C1387-1396.

148. A. Zeidan, I. Nordstrom, K. Dreja, U. Malmqvist, P. Hellstrand, Stretch-dependent modulation of contractility and growth in smooth muscle of rat portal vein, Circulation research 87 (2000) 228-234.

149. A. Zeidan, K. Sward, I. Nordstrom, E. Ekblad, J.C. Zhang, M.S. Parmacek, P. Hellstrand, Ablation of SM22alpha decreases contractility and actin contents of mouse vascular smooth muscle, FEBS letters 562 (2004) 141-146.

150. K.R. Chien, E.N. Olson, Converging pathways and principles in heart development and disease: CV@CSH, Cell 110 (2002) 153-162.

151. W.C. Claycomb, Control of cardiac muscle cell division, Trends in cardiovascular medicine 2 (1992) 231-236.

152. W.R. MacLellan, M.D. Schneider, Genetic dissection of cardiac growth control pathways, Annual review of physiology 62 (2000) 289-319.

153. M.H. Soonpaa, L.J. Field, Survey of studies examining mammalian cardiomyocyte DNA synthesis, Circulation research 83 (1998) 15-26.

154. M.A. Laflamme, C.E. Murry, Heart regeneration, Nature 473 (2011) 326-335.

155. J. Sadoshima, S. Izumo, Mechanical stretch rapidly activates multiple signal transduction pathways in cardiac myocytes: potential involvement of an autocrine/paracrine mechanism, The EMBO journal 12 (1993) 1681-1692.

156. D. Sedmera, T. Pexieder, V. Rychterova, N. Hu, E.B. Clark, Remodeling of chick embryonic ventricular myoarchitecture under experimentally changed loading conditions, Anat Rec 254 (1999) 238-252.

157. D. Sedmera, R.P. Thompson, F. Kolar, Effect of increased pressure loading on heart growth in neonatal rats, Journal of molecular and cellular cardiology 35 (2003) 301-309.

158. K. Tobita, J.B. Garrison, L.J. Liu, J.P. Tinney, B.B. Keller, Three-dimensional myofiber architecture of the embryonic left ventricle during normal development

and altered mechanical loads, The anatomical record. Part A, Discoveries in molecular, cellular, and evolutionary biology 283 (2005) 193-201.

159. G.E. Burch, R.B. Romney, Functional anatomy and throttle valve action on the pulmonary veins, American heart journal 47 (1954) 58-66.

160. J.V. Klavins, Demonstration of striated muscle in the pulmonary veins of the rat, Journal of anatomy 97 (1963) 239-241.

161. H. Nathan, H. Gloobe, Myocardial atrio-venous junctions and extensions (sleeves) over the pulmonary and caval veins. Anatomical observations in various mammals, Thorax 25 (1970) 317-324.

162. M. Chard, R. Tabrizchi, The role of pulmonary veins in atrial fibrillation: a complex yet simple story, Pharmacology & therapeutics 124 (2009) 207-218.

163. S.A. Chen, M.H. Hsieh, C.T. Tai, C.F. Tsai, V.S. Prakash, W.C. Yu, T.L. Hsu, Y.A. Ding, M.S. Chang, Initiation of atrial fibrillation by ectopic beats originating from the pulmonary veins: electrophysiological characteristics, pharmacological responses, and effects of radiofrequency ablation, Circulation 100 (1999) 1879-1886.

164. M. Haissaguerre, P. Jais, D.C. Shah, A. Takahashi, M. Hocini, G. Quiniou, S. Garrigue, A. Le Mouroux, P. Le Metayer, J. Clementy, Spontaneous initiation of atrial fibrillation by ectopic beats originating in the pulmonary veins, The New England journal of medicine 339 (1998) 659-666.

165. P. Jais, M. Haissaguerre, D.C. Shah, S. Chouairi, L. Gencel, M. Hocini, J. Clementy, A focal source of atrial fibrillation treated by discrete radiofrequency ablation, Circulation 95 (1997) 572-576.

166. M.P. Kracklauer, H.-Z. Feng, W. Jiang, J.L.C. Lin, J.J.C. Lin, J.-P. Jin, Discontinuous thoracic venous cardiomyocytes and heart exhibit synchronized developmental switch of troponin isoforms, FEBS Journal 280 (2013) 880-891.

167. A.W. Kramer, Jr., L.S. Marks, The occurrence of cardiac muscle in the pulmonary veins of Rodenita, Journal of morphology 117 (1965) 135-149.

168. Q. Wang, R.S. Reiter, Q.-Q. Huang, J.-P. Jin, J.J.-C. Lin, Comparative studies on the expression patterns of three troponin T genes during mouse development, The Anatomical Record 263 (2001) 72-84.

169. H.Z. Feng, B. Wei, J.P. Jin, Deletion of a genomic segment containing the cardiac troponin I gene knocks down expression of the slow troponin T gene and impairs fatigue tolerance of diaphragm muscle, The Journal of biological chemistry 284 (2009) 31798-31806.

170. J.P. Jin, A. Chen, Q.Q. Huang, Three alternatively spliced mouse slow skeletal muscle troponin T isoforms: conserved primary structure and regulated expression during postnatal development, Gene 214 (1998) 121-129.

171. J.J. Lin, Monoclonal antibodies against myofibrillar components of rat skeletal muscle decorate the intermediate filaments of cultured cells, Proceedings of the National Academy of Sciences of the United States of America 78 (1981) 2335-2339.

172. Z.B. Yu, H. Wei, J.P. Jin, Chronic coexistence of two troponin T isoforms in adult transgenic mouse cardiomyocytes decreased contractile kinetics and caused dilatative remodeling, Am J Physiol Cell Physiol 303 (2012) C24-32.

173. A. Redel, W. Baumgartner, K. Golenhofen, D. Drenckhahn, N. Golenhofen, Mechanical activity and force–frequency relationship of isolated mouse papillary muscle: effects of extracellular calcium concentration, temperature and contraction type, Pflugers Arch - Eur J Physiol 445 (2002) 297-304.

174. E. Monuszko, S. Halevy, K. Freese, M. Liu-Barnett, B. Altura, Vasoactive actions of local anaesthetics on human isolated umbilical veins and arteries, British journal of pharmacology 97 (1989) 319-328.

175. M.P. Revuelta, B. Cantabrana, M. Sanchez, A. Hidalgo, Effect of spermine and alpha-difluoromethylornithine on KCl- and CaCl2-induced contraction in rat uterine smooth muscle, Journal of autonomic pharmacology 18 (1998) 223-230.

176. Z. Zhang, B.J. Biesiadecki, J.-P. Jin, Selective Deletion of the NH2-Terminal Variable Region of Cardiac Troponin T in Ischemia Reperfusion by Myofibril-Associated μ-Calpain Cleavage†, Biochemistry 45 (2006) 11681-11694.

177. H. Nathan, M. Eliakim, The junction between the left atrium and the pulmonary veins. An anatomic study of human hearts, Circulation 34 (1966) 412-422.

178. O. Paes de Almeida, C.M. Bohm, M. de Paula Carvalho, A. Paes de Carvalho, The cardiac muscle in the pulmonary vein of the rat: a morphological and electrophysiological study, Journal of morphology 145 (1975) 409-433.

179. N. Hamdani, M. de Waard, A.E. Messer, N.M. Boontje, V. Kooij, S. van Dijk, A. Versteilen, R. Lamberts, D. Merkus, C. Dos Remedios, D.J. Duncker, A. Borbely, Z. Papp, W. Paulus, G.J. Stienen, S.B. Marston, J. van der Velden, Myofilament dysfunction in cardiac disease from mice to men, Journal of muscle research and cell motility 29 (2008) 189-201.

180. R. Cooke, The mechanism of muscle contraction, CRC critical reviews in biochemistry 21 (1986) 53-118.

181. K.E. Kamm, J.T. Stull, Signaling to myosin regulatory light chain in sarcomeres, The Journal of biological chemistry 286 (2011) 9941-9947.

182. J.M. Metzger, R.L. Moss, Myosin light chain 2 modulates calcium-sensitive cross-bridge transitions in vertebrate skeletal muscle, Biophysical journal 63 (1992) 460-468.

183. D. Szczesna, J. Zhao, J.D. Potter, The regulatory light chains of myosin modulate cross-bridge cycling in skeletal muscle, The Journal of biological chemistry 271 (1996) 5246-5250.

184. M.T.M. Mommersteeg, N.A. Brown, O.W.J. Prall, C. de Gier-de Vries, R.P. Harvey, A.F.M. Moorman, V.M. Christoffels, Pitx2c and Nkx2-5 Are Required for the Formation and Identity of the Pulmonary Myocardium, Circulation research 101 (2007) 902-909.

ABSTRACT

CALPONIN AND CYTOSKELETON DYNAMICS IN MACROPHAGE FUNCTIONS AND THE PATHOGENESIS OF ATHEROSCLEROSIS

by

Rong Liu

December 2016

Advisor: Dr. J.-P. Jin

Major: Physiology

Degree: Doctor of Philosophy

Arterial atherosclerosis is an inflammatory disease. Macrophages play a major role in the pathogenesis and progression of atherosclerotic lesions. Modulation of macrophage function is a therapeutic target for the treatment of atherosclerosis. Calponin is an actin-filament-associated regulatory protein that inhibits the activity of myosin-ATPase and dynamics of the actin cytoskeleton. Encoded by the *Cnn2* gene, calponin isoform 2 is expressed at significant levels in macrophages. Deletion of calponin 2 increases macrophage migration and phagocytosis. In the present study, we investigated the effect of deletion of calponin 2 in macrophages on the pathogenesis and development of atherosclerosis. The results showed that macrophages isolated from *Cnn2* knockout mice ingested the same level of acetylated low-density lipoprotein (LDL) as that of wild type (WT) macrophages but the resulting foam cells had significantly less impaired velocity of migration. Systemic or myeloid cell-specific *Cnn2* knockouts effectively attenuated the development of arterial atherosclerosis lesions with less macrophage infiltration in apolipoprotein E knockout mice. Consistently, calponin

2-null macrophages produced less pro-inflammatory cytokines than that of WT macrophages, and the up-regulation of pro-inflammatory cytokines in foam cells was also attenuated by the deletion of calponin 2. Calponin 2-null macrophages and foam cells have significantly weakened cell adhesion, indicating a role of cytoskeleton regulation in macrophage functions and inflammatory responses, and a novel therapeutic target for the treatment of arterial atherosclerosis.

To contribute to the greater field of vascular physiology and medicine, this dissertation research also pursued studies on the generation of anti-ApoE monoclonal antibodies, mechanoregulation in vascular smooth muscle and non-muscle cells, and a characterization of physiologically contractile cardiomyocytes in thoracic veins. The results add valuable contributions to our understanding of cardiovascular biology and diseases.

AUTOBIOGRAPHICAL STATEMENT

Rong Liu

Education

2016	Ph.D. in Physiology, Wayne State University, School of Medicine
2011	M.Sc. in Cardiology, Shandong University, School of Medicine
2009	B.M. (M.D.), Shandong University, School of Medicine

Honors, Awards, Distinctions

09/2012-04/2013	Thomas C. Rumble University Graduate Fellowship
02/2014	Graduate Student Travel Award, Wayne State University
09/2014-04/2015	Thomas C. Rumble University Graduate Fellowship
08/2014	Marion I. Barnhart Graduate Student Achievement Award, Department of Physiology, Wayne State University
02/2015	Graduate Student Professional Travel Award, Wayne State University School of Medicine
02/2015	2015 Biophysical Society Education Committee Travel Award
02/2015	2015 Biophysical Society Student Research Achievement Award
06/2015	Richard Barber Interdisciplinary Research Scholarship, Depart. Physics, Wayne State University
08/2015	Marion I. Barnhart Graduate Student Achievement Award, Department of Physiology, Wayne State University
08/2016	Graduate Student Achievement Award, Department of Physiology, Wayne State University

Peer Reviewed Publications

1. **Liu R,** Wang X, and Bu P. Omentin-1 is associated with carotid atherosclerosis in patients with metabolic syndrome. *Diabetes Research and Clinical Practice* 93: 21-25, 2011. PMID: 21497934
2. Wang F, Zhao XQ, Liu JN, Wang ZH, Wang XL, Hou XY, **Liu R,** Gao F, Zhang MX, Zhang Y, and Bu PL. Antagonist of microRNA-21 improves balloon injury-induced rat iliac artery remodeling by regulating proliferation and apoptosis of adventitial fibroblasts and myofibroblasts. *Journal of Cellular Biochemistry* 113: 2989-3001, 2012. PMID: 22565856